Why Are There No Low-$\delta^{18}O$ Magmas In Convergent Margins?

A Case of The Central Andes, Northern Chile.

A thesis presented for the degree of Master of Science in Geology, submitted to the Department of Geological Sciences, University of Cape Town.

Connie Sigauke

Supervised by Chris Harris

April 2021

Dedication

This work is dedicated to my late parents Adam and Samaria, whose memory has pushed me to work harder and become a better person. I also dedicate this work to my late guardian sister Sandile, I carry your love and teachings everywhere I go.

Declaration

I, Connie Sigauke, hereby declare that this thesis, submitted to the Department of Geological Sciences, University of Cape Town, is my own work and that neither the whole nor any part of it has been, is being, or is to be submitted for other academic purposes at this or any other institution of higher learning. All the assistance and reference material cited have been fully acknowledged.

Signed by candidate

28 April 2021

Acknowledgements

I extend my sincere gratitude to my supervisor Prof. Chris Harris for his guidance, the time he spent teaching me how to run the laser line, and the knowledge he shared with me throughout this project,. I am grateful for the NRF scholarship that was awarded to me through him.

I thank Dr. Petrus Le Roux, Dr. Benigno Godoy and Osvaldo Gonzales-Maurel for all the assistance during the fieldwork in Chile, and Sherissa Roopnarain for her assistance in analysing the samples.

Abstract

It has long been thought that low-$\delta^{18}O$ magmas (<5.7‰) are only found in extensional tectonic settings. Low-$\delta^{18}O$ magmas are rare, worldwide, especially in subduction zone settings. The main objective of this study was to conduct a search for low-$\delta^{18}O$ magmas in the Central Volcanic Zone (CVZ) of the Andes, to verify if their rarity is due to undersampling. If no low-$\delta^{18}O$ magmas were found, the question of why low-$\delta^{18}O$ magmas have appeared to be absent from the region would be addressed. This study has determined the variation in oxygen isotope composition of rocks across the CVZ, ranging in age from about 12 Ma to Recent. The $\delta^{18}O$ values were measured in selected bulk rock samples and separated quartz phenocrysts in order to identify potential low-$\delta^{18}O$ rocks (from whole rock analyses) and magmas (from the quartz phenocrysts). The average $\delta^{18}O$ values for quartz phenocrysts and whole rocks are 8.6‰ and 10.5‰ respectively, and no low-$\delta^{18}O$ magmas were found. Hydrogen isotope values range from -32 to -119‰, with the highest value in the most altered rock. The results from this study show no evidence for low-$\delta^{18}O$ magmas; the lowest value (5.0‰) was found in one sample (for both quartz and whole rock) and this sample appears to have been affected by interaction with meteoric water. The overall high $\delta^{18}O$ values in the CVZ rocks are best explained as the result of alteration by fluids having high $\delta^{18}O$ values. These were probably meteoric waters whose $\delta^{18}O$ were enriched due to fluid-rock exchange. The high $\delta^{18}O$ values of the magmas must reflect the absence of low-$\delta^{18}O$ rocks that could be melted and assimilated, as well as a relative crustal input to magmas. This study agrees with the conclusions of Folkes et al. (2013), which explains the absence of low-$\delta^{18}O$ magmas as a result of tectonic history and climatic conditions of the Central Andes; where low precipitation and high evaporation rates, high aridity, limited supply of meteoric waters, and high elevation all played significant roles in the lack of low-$\delta^{18}O$ magmas in the region.

Table of Contents

List of Tables

List of Figures

CHAPTER 1

Introduction

Low-$\delta^{18}O$ magmas are those that have $\delta^{18}O$ values lower than that of mantle-derived magma, that is about <5.7‰. Magma in this context refers to the semi or totally molten material found deep beneath the Earth's surface, this material may be derived from the mantle, crust or both and when it reaches the earth's surface, it solidifies to form different kinds of igneous rocks, depending on the composition of the melt (Bowen, 1947). Low-$\delta^{18}O$ magmas are globally rare, with classic and famous occurrences in the Yellowstone and Iceland (Bindeman et al., 2001). The rarity of these magmas is puzzling, and the mechanisms by which they form is still a controversial subject, e.g. (Balsley and Gregory, 1998; Boroughs et al., 2005; Troch et al., 2020). However, remelting, assimilation, exchange with hydrothermally altered wall rocks, partial melting of hydrothermally altered wallrocks, and stoping of altered material into the roof of the magma chamber are the popular explanations for the formation of low oxygen isotope magmas (Beard et al., 2005; Bacon and Lowenstern, 2005; Dungan and Davidson, 2004; Garcia et al., 1998; Taylor, 1986; Troch et al., 2020).

Larson and Taylor (1986), in their study of the oxygen isotope ratios of ash-flow tuffs in Lake City caldera, concluded that factors such as the duration of magmatism, the extent of hydrothermal alteration and the magnitude of extensional tectonic activity may play a chief role in the rarity of low-$\delta^{18}O$ magmas. Balsey and Gregory (1998), proposed that the solubility of water in high-silica magmas and its profound effect on the solidus are key aspects to understanding why low-$\delta^{18}O$ magmas are rare. Direct influx of meteoric water into the magma is also another mechanism that was proposed to have resulted in the ^{18}O depletion at the Yellowstone Timber Mt. Caldera Complex, (Hildreth et al., 1984; Lipman and Friedman, 1975; Taylor, 1986). Low-$\delta^{18}O$ magmas contain oxygen that was derived from surface waters, and Hamilton (1994), suggested that in high latitudes, the generation of low-oxygen isotope magmas may be enhanced by the presence of surface water with low-$\delta^{18}O$ values. In this context, glaciers could contribute extremely negative meteoric waters ($\delta^{18}O$ <-25‰) to pre-caldera hydrothermal systems, which then introduce a depletion of oxygen isotopes in country rocks in the vicinity of the magma chamber.

Subduction zone settings do not apparently yield low-$\delta^{18}O$ magmas. Normally, low-$\delta^{18}O$ values characterize caldera systems and rift zones that involve shallow crustal recycling of rocks that have interacted with meteoric waters at elevated temperatures. Bindeman et al. (2010), strongly believed that there are more low-$\delta^{18}O$ magmas than documented, they further outlined that these magmas are often underrepresented in recent geologic record due to their being of shallow genesis, which puts them in high chances of getting eroded away. Common examples of well-known low-$\delta^{18}O$ magmas include the Yellowstone rhyolites, Iceland basalts, and the Koegel Fontein granites/gneisses. Table 1 gives examples of the documented low-$\delta^{18}O$ magmas from some of the world's subduction zone settings.

Table 1: A summary of some examples of low-$\delta^{18}O$ magmas from subduction zone settings around the world.

Locality	**Material analysed**	**$\delta^{18}O$ Values**	**Publication**
Kamchatcka	Ignimbrites	4.0-5.0‰	Bindeman et al., 2004
Aleutians	Andesites, dacites	4.4-4.9‰	Bindeman et al., 2001
Calabozos	Andesitic tuffs	5.0-6.3‰	Grunder, 1987
Banda arc	Biotite, garnet and olivine	4.86-5.10‰	Vroon et al., 2000
Yusin pluton	Zircons	4.1-5.1‰	Suzuki et al., 2015
Casto pluton	Granites	2.7-5.4‰	Criss et al., 1984
Kermadic arc	Pyroxenes	5.23-5.39‰	Macpherson et al., 1998

The Central Andes is one of the best examples on Earth of a continental margin volcanic arc. Along the margin, a diverse geochemical composition of erupted magmas can be spatially and temporally distinguished in terms of their tectonic setting and crustal composition. In this regard, numerous geochemical and petrological studies (e.g. James and Sacks, 1999; Beck and Zandt, 2002; Yuan et al., 2002; McGlashan et al., 2008) have shown that primary mantle-derived melts passing through the 50-70 km tectonically thickened Andean crust are to a great extent modified by crustal level processes such as fractional crystallization, magma mixing and crustal assimilation (Kay et al., 1991, 1999; Wörner et al., 1992). In view of these findings, this study aims to understand why there have not been any discoveries of low-$\delta^{18}O$ magmas in the Central Andes or in the Andes as a whole, except for the Calabozos complex in the Southern Andes (Grunder, 1987).

Similar to this current study is the one that Feeley and Sharp (1995) conducted for Volcàn Ollagüe, where they recorded $\delta^{18}O$ variation values ranging from 7.1-8.1‰ for the basaltic andesite and dacitic lavas. They found that the $\delta^{18}O$ values for basaltic andesite lavas were lower than those of dacitic lavas and explained this variation through a two-staged process called the 'intracrustal contamination model'. The model explained the first stage to be associated with the assimilation of significant amounts of high-$^{18}O/^{16}O$ lower continental crust with the parental basalt and basaltic andesite magmas, and the andesitic and dacitic magmas melting and assimilating low-$^{18}O/^{16}O$ hydrothermally altered wall rocks during differentiation in shallow crustal magma chambers in the second stage. Their study concluded that this model could be applicable to the explanation of the relative scarcity of low-$\delta^{18}O$ magmas at Volcàn Ollagüe.

The Central Volcanic Zone of the Central Andes, is in a zone of active subduction and has quite a magnificent exposure of the volcanic material. There is a clearly defined sequence of igneous activity in the last 12 Ma, with the oldest being the eruption of large ignimbrite sheets and the youngest being the intrusion of various crystal-rich dacitic-rhyolitic domes and scattered stratovolcanoes along the active arc and the Altiplano plateau.

The features of the CVZ that make it an ideal area for this study include; its magmas that contain high crustal component, a systematic E-W compositional variation, and the 12 Ma great caldera structures (Coira et al., 1982; de Silva, 1989; de Silva and Francis, 1991; Freymuth et al., 2015; Godoy et al., 2017; Hildreth, 1981) that may have been sites of ^{18}O depletion due to hydrothermal activity.

Although this study aims to find low-$\delta^{18}O$ magmas, reasonable hypotheses to why low-$\delta^{18}O$ magmas might not be found in the area are drawn from previous studies, however, there appears not to have been a systematic search undertaken for low-$\delta^{18}O$ magmas and that could be one of the reasons why they have not been documented in the area. Other reasons for the non-recognition of low-$\delta^{18}O$ magmas in the Central Andes are that (i) it, especially the CVZ belongs to the Northern region of Chile, which is dominated by arid climate, with very little precipitation, which must reduce the possibility of hydrothermal activity (Folkes et al., 2013); (ii) Balsley and Gregory (1998) also proposed that assimilation of water-rich low-$\delta^{18}O$ material combined with fractional crystallization would drive magmas to water oversaturation, such magmas would either erupt explosively or quench beneath the surface before the magma $\delta^{18}O$

value lowers significantly; and (iii) insufficient heat input to melt or assimilate enough hydrothermally altered material to produce low-$\delta^{18}O$ magmas (Bindeman, 2008).

The objectives of the study are to:

- Measure $\delta^{18}O$ values in a wide variety of bulk rock samples and separated quartz phenocrysts to identify low-$\delta^{18}O$ rocks from whole rock analyses and low-$\delta^{18}O$ magmas from the quartz phenocrysts;
- Construct a map of $\delta^{18}O$ variation and transect of the CVZ whole rocks;
- Focus special attention on any volcano of rock unit where low-$\delta^{18}O$ values are found in any of the material analysed;
- Address the possible reasons why low-$\delta^{18}O$ magmas have not been found in the Central Andes;
- Construct models for the magmatic evolution of the CVZ felsic magmas using O-isotopes and existing data.

CHAPTER 2

Review Of Literature

2.1. Geological Setting

The Andean volcanic chain (Figure 2.1) is a major volcanic chain along the Andean Cordillera running through Argentina, Bolivia, Chile, Colombia, Equador and Peru.

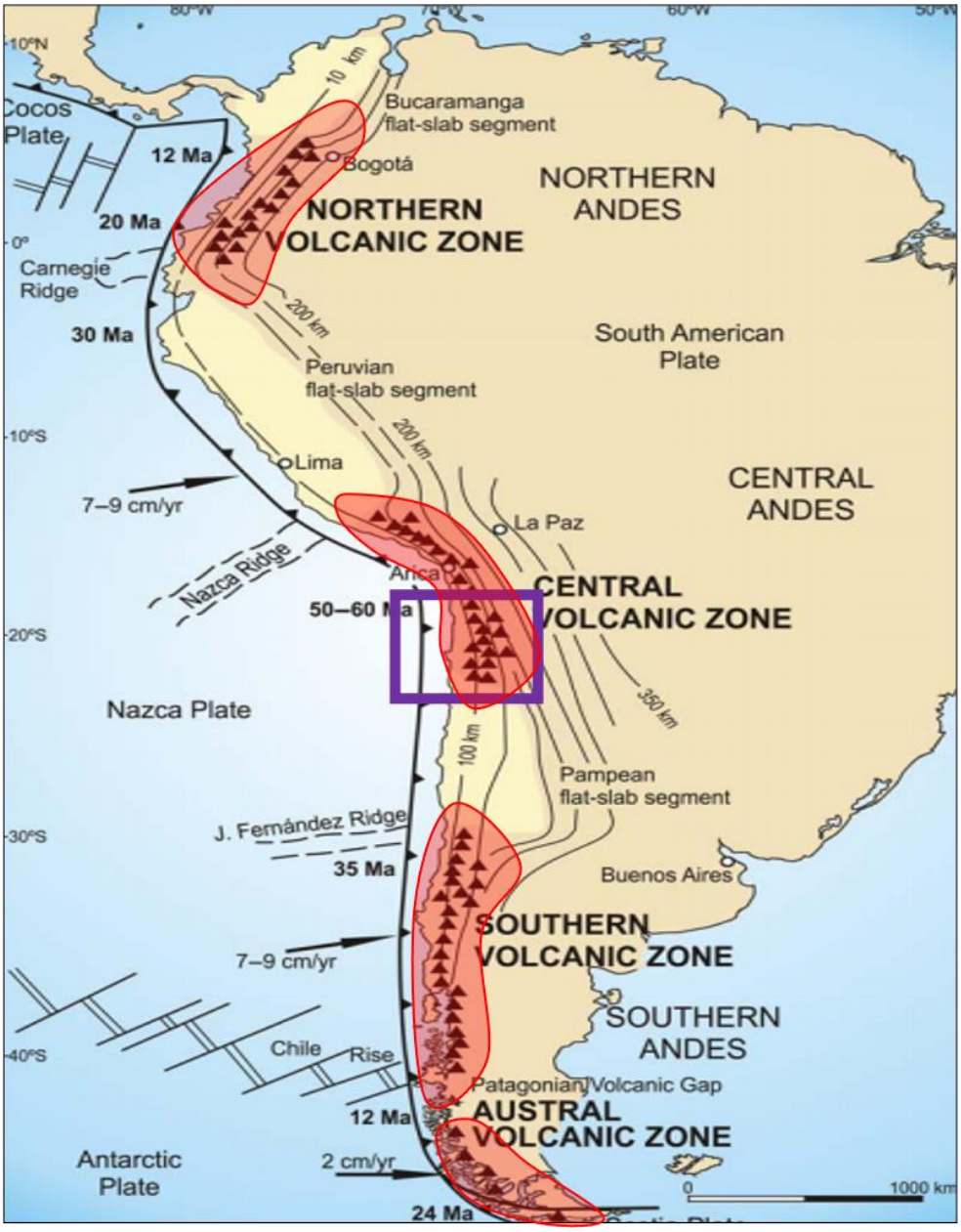

Figure 2.1: Map of South America showing the Andean Volcanic Belt and its four volcanically active segments (highlighted), and the study area demarcated by the square (Stern, 2004).

This volcanic chain was formed as a result of subduction of the Nacza plate and Antarctic plate underneath the South American plate. Four main volcanic zones are identified in this chain and are separated by volcanic gaps. The volcanoes in this chain are diverse in terms of activity style, products and morphology. Some differences can be explained by which volcanic zone a volcano belongs to; however, there are differences within volcanic zones and their neighbouring volcanoes. The Andean Chain is a typical calc-alkaline and subduction volcanism location with a broad range of volcano-tectonic settings (de Silva and Francis, 1991; Ort, 1993; Stern, 2004). The focus of this study is in the Central Volcanic Zone of the Andean chain.

2.1.1. The Central Volcanic Zone (CVZ)

The CVZ (Figure 2.2) extends from 16°S-28°S including southern Peru, northern Chile and adjacent parts of Bolivia and Argentina (Grunder, 1987). This zone is characterized by an exceptionally thick continental crust of about 70 km and large number of active volcanoes. The crust below the Altiplano of the CVZ reaches a maximum thickness of about 75 km in the vicinity of the Arica bend.

The history of the Nacza plate subduction and arc evolution is displayed by the geology of the area along the western margin of central South America during the past 200 Ma (Allmendinger et al., 1997; Beck et al., 1996; Michelfelder et al., 2013). Submarine early Jurassic andesitic volcanoes and sediments are the earliest products of this magmatic cycle and are found near the coast. These are overlain by Mesozoic igneous and marine sedimentary units that are covered by continental sediments, intruded by younger plutonic rocks and capped by a thin veneer of Miocene to Recent volcanics (Wörner et al., 1998). A simplified geological map of the Central Andes is shown in Figure 2.3.

Within the CVZ, there are forty-four major and eighteen minor volcanic centres that are considered active (Figure 2.2). It consists of not less than six potentially active massive silicic volcanic systems, which include those of the Altiplano Puna Volcanic Complex (Cerro Panizos, Pastos Grandes, Cerro Guacha and La Panaca), other silicic systems are Los Frailes ignimbrite plateau in Bolivia (~319 km from the APVC) and the caldera complexes of Incapillo and Cerro Galan in Argentina, which are located ~318 km from the APVC. Four main phases of activity are identified during the eastward migration of the volcanic front. The first phase was the Jurassic to upper Cretaceous arc with effusive products that mainly erupted in the coastal range of Chile; the second phase was the mid-Cretaceous arc of the longitudinal valley and Sierra de Moreno in Chile; the late Cretaceous-paleogene arc after the flat slab subduction

and lastly, the Miocene-Holocene active arc eruptive products located in the Western Cordillera, which is related to steepening of the Nacza plate below the South American plate (Francis et al., 1991; Scheuber and Giese, 1999; Coira et al., 1982).

Figure 2.2. Sketch map of the Central Andes showing the distribution of Quaternary arc volcanoes, major salars and the approximate outcrop extent of Neogene ignimbrites with known calderas (Schilling et al., 2006).

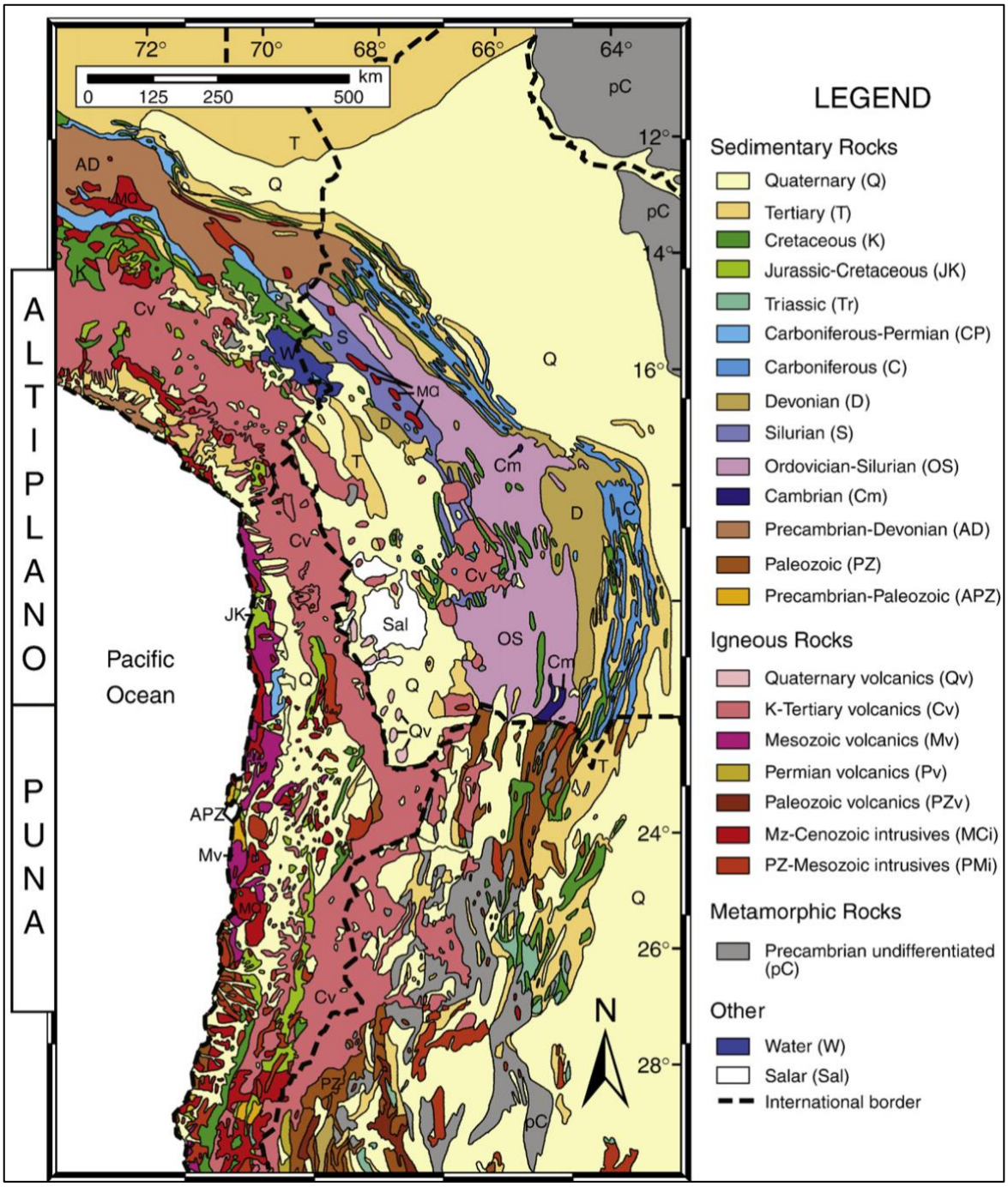

Figure 2.3: A simplified geological map of the Central Andes, showing principal geomorphogical units, locations of main Mesozoic and Early Cenozoic intrusions, and Neogene volcanism (Barnes and Ehlers, 2009).

Volcanism and tectonic setting in the CVZ

Known for its high elevations (~4-6 km above sea level), the Central Andes has been divided into two segments by de Silva and Francis (1991). The first segment (forearc) is oriented northwest-southwest in southern Peru and the other (backarc) oriented north-south in northern Chile; and further divided into eight north-trending trench-parallel structure belts from west to east across the orogeny, defining the changes in structure, distribution of magmatism, and geomorphology around the area. These separate segments are based on the separation of volcanic centres along and behind the volcanic front (Wood et al.,1987).

The forearc consists of the Coastal Cordillera, Longitudinal Valley, and the Pre-Cordillera (Wörner et al., 1992). The predominant rock units in this arc range from the Mesozoic to Paleogene and decrease in age eastwards. This marks the migration of the Andean arc since the Jurassic to its location in the Western Cordillera from the Late Miocene to Recent. Upper Miocene to Recent stratovolcanoes in the Western Cordillera comprise a nearly continuous volcanic zone aligned N-S containing almost 1100 active volcanoes (de Silva and Francis, 1991). The backarc is defined by four structural belts; the Altiplano-Puna, Eastern Cordillera, Inter-Andean Zone, and the Chaco Plain. The Altiplano-Puna is a high plateau sitting at a mean elevation of 4 km; the Eastern Cordillera mountain belt is dominated by folding and thrusting of Palaeozoic to Cenozoic rocks.

Since the late Oligocene, Palaeozoic to Cenozoic sediments accumulated in the backarc and have undergone compressional deformation with doubling of the continental crust as a result of contraction and compression, leading to thrusting of the Andean orogen over the foreland (Isacks, 1988; Lamb and Hoke, 1997). Figure 2.4 shows the crustal profile of the Central Andes with its major tectonic segments.

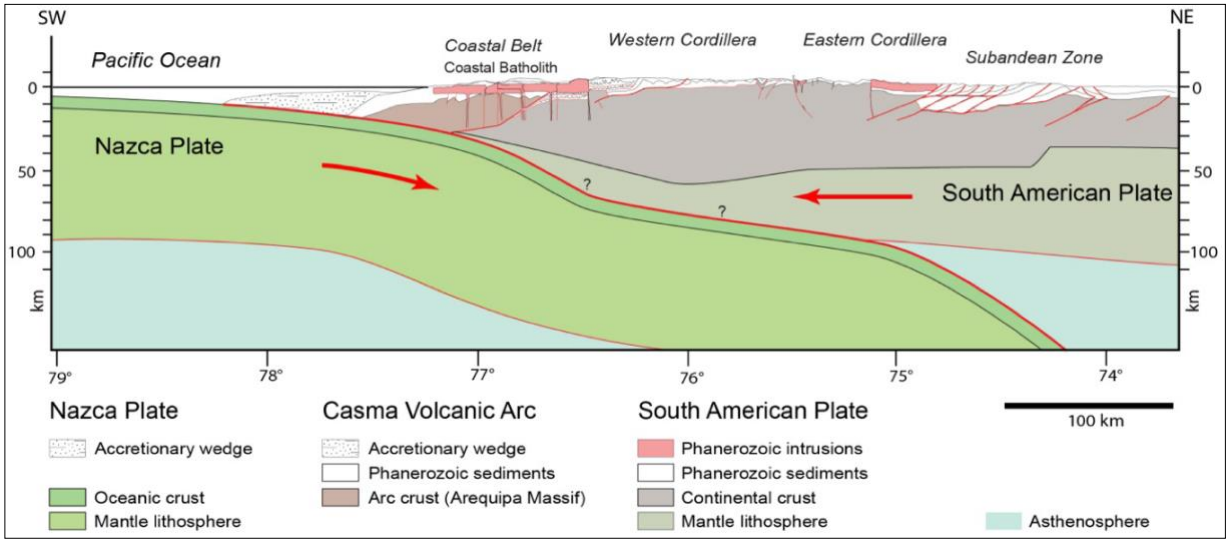

Figure 2.4: A general cross-section showing the geometry of the plate boundary in the subduction zone and the crustal structure of the Andes, with its major tectonic segments (Tassara et al., 2006).

The active volcanoes in the CVZ overlie volcanic rocks of late Oligocene to Quaternary age, including large ignimbrite sheets, stratovolcanoes and caldera systems (Mpodozis and Ramos, 2008; de Silva, 1989; Lindsay et al., 2001). Many of these volcanic centres (Figure 2.5) are extremely well preserved due to the hyper-arid conditions prevalent in the region. Based on the concentrations of the older centres, de Silva and Francis (1991) suggested that the onset volcanism in the CVZ was earlier in the south and more recent northwards. At the other end of the compositional spectrum, the Central Andes contains one of the largest ignimbrite provinces on Earth (de Silva and Kay 2018). Monotonous or crystal-rich dacites to rhyolites of Miocene age contain individual flows of thousands of cubic kilometres, de Silva and Kay (2018) proposed that these "ignimbrite flare-ups" are related to increased mantle input and to a zone of anomalously low seismic velocities in the middle crust of the southern Central Andes (Ward et al., 2014).

Below the CVZ, the <60 Ma Nacza plate is being subducted at 7-9cm/year (Geise et al., 1999), in a direction that varies from 20°-24° southeast orthogonal with the trench below the northern part of the CVZ in southern Peru to 27 degrees northeast of Chile. The subduction slab descends at a dip of 25° to a depth of >400 km. The volcanic front is located in the Western Cordillera, at about 120 km above the subducted slab and 240-300 km east of the trench, which reaches a maximum depth of 8055 m above sea level at 23°.

Crustal thickness below the CVZ reach about 70 km and basement ages that range from as old as ~2000 Ma below the northern portion of the segment in Peru and northern Chile as well as Bolivia to late Precambrian and Palaeozoic below northern Chile and Argentina. The northern end of the CVZ coincides with the locus of subduction of the Nacza ridge and the Abancay deflection (Davidson et al., 1990; Lindsay et al., 2001; Schmitt et al., 2002).

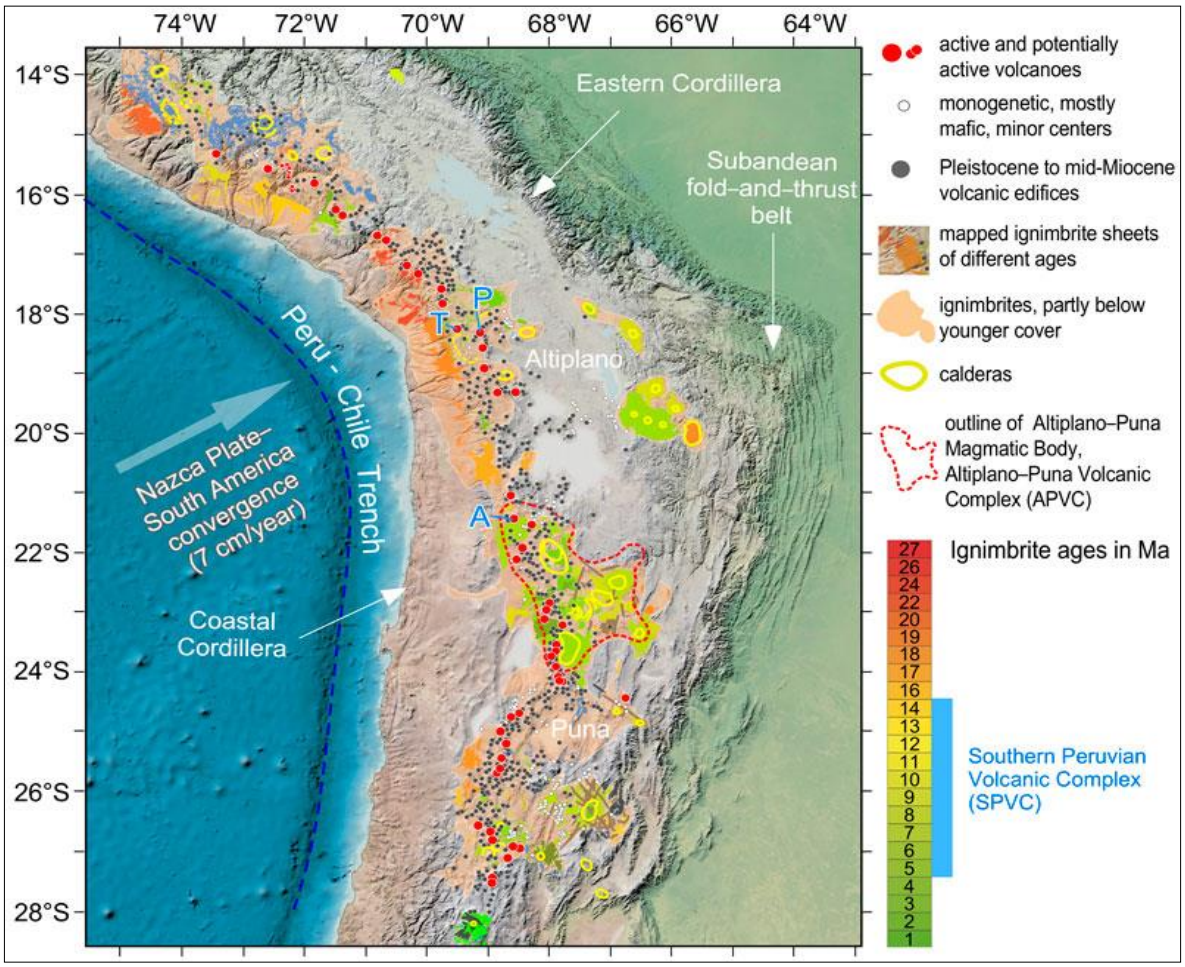

Figure 2.5: Distribution of stratovolcanoes (Miocene to Holocene) and monogenetic volcanic centres (Pliocene to Holocene) in the Central Andes; large-volume ignimbrites are also shown and color-coded according to age; caldera structures are outlined in yellow as well as the location of the mid-crustal Altiplano-Puna Magma Body represented in a red dashed line (Freymuth et al., 2015; Wörner et al., 2018).

Magma genesis and evolution in the CVZ

There is a systematic evolution of magma compositions in the CVZ through space and time. The volcanic front has migrated eastwards and magma compositions have become more enriched in both incompatible trace element and isotopic properties since the Jurassic era (Davidson et al., 1990). A study by Taylor and McLennan (1985) revealed that the andesites in the CVZ are compositionally similar to estimates for the composition of an average continental crust, presenting a reliable mantle-to-crust compositional ratios. Andesites, dacites and rhyolites are the dominant lithologies in the CVZ, although basaltic andesites and occasional basalts also occur.

CVZ magmas have elevated bulk rock $^{87}Sr/^{86}Sr$ and $\delta^{18}O$ and lower $^{143}Nd/^{144}Nd$ ratios as compared to the SVZ of the Andean volcanic belt (James, 1982; Davidson et al., 1990). These data imply that greater amounts of continental crust have been incorporated in the CVZ than in the SVZ magmas. Correlated variations of strontium, neodymium and oxygen isotopes with increasing silica content and regional correlations of lead isotopic compositions and Andean age indicate that an essential part of the process of crustal contamination in the CVZ magmas occurred through intra-crustal assimilation coupled with crystallization of these magma, which is combined with anatexis (Francis et al., 1984; Wörner et al., 1992, 1994; Hawkesworth et al., 1982; Davidson and de Silva, 1995).

The volcanoes in the CVZ belong to a north-northwest trending belt of late Cenozoic calc-alkalic and alkali volcanic rocks, this is a consistent chain of evenly spaced volcanoes from 16˚ to 22˚S making up the northern segment of the CVZ, while the southern segment between 22˚ and 28˚ S moves farther east and becomes wider and more irregular (Wörner et al., 1992). The crust beneath the Western Cordillera exceeds a thickness of 70 km and decreases towards the eastern-most margin to ~60 km (James, 1971). At 25˚S, the late Cenozoic chain is roughly 100-150 km wide and overlies a 150,000 km^2 Tertiary rhyolitic to dacitic ignimbrite plateau. The upper crust beneath the volcanic front consists of Palaeozoic and Mesozoic rocks, with early Cenozoic volcanic rocks to the west. West of the Andean Cordillera are exposed Palaeozoic granitoids and siliceous volcanic rocks. The Jurassic and Cretaceous marine and continental sedimentary and volcanic rocks are situated on each side of the Palaeozoic rocks (Naranjo, 1992). Geophysical studies suggest that the upper 20 km of crust is composed of granitic and intermediate composition plutonic rocks comagmatic with the late Cenozoic rocks. The lower 40-50 km terrane is likely composed of amphibolite or more siliceous anhydrous metamorphic

rocks, pyroxene gneisses, and gabbros (Feeley and Hacker, 1995; Schmitz et al., 1999). Published K-Ar dates suggest that late Cenozoic volcanic activity initiated during the Miocene and is characterized by two episodes based on composition and style; with the first episode defined by large scale regionally extensive rhyolite to dacite ignimbrite volcanism beginning ~23 Ma, and the second episode overlapping in time and represented by eruptions of basaltic andesite to dacite lavas ranging from 23 Ma to present (Baker and Francis, 1978). This group, confined to the Western Cordillera, comprise of large stratovolcanoes and is not as regionally extensive. Baker and Francis (1978) described the CVZ volcanic stratigraphy as an indication that volcanic activity was dominated by early eruptions of silicic material, and that a greater proportion of mafic relative to felsic material has been erupted over time.

Geophysical investigations interpret the crustal structure having been altered by partial melting. Temporal variations of these magmas show that the extent of crustal contamination of these magmas increased through time, from pre-Miocene to Recent Miocene as the crust has thickened to about >70 km (Schmitz et al., 1997; Rogers and Hawkesworth, 1989).

2.1.2. The Altiplano-Puna Volcanic Complex (APVC)

The Altiplano-Puna volcanic complex (APVC) is a major Andean volcano-tectonic province that has developed between 21° and 24°S (Olivier, 1967; de Silva, 1989). In the context of this project, it is important to consider the evolution and development of the Altiplano-Puna Volcanic Complex, where the main area of interest of this study (SPLVC) is found. The APVC (Figure 2.6) is located at about 100-250 km above the Benioff zone of the Nacza plate, and at the southward transition between the Altiplano Plateau and the Puna (Allmendinger et al., 1997).

The evolution of the APVC began with episodic ignimbrite flare-ups, with steady-state and waning stages identified between each flare-up. Stratovolcanoes were produced with these stages. The evolution then shifts to more mafic eruptions occurring during the steady-state and waning stages. During the waning stages, eruptions as young as (<0.2 Ma) took place, corresponding to monogenetic scoria cones such as Cerro Overro and La Poruña. Lava flow complexes (San Pedro, Lascar) are also products of the waning stage. The eruption of the young silicic domes appears to have been triggered by some of the young mafic magmas, as attested by the widespread presence of mafic enclaves found in the rocks of the silicic domes intruding the SPLVC. This in turn becomes a clear indication that mafic magmas were high in volume to have been able to transfer a significant amount of heat to the highly viscose magma

chambers, thereby allowing the mobilization and eruption of the dacite/rhyodacitic domes (de Silva, 1989; de Silva et al., 1994; Burns et al., 2015; Tierney et al., 2016; Godoy et al., 2017).

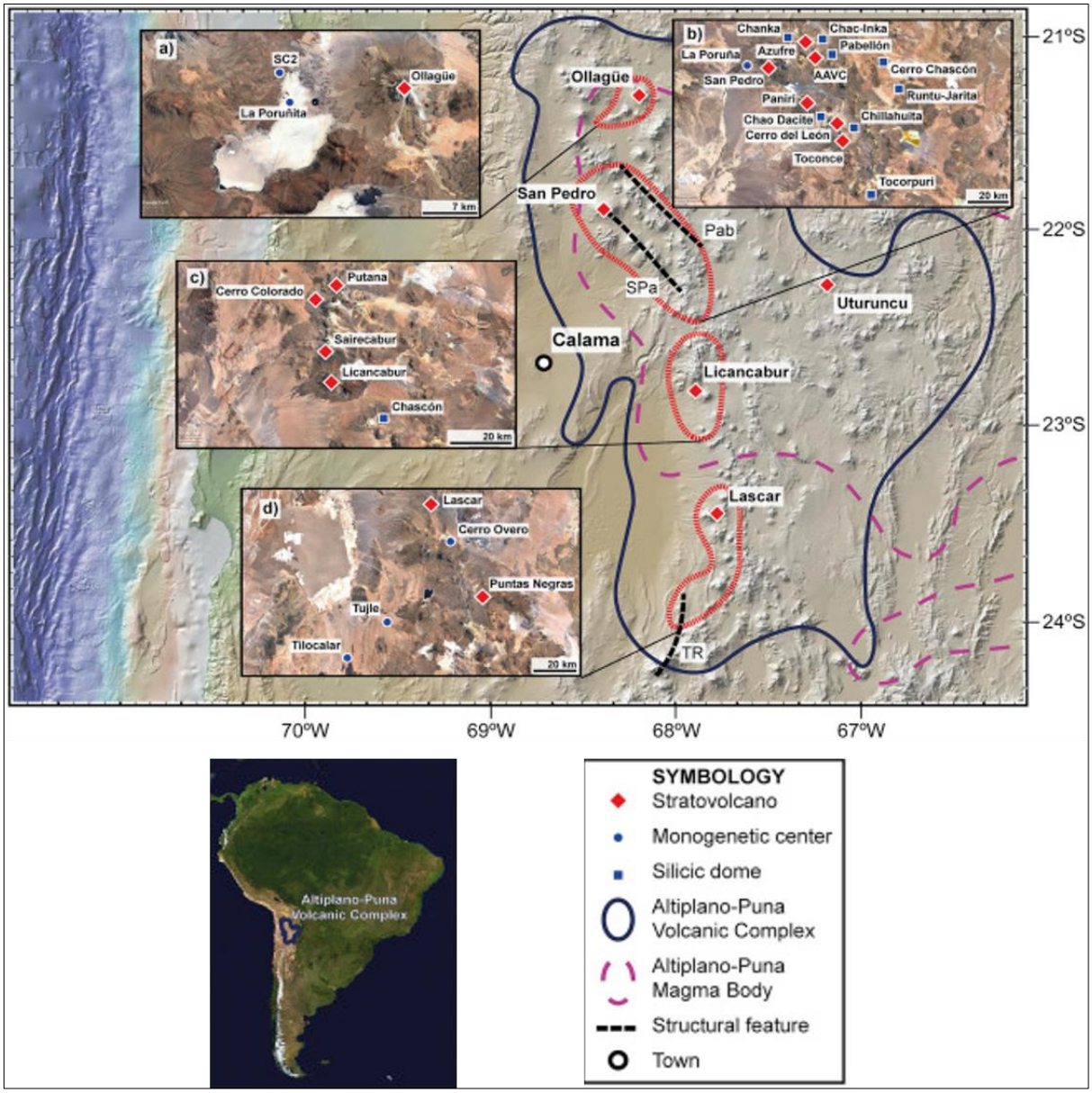

Figure 2.6: Satellite image showing the coverage of the APVC (black circle), the APMB in purple dotted lines. The inserts show the distribution of the monogenetic centres, main stratovolcanoes, domes and mafic flows; which some were sampled in this project (Godoy et al., 2019 after de Silva, 1989 and Zandt et al., 2003)

The Southern Puna and Altiplano host mafic rocks associated with strike-slip faults and normal faults. Andesites erupted after about 7 Ma in the Southern Puna, with the least evolved magmas being the 6.7 Ma Cerro Morado and 8-7 Ma Rachaite complex flows. In the Southern Altiplano, basaltic on top of shoshonitic to andesitic (post-Miocene) lavas are found (Kay et al., 2010).

Repeated ignimbrite eruptions are the main element in the development of the APVC. Four pulses of major ignimbritic eruptions are identified, which signify a high influx of mantle-derived magmas. A new phase magmatism was recognized as being late Quaternary (< 0.2 Ma), this phase is defined by silicic dome eruptions, which are dacitic and rhyolitic in composition, with high crystal content (50%) (Godoy et al., 2019). Dacitic ignimbrites underlie the SPLVC.

Since the Miocene, the evolution of the Altiplano-Puna Volcanic Complex within which the SPLVC erupted, has been driven by cyclic arc magmatic stages. The ignimbrites of the SPVC are believed to have been deposited during the eruptions of the APVC volcanoes, and the deposition of these ignimbrites to have been influenced by the so called "boiling over" eruptions. These eruptions were from magma chambers that housed viscous, crystal-rich and volatile-poor magmas, erupted in a non-explosive manner; which is evident through the massive, homogeneous and minor fluidization nature of ignimbrite deposits (Kay et al., 2010).

Below depths of about 20 kilometres, a low velocity zone called the Altiplano-Puna Magma Body (APMB) is proposed to exist (Figure 2.6). Seismic data is consistent with the presence of melts in this layer. This zone represents the world's largest known zone of partial melting, with a volume of about 500 000 km^3 and has been interpreted as a batholith-like body (de Silva and Gosnold, 2007), corresponding to a zone of melting, assimilation, storage and homogenization at upper crustal levels. The repeated eruptions of ignimbrite sheets followed by the eruption of young (<100 ky) rhyodacitic domes are the most prominent features expressing the influence of the Altiplano-Puna Magma Body on the APVC.

An extensive low-density area beneath the APVC (around Uturuncu volcano), and partial melting have been reported in the studies of Ward et al. (2014); Götze and Krause (2002). The influence of this magma body on the magmatic evolution of the SPLVC has been revealed by geophysical studies, where S-wave velocities indicate an increase in melt/ fluid percentage from the margin to the centre of the partially molten body (Ward et al., 2014). Petrographically, mafic magmatism in the Altiplano-Puna Volcanic Complex shows textural disequilibria and skeletal morphologies of olivine crystals, latter is related to the fast ascent and cooling of mafic magmas facilitated by structural and crustal weakness in the APVC region (Mattioli et al., 2006; van Alderwerelt, 2017; González-Maurel et al., 2019).

Evidence of crustal assimilation with the partially melted AMPB, facilitated by magma mixing or mingling has been observed in almost all the mafic products erupted in the APVC, the textural properties of these mafic products represent a more differentiated magma source (Godoy et al., 2019). Quartz xenocrysts found in the rocks of this region indicate basement material incorporated into magmas erupted from the monogenetic centres (Ortega, 2008). The effect of the APMB is furthermore seen on the lava flows that have rimming and banding mineralogical phases of inter alia, clinopyroxene-hornblende and plagioclase-biotite.

These features are associated with thermal and chemical disequilibria between two compositionally distinct magmas mingling with each other (O'Callaghan and Francis, 1986; González-Maurel et al., 2019; Taussi et al., 2019). Burns et al. (2015), Godoy et al. (2017), de Silva and Kay (2018), González-Maurel et al. (2019) and Taussi et al. (2019) have recognized that the abovementioned interaction processes are all influenced if not directly driven by the presence of the Altiplano-Puna Magma Body, which is an important feature when defining the magmatic evolution of the Altiplano-Puna Volcanic Complex, within which the San Pedro-Linzor Volcanic Chain (main area of interest for this study) is located.

2.1.3. The San Pedro-Linzor Volcanic Chain (SPLVC)

The SPLVC (Figure 2.7) is a 65 km long linear chain of volcanoes, it is part of the Plio-Pleistocene evolution of the Central Andean magmatic arc (Godoy et al., 2015). It strikes at an angle to the general N-S direction of the Central Andes' active front and crosses the western margin of the surficial projection of the upper crustal Altiplano-Puna Magma Body (APMB). The San Pedro-Linzor Volcanic Chain form a NW-SE trending lineament of stratovolcanoes between 21°53'S/ 68° 23´W and 22°09'S/ 67°58'W. These stratovolcanoes erupted in the NW margin of the Altiplano-Puna Volcanic Chain (APVC) and cross the western border of the APMB. It includes a series of large and partly complex volcanic edifices such as the San Pablo volcanic complex, Panini, Cerro de Leon, Toconce and Linzor volcanoes.

The SPLVC consists of lava, pyroclastic and scoria flows as well as breccias. Petrographically, the lava flows from these volcanoes vary from basaltic-andesite to hornblende-dacite with pyroxene and andesites as main lithologies. Pyroclastic flows are dacitic, while scoria flows and breccias vary from basaltic-andesite to andesite.

The Chillahuita and the Chao dacite dome are great parts of the chain, as well as the La Poruña basaltic-andesite cone, which is the source of an 8 km long lava flow located at the far north-western part of the chain. Underlying the SPLVC is the dacitic ignimbrite, which is 8.3 Ma and the volcaniclastics of the 6.5-5.6 Ma Toconce formation (Ramirez and Huete, 1981; Laznaco et al., 2012; Lopez, 2014; de Silva, 2015; O'Collaghan and Francis, 1986).

Magmatic evolution in the SPLVC shows a south-eastward increase of $^{87}Sr/^{86}Sr$ with decreasing Sr concentration. This observation reflects increasing proportions of assimilated crustal rocks in magmas together with higher degrees of low-pressure differentiation (Davidson et al., 1990; Mamani et al., 2010). The apparent absence of a deep-crustal geochemical signature for lavas from SPLVC suggests that magma genesis is dominated by shallow assimilation of crustal melts that are derived from the APMB; therefore, lavas erupted at this volcanic chain evolved and assimilated crustal material at shallow depths (Godoy et al., 2014; Martínez, 2014).

Over the past 2 Ma, the SPLVC has grown and evolved, it developed across the western margin of the APMB, an upper crustal, partially molten zone with decreasing proportion of crustal melts towards its margins and during the ignimbrite waning stage. During the evolution of the SPLVC, arc magmas that interacted with the lower crust prior to their ascent mixed with different proportions of this upper-crustal melt zone (APMB), and produced magmas with variable radiogenic Sr and Nd isotope compositions.

Increasing strontium isotope ratios across the margins of the APMB, and the volcanoes found outside the margins of the APMB that are less radiogenic all represent the influence that the APMB had on the magmatic evolution of the SPLVC in the last 2 Ma (Godoy et al., 2017). The formation of magmas with variable radiogenic Sr and Nd isotope compositions in the SPLVC is explained by arc magmas that interacted with the lower crust before their ascent and mixed with different proportions of the upper crustal melt zone, the so called APMB. Increasing Sr-isotope ratios of between 0.709 and 0.707 are detected in transects across the margins of the APMB reaching maximum values (0.710-0.717) in lavas of Uturuncu volcano (Figure 2.6) above the centre of this partially molten zone as suggested by Godoy et al. (2017).

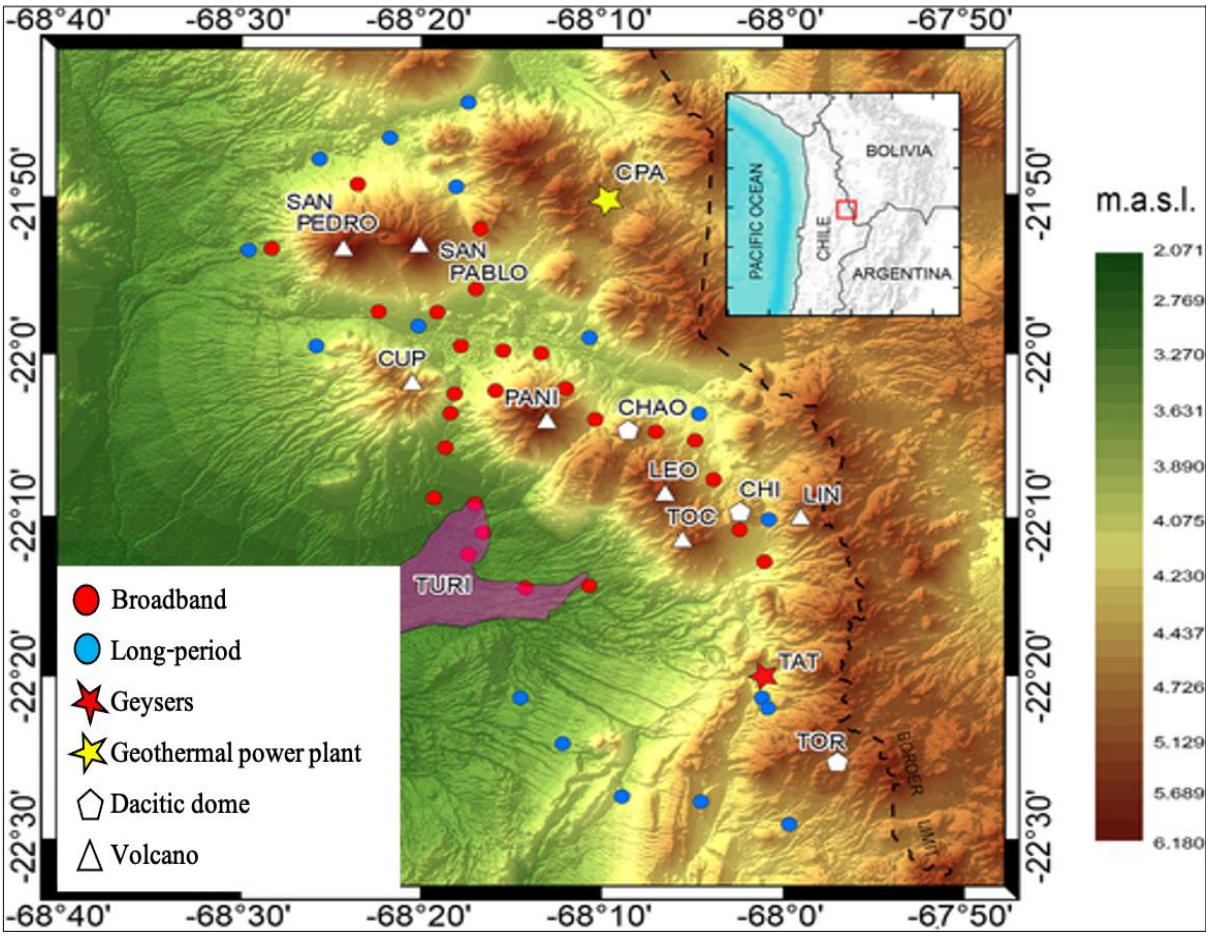

Figure 2.7: The San Pedro-Linzor Volcanic Chain and its individual volcanic edifices striking NW-SE of the Central Andes (Mancini et al., 2019).

2.2. Climatic Conditions in the CVZ

The climate of northern Chile (Figure 2.8) is extremely arid, characterized by lack of precipitation, very low humidity and absence of clouds. These arid conditions are a result of the subtropical latitudes and the presence of cold waters in the pacific (Garreaud et al., 2010). The average rainfall in northern Chile (17°S-27°S) is about 1 mm per year, this is one of the driest regions on the planet, featuring the Atacama Desert, which is the driest desert in the world. In the Atacama desert, which has been hyperarid over many millions of years, temperatures may reach closer to 90°F during the day and drop down to freezing point at night (Placzek et al., 2009). The arid and hyper-arid climatic conditions developed in the Andes from the beginning of the Miocene and this may have decreased the rates of sediment supply to the trench and thus increased the rate of subduction erosion of the continental margin (Stern, 2004).

According to Houston and Hartley (2003), the hyperaridity in Northern Chile is due to a combination of the extreme rain shadow created by the high Andes and Altiplano, which excludes moisture from the Amazon Basin; a strong temperature inversion along the Pacific coast, which effectively blocks Pacific moisture at an elevation of 1000 m along the western flank of the Coastal Cordillera; and lastly, the northern limit of the southern Westerlies. Over millions of years, the rain shadow created by the high Andes and the Altiplano plateau was primarily responsible for the prolonged aridity of the Atacama Desert. Andean elevation of at least 2000 m is considered high enough to exclude much of the moisture originating in the Amazon Basin from the Atacama (e.g., Masek et al., 1994; Rech et al., 2006).

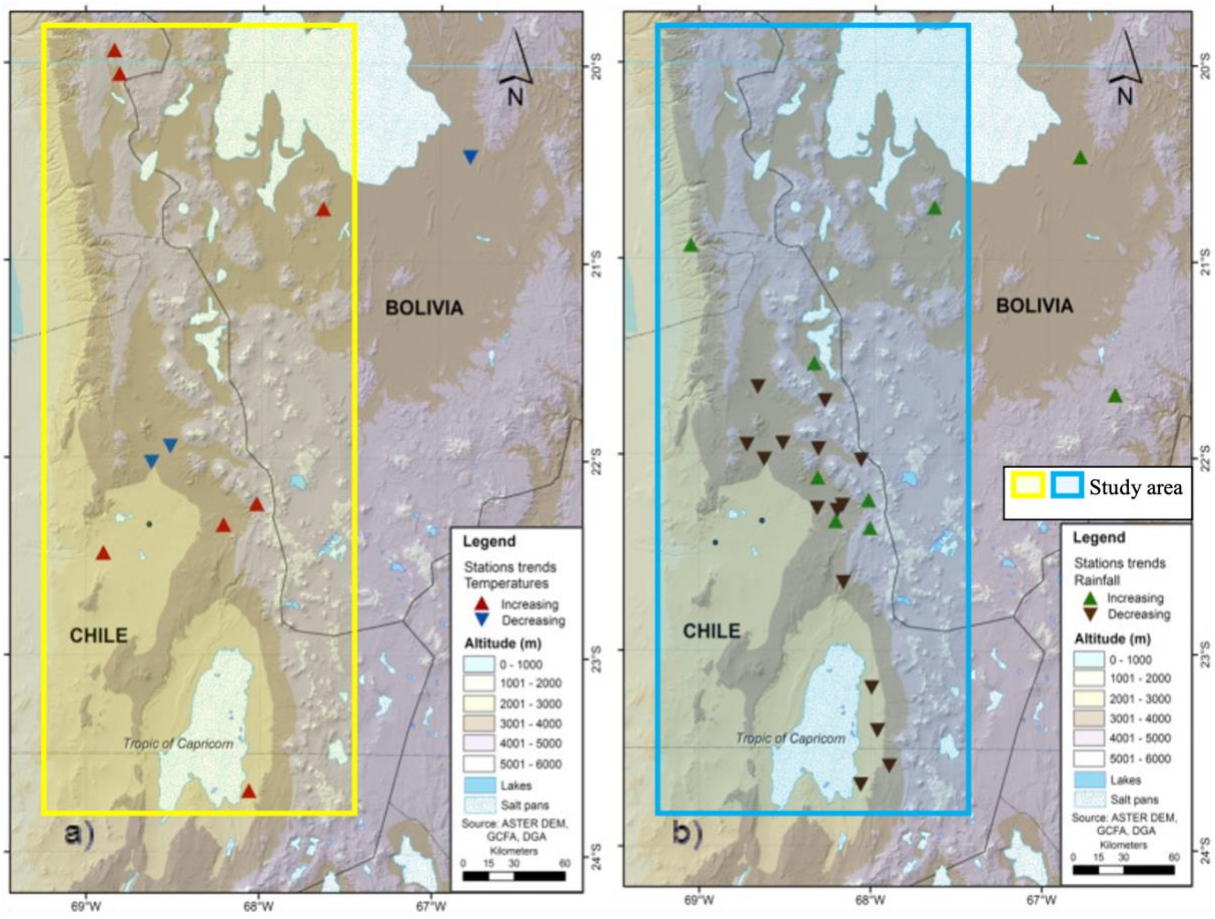

Figure 2.8: Trends in a) temperatures and b) rainfall in the Central Andes over 3 decades (1980-2010), showing increasing temperatures and decreasing rainfall (Adapted from Bennett et al., 2016)

2.3. Volcanism at Convergent Plate Margins

Subduction zones are the principal sites for the production of new continental crust through the production of arc magmas (Vroon et al., 2001). Converging plates can be oceanic, continental or one of each (Figure 2.9). If they are both continental, they will smash together and form a mountain range; if one is oceanic, it will subduct beneath the continental plate and create a volcano. The subducting plate heats up as it sinks into the mantle and introduce a degree of melting, water is also mixed with the overlying sediments and as these sediments subduct, the water rises into the overlying mantle material and lowers the melting point. Melting of the mantle above the subducting plate creates a volcano within an island or oceanic arc (Tackley, 2000; Conrad et al., 2004).

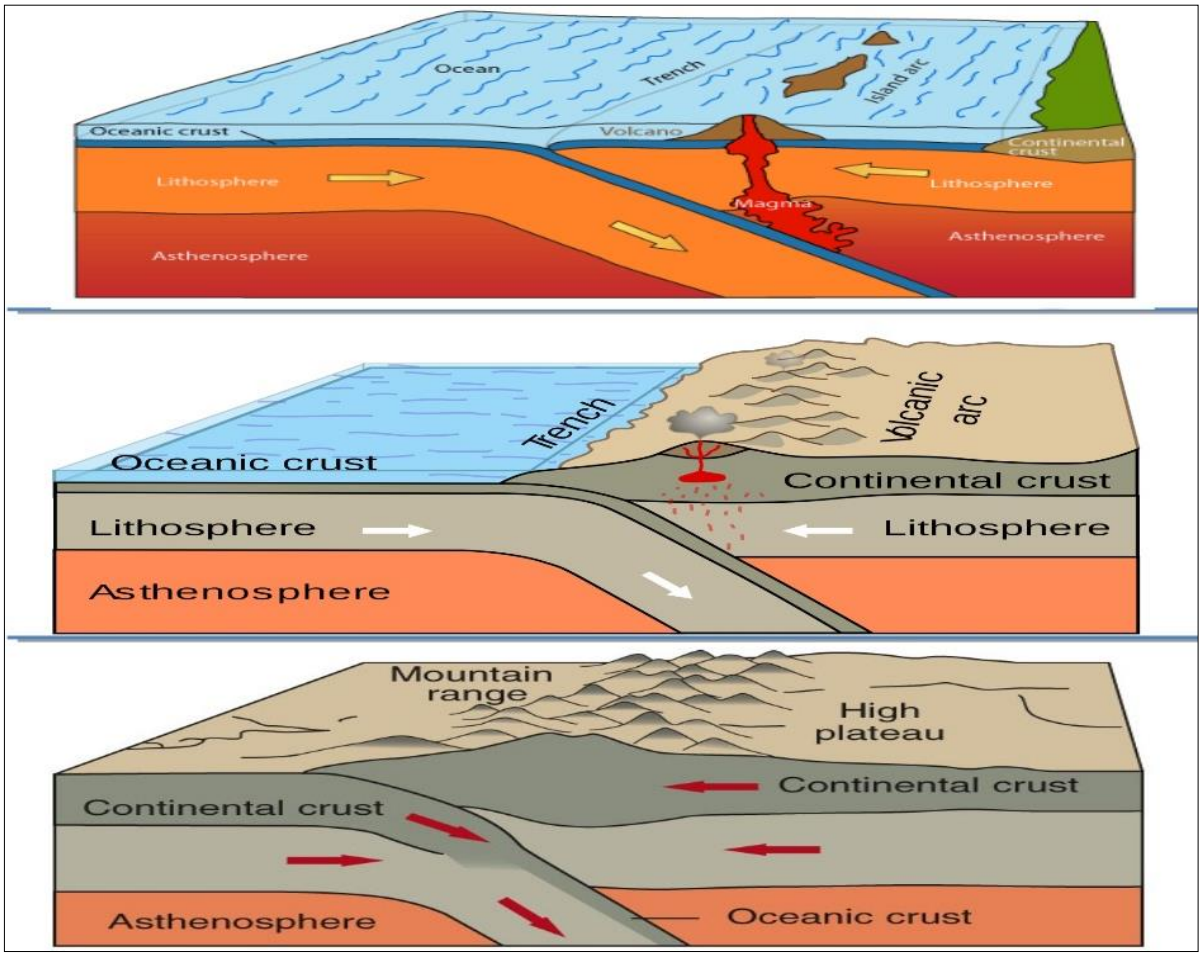

Figure 2.9: Schematic representation of subduction volcanism and its three mechanisms of convergence with the resultant topography (Tackley, 2000).

Volcanoes at destructive boundaries all lie along the Pacific Ocean basin, primarily at the edges of the pacific, Cocos and Nacza plates, between all subduction zones, trenches are found (Sigurdson et al., 2015). Subducting components such as sediments, oceanic crust, and pre-existing crust, are key to quantifying rates of crustal growth and recycling over time. Crustal material can either be incorporated into arc magmas in the melt source region, due to the subduction of sediments/subduction erosion of the overriding lithosphere, and/or due to the assimilation of the overlying crust as arc magmas migrate towards the surface. The Andean margin has been an important site for continental crust production throughout the Cenozoic and is a type locality of an ocean-continent convergent margin (Taylor and Martinez, 2002).

Volcanics at destructive plate boundaries are believed to be derived from variable portions of partial melting of the mantle wedge in response to the addition of aqueous fluids that evolved from the subducting oceanic lithosphere; decompression-melting, in this case, the mantle upwells beneath the upper plate; direct melting of the lithosphere; and melting of the pre-existing crustal rocks within the upper plate. The relative contributions of all these processes to the overall magmatic output or arcs vary significantly; however, present day basaltic lavas in convergent margins appear to be products of hydrous melting of the mantle wedge that contains only trace, cryptic components derived from the slab (Bindeman et al., 2005).

At present times, convergent plate boundaries are the most intense areas of active magmatism above sea level. Within the volcanic arcs, the most imposing features of the landscapes are large stratovolvanoes, these are predominantly andesitic lava flows that are embedded by pyroclastic materials like dacites and rhyolites. Most of these stratovolcanoes undergo a stage where their uppermost portion collapse in a downward motion, forming caldera systems. The caldera forming mechanisms are usually associated with explosive eruptions that emit silicic pyroclastic material in massive volumes and the sudden evacuation of the underlying magma chambers are responsible for the collapse of the volcanoes to form calderas (Kent, 2016).

The most distinguishing feature of subduction-related volcanics is their generally porphyritic nature and their petrographic clusters of phenocrysts. Andesites and dacites have plagioclase, quartz, augite and may contain hornblende phenocrysts (Eiler et al., 1998). The features present in these volcanics are a result of kinetic factors during their formation such as crystal growth, whereby a zone of the crystal is precipitated and a liquid immediately surrounding the crystal becomes depleted in the components that are responsible for further growth, therefore a new composition is precipitated until diffusion has had enough time to renourish the surrounding

liquid necessary for the formation of an equilibrium composition; cycling through chemically zoned magma during cell convection; and magma mixing, which sometimes present disequilibrium mineral assemblages. Xenoliths of crustal rocks are also found in some cases, particularly in continental margin arcs, suggesting that assimilation or partial melting of the pre-existing crust can in some cases be an important process in this environment (Tatsumi et al., 1989; Vroon et al., 2001; Taylor and Martinez, 2002).

2.4. Low-$\delta^{18}O$ Magmas

It is generally believed that in most cases low-$\delta^{18}O$ magmas are related to melting or assimilation of geochemically similar, but hydrothermally altered volcanics of a previous volcanic cycle (Bindeman and Valley, 2000; Bindeman et al., 2001). These magmas have $\delta^{18}O$ values that are lower than that of mantle-derived magmas. Several factors are involved in the formation of low-$\delta^{18}O$ magmas. Magmatic factors that favour the lowering of $\delta^{18}O$ are, the position of magma chambers in shallow depths, high temperatures of assimilating magmas and extended magmatic and hydrothermal pre-history; other factors include the earlier-caldera formation, which is necessary for burying hydrothermally altered low-$\delta^{18}O$ rocks; and lastly, climatic factors, low-oxygen isotope magmas tend to be more widespread in areas where annual precipitation is high, and where the weighted mean $\delta^{18}O$ values of precipitation is low (Yurtsever and Gat, 1981).

Fresh silicic igneous rocks show a wide range in oxygen isotope ratios, which are attributed to eruption and crystallization of magmas with variable petrogenetic histories. Silicic magmas with low-$\delta^{18}O$ have been a focus for numerous studies (eg: Grunder, 1987; Bacon et al., 1989; Larson and Geist, 1995; Balsley and Gregory, 1998; Harris and Ashwal, 2001; Bindeman and Valley, 2001; Bindeman et al., 2008; Riishuus et al., 2015; Ellis et al., 2017), these magmas are examples of products of the interaction between magma and meteoric water or the upper crust that has been hydrothermally altered by meteoric water (Lipman and Friedman, 1987; Taylor, 1977; Wolff et al., 2002).

Isotope studies have been particularly helpful in identifying significant crustal and mantle reservoirs that contribute to magma diversity. These studies are well suited for clarifying the ambiguity of magma sources and contamination process. Low temperature fractionation of oxygen isotopes in the presence of water introduce unambiguous $\delta^{18}O$ for supra-crustal signatures in sedimentary rocks that form at the surface of the earth or igneous and metamorphic rocks that are hydrothermally altered.

When such rocks partially melt, the $\delta^{18}O$ signatures of these melts contrast with the restricted range of the primitive mantle (Taylor and Sheppard, 1986). Oxygen isotope data also have the potential to constrain the amounts of slab melt contributing to arc lavas and possibly even the part of the slab from which the melt was derived. All common rocks and geological fluids have similar concentrations of oxygen, making it relatively simple to relate variations in $\delta^{18}O$ of lavas to mixing ratios of isotopically distinct components in their sources. For example, most mantle-derived peridotites span a narrow range of $\delta^{18}O$ values (5.5per mil ±0.2per mil), whereas oceanic lithosphere contains several materials that are distinct from this range and from each other. Marine carbonates, weathered and hydrothermally altered lower oceanic crust all have higher $\delta^{18}O$ values than peridotites.

2.5. A Review of Some Known Low-$\delta^{18}O$ Magmas

2.5.1. The Yellowstone rhyolites

The Yellowstone Plateau is one of the largest centres of rhyolitic magmatism on Earth, with great caldera-forming eruptions that are then followed by unusual low-$\delta^{18}O$ rhyolites. Bindeman and Valley (2001), presented oxygen, petrological and geochemical data from rhyolites belonging to the 2.0 Ma history of Yellowstone. In their work, most emphasis was put on Huckleberry Ridge Tuff and Lava Creek Tuff, which are 2.0 Ma and 0.6 Ma respectively. They analysed individual quartz and sanidine phenocrysts, as well as obsidian and zircons from low-$\delta^{18}O$ lavas. The data revealed variation in $\delta^{18}O$ values from 1-2‰ (quartz); oxygen isotope disequilibria between quartz, zircon and homogeneous host glass where zircon cores and some quartz phenocrysts have higher $\delta^{18}O$ values and up to 5‰ zoning within zircons. Bindeman and Valley (2001); in view that these features are only present in low-$\delta^{18}O$ intra-caldera lavas that erupted shortly after caldera-forming eruptions, proposed that the older, hydrothermally altered, oxygen isotope depleted and chemically similar rhyolites in the subducted block were dropped closer to the magma chamber. This then caused remelting and formation of almost entirely molten stacks of low-$\delta^{18}O$ melt, which then erupted in various parts of the caldera as low-oxygen isotope lava flows (Bindeman and Valley, 2001).

Figure 2.10 shows the stage-wise model of formation and evolution of the rhyolites to low-$\delta^{18}O$ magma. In the figure, stage (i) describes the hydrothermal alteration that creates low-$\delta^{18}O$ country rocks adjacent to the magma chamber, and more alteration occurring closer to the magma at elevated temperatures; in this stage, quartz and zircons remain unaltered by hydrothermal fluids and retain their pre-caldera low-oxygen isotope signatures. In stage (ii);

caldera collapse brings about low-oxygen isotope rocks with unaltered quartz and zircon into the magma chamber, promoting an almost complete and abrupt melting; however, zircon and quartz remain as normal $\delta^{18}O$ xenocrysts in newly formed low-$\delta^{18}O$ magma stacks. Prior to eruption, these quartz and zircon xenocrysts begin to be variably exchanged with low-$\delta^{18}O$ melt, with the amount of exchange reflecting the longevity of the magma.

The final stage (iii) shows low-$\delta^{18}O$ magma erupting in different parts of the caldera (Bindeman and Valley, 2001). Further isotopic studies in the Yellowstone were also conducted recently by Loewen and Bindeman (2016); Stelten et al. (2017); and Troch et al. (2018 and 2020), who did not agree with this model.

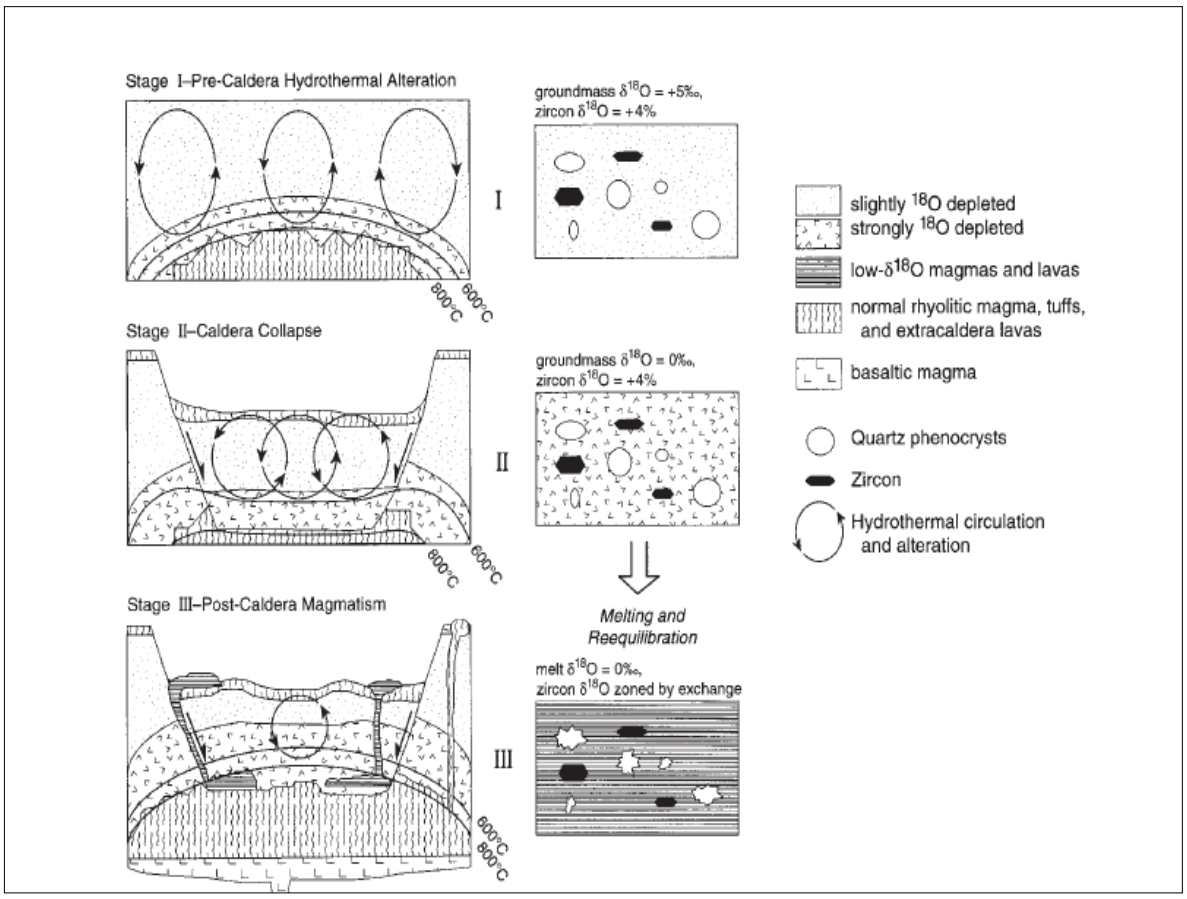

Figure 2.10: Showing the melting-caldera collapse model for the genesis of low-$\delta^{18}O$ magmas (Bindeman and Valley, 2001).

2.5.2. Iceland basalts

A study by Muehlenbachs et al. (1974), documented the low-$\delta^{18}O$ of basalts in Iceland, their findings revealed that the volcanic rocks are anomalous in their oxygen isotope content. The study found that tholeiitic and transitional alkali basalts from Iceland range from 1.8-5.7‰ and that most of the tholeiitic basalts and their phenocrysts are at least 1% lower in $\delta^{18}O$ than unaltered basalts from other oceanic islands or oceanic ridges. This study proposed that secondary alteration processes have lowered the $\delta^{18}O$ values of some Icelandic rocks, however in some cases have risen the values; which then means that surface mechanisms cannot entirely account for the distribution of oxygen isotopes in the Recent Icelandic basalts. Three mechanisms that could have played a role in bringing about low-$\delta^{18}O$ were identified in this study, these mechanisms include; (i) exchange of oxygen between magma and low-$\delta^{18}O$ hydrothermally altered rock, (ii) exchange with low-$\delta^{18}O$ meteoric water, or (iii) an exceptional low-$\delta^{18}O$ mantle under Iceland. (Muehlenbachs et al., 1974).

2.5.3. Low-$\delta^{18}O$ silicic magmas of Kamchatka

Kamchatka is a region of isotopic diversity, with high-$\delta^{18}O$ basaltic magmas and low-$\delta^{18}O$ silicic volcanism from the upper crust. In this region, one half of the hundred Holocene and Pleistocene eruptive units are low-$\delta^{18}O$ magmas (4.0-5.0‰). Most of these are voluminous, silicic ignimbrites that are associated with large 10 km^3 caldera-forming eruptions and intra-caldera lavas and domes, namely; Holocene multi-caldera Ksudach volcano, Karymsky and Kurile Lake-Iliinsky calderas, and Late Pleistocene Maly Semyachik, Akademy Nauk, and Uzon calderas (Bindeman et al., 2004; Seligman et al., 2014). A study conducted by Bindeman et al. (2004) suggested that the widespread and volumetric abundance of low-$\delta^{18}O$ magmas in Kamchatka is possibly related to a combination of near-surface volcanic processes, the effects of the last glaciation on high-latitude meteoric waters, and extensive geyser and hydrothermal systems that are matched only by Iceland.

Strontium and lead isotopic compositions of Kamchatka magmas show a negative correlation in $\delta^{18}O$ values, a similar trend observed from those in Iceland. This led to a conclusion that these magmas were largely produced by remelting of older, more radiogenic, hydrothermally altered crust that suffered a $\delta^{18}O$ depletion during a 2 Ma Pleistocene glaciation. Bindeman et al. (2004), studied intermediate to silicic rocks associated with some caldera systems, they analysed 100 units of 23 volcanic centres and found unusually low-$\delta^{18}O$ signatures (+4 to 5‰).

Such abundance of low-$\delta^{18}O$ magmas makes Kamchatka one of the largest Quaternary low-$\delta^{18}O$ volcanic areas on Earth (Bindeman et al., 2004). Recent isotopic studies in Kamchatka were also conducted (Auer et al., 2009; Seligman et al. 2014; Bindeman et al., 2019).

2.5.4. Low-$\delta^{18}O$ tephra in Aleutian Islands

Bindeman et al. (2001) presented a study on the phenocrysts in pumice clasts and ash layers of the Fisher Caldera in the Aleutians. Analyses were carried on eleven samples of Fisher tephra from eight different localities, which are representative of ash fall, welded ignimbrite and lapilli bomb beds. Low-$\delta^{18}O$ magmas contain plagioclase and clinopyroxene phenocrysts, with values ranging from 4.9±0.24‰ and 3.81±0.23‰, respectively. Other products of the eruption (dacitic and overlying basaltic-andesitic tephra, intra-caldera basaltic to andesitic lavas) were also found to have low-$\delta^{18}O$ signatures. Bindeman et al. (2001) proposed a model that describes the origin of these magmas, where normal mantle-derived basaltic magma coalesced in a large shallow pre-caldera magma chamber during the Late Wisconsin glaciation. They concluded that the lowering of magmatic $\delta^{18}O$ values must have resulted from prolonged assimilation of about ~5-10% of syn-glacial hydrothermally altered country rocks.

CHAPTER 3

Local Geology And Fieldwork

3.1. Fieldwork and Sampling

In search for low-$\delta^{18}O$ magmas, comprehensive fieldwork was conducted within the accessible vicinity of the Andean CVZ between the 15th and 24th of April 2019, following preliminary sample collection in 2017. Figure 3.1 shows the location of active volcanoes and ignimbrite sheets that were sampled, which are all within the area of interest, the SPLVC.

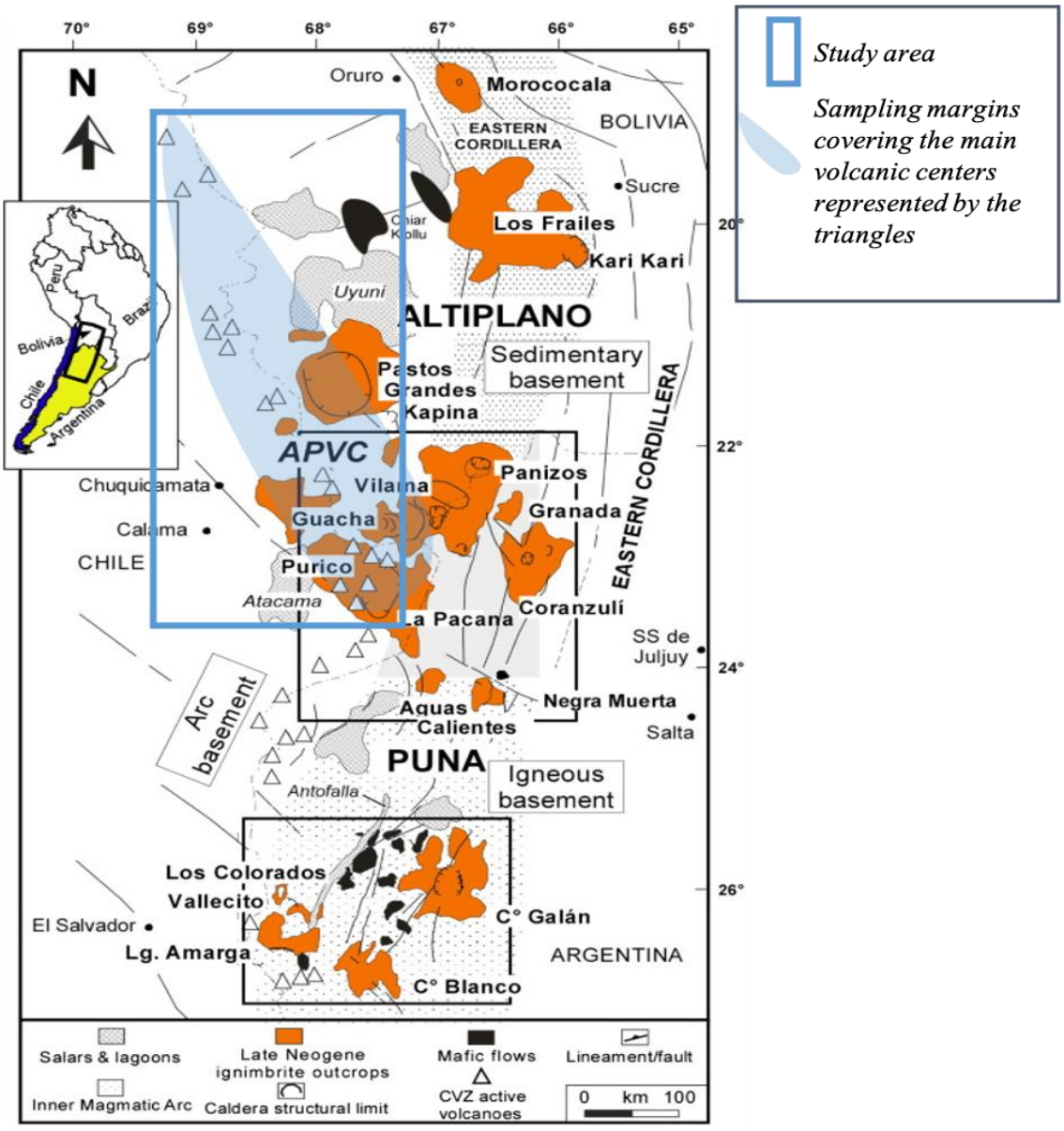

Figure 3.1: A map showing the location of the active volcanoes and earlier ignimbrite sheets under study (Adapted from Kay et al., 2010); with the blue outline demarcating the SPLVC, which is the main area of interest. The volcanoes are represented by small triangles.

Fieldwork was aimed at collecting rock samples that contain quartz or feldspar phenocrysts to allow for full house analyses. Preliminary research was conducted prior to the actual field work, where data from collaborators and locality maps were collated to secure prior knowledge of the area under study. The Global Positioning System (GPS) was used to determine the location and elevation of all sampling points. At each sampling site, records of the rock types and physical characteristics of volcanic outcrops were made in a field book, and photographs were taken. Courtesy of our Chilean collaborators, field trucks were organized to ensure smooth movement from one sampling location to the next.

Sampling was done across the San Pedro-Linzor Volcanic Chain (SPLVC), which is a ~65 km long NW-SE stretching lineament of stratovolcanic edifices. Rock samples were collected from the domes, lava flows and ignimbrite sheets that are widespread in the area. The main sampled areas include; the Chao dome, Turi lava, Toconce volcano, San Pedro de Atacama, Chillahuita dome, Cabanas sulphur mine, Ollagüe volcano, Cerro Overro maar and El Laco. These areas are all within the vicinity of the SPLVC. In each sampling area, the sampling points were selected based on features visible on the outcrop (phenocrysts, preferably quartz), accessibility of the area; in this regard, sampling was mostly judgemental. The number of samples and sampling intervals were a function of the availability of the outcrop, the size, and differences in rock characteristics of the outcrops. A combination of fresh and variably altered rock samples were collected across the field area, from dacite domes, ignimbrite sheets and lava flows. Each sample was obtained using a geological hammer or a sledgehammer, depending on its competency, then bagged up in a labelled sample bag to avoid mixing and confusion during sample preparation. These samples summed up to sixty-six, most of them were still fresh and well preserved, favoured by the arid climate of Northern Chile. All samples were then carried back to the University of Cape Town, Department of Geological Sciences for analyses. Table 2 shows the sample locations and the rock types encountered throughout the fieldwork, while Figure 3.2 shows the sample locations.

Table 2: Description of samples and their locations from selected active volcanoes of the CVZ.

Sample	Location	Latitude	Longitude	Comments
CS-19-01	Chao	22° 11' 41" S	-68° 11' 33" W	Dacite, glassy matrix, intermediate
CS-19-02	Chao	22° 11' 41" S	-68° 11' 33" W	Dacite, crystalline and dark
CS-19-03	Chao	22° 11' 41" S	-68° 11' 33" W	Dacite, glassy and darker
CS-19-04	Chao	22° 11' 41" S	68° 11' 36" W	pumice, from the pyroclastic flow, by first cactus
CS-19-05	Chao	19° 29' 04" S	68° 12' 27" W	semi-pumice, pyroclastic flow, high up
CS-19-06	Chao	22° 11' 39" S	68° 11' 36" W	from the dome, higher up, 3rd cactus
CS-19-07	Turi lava	-22° 14' 22" S	-68° 10' 07" W	Dacite, from the dry river
CS-19-08	Turi lava	-22° 14' 22" S	-68° 10' 07" W	Dacite, finer-grained, probably from Toconce flow
CS-19-09	Toconce	-22° 15' 28" S	-68° 11' 47" W	Andesite, Dark colored with vesicles
CS-19-10	Toconce	-22° 15' 28" S	-68° 11' 47" W	Ignimbrite, rubbly and highly weathered
CS-19-11	Toconce	-22° 15' 31" S	-68° 11' 40" W	Pumice, elongated vesicular texture, small crystals
CS-19-12	Toconce	-22° 15' 57" S	-68° 09' 45" W	Ignimbrite, 7myo
CS-19-13	S.P river	-21° 56' 00" S	-68° 31' 02" W	Ignimbrite, with quartz enclaves, 8myo
CS-19-14	S.P river	-21° 56' 30" S	-68° 31' 48" W	Ignimbrite, loose and crumbly
CS-19-15	Toconce	-22° 05' 49" S	-68° 03' 28" W	Dacite, with crystals
CS-19-16	Toconce	-22° 05' 49" S	-68° 03' 28" W	sulfur-rich altered rock
CS-19-17	Chillahuita	-22° 08' 54" S	-68° 02' 44" W	Flow banded and glassy rock
CS-19-18	Chillahuita	-22° 08’ 54’’ S	-68° 02’ 44’’W	Monocrystalline
CS-19-19	Chillahuita	-22° 14' 24" S	-67° 59' 02" W	altered rock, in-situ uphill
CS-19-20	Chillahuita	-22° 14' 12" S	-67° 58' 58" W	sulfur-rich loose rock, down the road
CS-19-21	Cabanas	-22° 03' 52" S	-68° 03' 31" W	from the left hand side vein
CS-19-22	Cabanas	-22° 03' 52" S	-68° 03' 31" W	from the right hand side vein
CS-19-23	Cabanas	-22° 03' 52" S	-68° 03' 31" W	from the altered wall rock
CS-19-24	Cabanas	-22° 00' 26" S	-68° 19' 48" W	Dacite, fine-grained and partly altered
CS-19-25A	Ollague	-21° 12' 28" S	-68° 22' 12" W	Breccia with veins, from mineralized zone
CS-19-25B	Ollague	-21° 12' 28" S	-68° 22' 12" W	vein rock
CS-19-25C	Ollague	-21° 12' 28" S	-68° 22' 12" W	altered country rock
CS-19-25D	Ollague	-21° 12' 28" S	-68° 22' 12" W	black rock in altered zone
CS-19-25E	Ollague	-21° 12' 28" S	-68° 22' 12" W	opaline vein rock
CS-19-25F	Ollague	-21° 12' 28" S	-68° 22' 12" W	veined rock
CS-19-25G	Ollague	-21° 12' 28" S	-68° 22' 12" W	white, massive, low density rock
CS-19-26	Ollague	-21° 12' 07" S	-68° 22' 42" W	Fresh dacite, from up the mineralized zone
CS-19-27	Ollague	-21° 11' 46" S	-68° 22' 58" W	altered volcanic rock, porphyritic
CS-19-28	Ollague	-21° 11' 46" S	-68° 22' 58" W	honeycomb rock
CS-19-29	Ollague	-21° 11' 34" S	-68° 27' 15" W	porphyritic, taken high above the mast
CS-19-30	Ollague	-21° 11' 34" S	-68° 27' 15" W	porphyritic, taken high above the mast
CS-19-31	Ollague	-21° 11' 34" S	-68° 27' 15" W	porphyritic, taken high above the mast
CS-19-32	Ollague	-21° 11' 19" S	-68° 27' 01" W	Mafic and dense rock, taken close to the signal tower
CS-19-33	Ollague	-21° 12' 34" S	-68° 22' 06" W	altered zone
CS-19-34	Ollague	-21° 16' 17" S	-68° 13' 53" W	quartz dacite, altered, by road from ollague dome
CS-19-35	San Pedro	-23° 30' 56" S	-67° 39' 38" W	altered dacite, from Cerro Overo maar
CS-19-36	Cerro Overo	23° 30' 55" S	67° 39' 38" W	unaltered dacite enclaves within basalt

CS-19-37	Cerro Overo	23° 30' 55" S	67° 39' 38" W	unaltered dacite, whitish, from crater bottom
CS-19-38	Cerro Overo	23° 31’ 01" S	67° 39' 50"W	unaltered dacite, pinkish, bottom of the crater
CS-19-39	Cerro Overo	23° 31' 01" S	67° 39' 50" W	green pumice
CS-19-40	Cerro Overo	23° 31' 01" S	67° 39' 50" W	white pumice
CS-19-41	Cerro Overo	-23° 31' 03" S	-67° 39' 53" W	Brownish, glassy, with quartz crystals, maar crater
CS-19-42	Cerro Overo	-23° 31' 03" S	-67° 39' 53" W	darker rock, crumbly, quartz crystals, darker matrix
CS-19-43	To Atacama	-23° 25' 57" S	-67° 46' 15" W	partially altered, porphyritic dacite
CS-19-44	To Atacama	-23° 19' 24" S	-67° 47' 41" W	ignimbrite, from down the valley
CS-19-45	To atacama	-23° 19' 04" S	-67° 51' 46" W	Ignimbrite, Close to the big NW striking trench
CS-19-46	EL Laco	-23° 50' 23" S	-67° 29' 25" W	Magnetite/hematite
CS-19-47	EL Laco	-23° 50' 33" S	-67° 29' 29" W	dacite in magnetite ore, from the quarry downslope
CS-19-48	EL Laco	-23° 50' 33" S	-67° 29' 29" W	similar rock, from opposite walls of the pit
CS-19-49	EL Laco	-23° 50' 33" S	-67° 29' 29" W	vein of coruscating magnetite
CS-19-50	EL Laco	-23° 50' 11" S	-67° 29' 37" W	altered lava
CS-19-51	EL Laco	-23° 50' 11" S	-67° 29' 37" W	white rock, 25m apart from the altered lava
CS-19-52	EL Laco	-23° 49' 58" S	-67° 29' 31" W	altered white rock from the road up
CS-19-53	EL Laco	-23° 49' 55" S	-67° 28' 38" W	less altered rock, heavy with quartz crystals
CS-19-54	EL Laco	-23° 49' 55" S	-67° 28' 50" W	less altered rock, heading downslope
CS-19-55	EL Laco	-23° 49' 51" S	-67° 29' 22" W	Fresh rock, could be andesite, Heading downhill,
CS-19-56	To the lakes	-23° 55' 05" S	-67° 33' 06" W	ignimbrite/dacite, enclaves, fresh, from silicic flow
CS-19-57	To the lakes	-23° 45' 10"S	-67° 50' 09"W	Ignimbrite, very altered, with xenoliths
CS-19-58	San Pedro	-23° 36' 58" S	-67° 50' 52"W	Ignimbrite, less altered, quartz phenocrysts, enclaves
CS-19-59	San Pedro	-22° 45' 07" S	-68° 04' 22"W	Ignimbrite sheet, next to the river at the base flow
CS-19-60	San Pedro	-22° 44' 31"S	-68° 03' 58"W	ignimbrite, altered, with nice quartz
CS-19-61	San Pedro	-22° 26' 21"S	-67° 58' 48"W	ignimbrite, white and altered, below the dome
CS-19-62	San Pedro	-22° 26' 07" S	-67° 59' 14"W	Dacite, solid, from the peak opposite the dome
CS-19-63	San Pedro	-22° 25' 38"S	-67° 59' 21"W	altered volcanic rock, from close to the road
CS-19-64	San Pedro	-22° 25' 38"S	-67° 59' 21’’W	could be dacite, flowbanded
CS-19-65	San Pedro	-22° 25' 43"S	-67° 59" 22"W	very altered volcanic rock, from the brecciation zone
CS-19-66	San Pedro	-22° 26' 14"S	-67° 59' 21’’W	brecciated material, have green stuff in the cavities

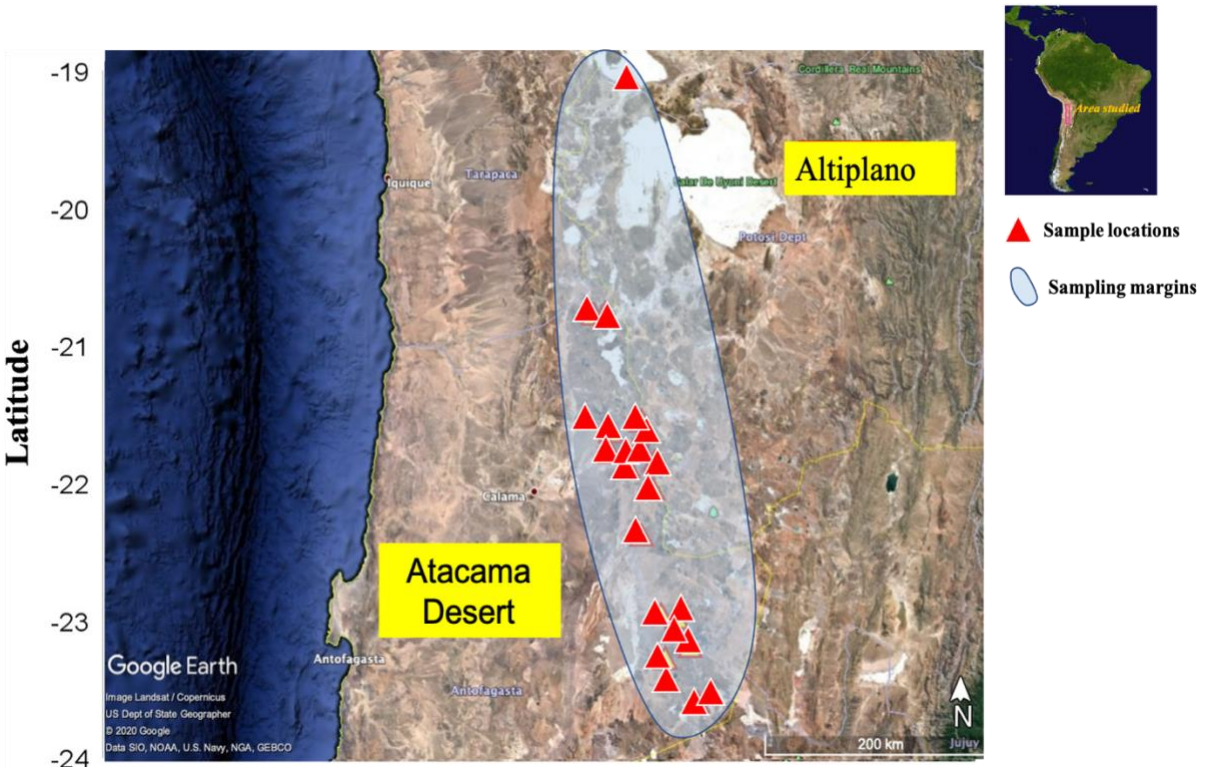

Figure 3.2: A map of sample locations along the CVZ, each triangle represents numerous sampling points.

3.1.1. Field observations

The fieldwork was undertaken from two camps, with the first one in Chiu Chiu, 30 km NE of Calama and the second one in San Pedro de Atacama. In this section, details of the fieldwork and sampling of selected volcanoes across the field area are given. Throughout the fieldwork, the usual rock types that were encountered and of interest for this project include; ignimbrites, dacites, lavas of variable composition and altered rocks; these were sampled.

The APVC Ignimbrites

The ignimbrites are one of the oldest rocks of the area. There is a remarkable distribution and volume of eruption of these silica-rich (>65wt% SiO_2) ignimbrites. The eruption of the ignimbrites corresponded to the highest magma production rates within the cyclic and episodic manner of continental magmatic arcs. The eruption of the ignimbrites occurred in four main pulses; 10, 8, 6, and 4 Ma respectively, and these pulses began with an increasing intensity, followed by a sudden drop after 4 Ma (Salisbury et al., 2011). The Altiplano-Puna ignimbritic eruption pulses are an indicator of high-flux of crustal magmas, also known as “flare ups” (de Silva and Kay, 2018; de Silva, 1989; de Silva and Gosnold, 2007; Ducea and Barton, 2007).

The ignimbrites are monotonous intermediates, with compositions dominated by calc-alkaline, high potassium dacites to rhyodacites with minor rhyolites. The eruption of these ignimbrites is related to structurally controlled caldera collapses. Phenocrysts of plagioclase, biotite, amphibole, quartz and Fe-Ti oxides are predominant in the ignimbrites, indicating a strong crustal composition. In total, these crystals make up 40% of the volume of these ignimbrites, classifying them as crystal rich (Lindsay et al., 2001; Schmitt et al., 2001).

Ignimbrites in the APVC are widespread across the area (Figure 3.1), all with distinct features. Samples of ignimbrites were collected from Toconce volcano, lower San Pedro river, around Salar de Atacama and San Pedro de Atacama. In Toconce village, the ignimbrites are about 7-8 Ma and mainly contain quartz, feldspar as well as minor biotite phenocrysts. At the upper San Pedro river, samples from the 8.1 Ma Sifon ignimbrite (Upper Rio San Pedro Ignimbrite) were collected. The outcrop represents the western-most portion of the ignimbrite that stretches northwards to San Pedro. This ignimbrite contains a lot of biotite and some lithic fragments as well as quartz phenocrysts. The lower Rio San Pedro ignimbrite is about 9.7 Ma, it is mainly a vesicular dacite with lithic fragments and pumice. It contains plagioclase, quartz and biotite. Figure 3.3 shows the ignimbrite outcrops that were sampled in Toconce, Lower and upper San Pedro river.

Figure 3.3: Ignimbrite outcrops across the study area. Frame (A) showing the 8 Ma ignimbrites in Toconce and Toconce volcano further ahead. Highly weathered ignimbrite outcrop found on the sidewall of the road to Toconce in Frame (C), with Frame (B) showing a layered ignimbrite wall on the road to Toconce village. Frame (D) and (E) show the 8.1 Ma Rio San Pedro ignimbrites found along the road upper (D) and lower (E) San Pedro river.

The Linzor Lavas and the domes intruding the SPLVC

Basaltic-andesite and andesite lava flows overlie the ignimbrites, such as the SC2 flow near Ollagüe volcano. It is assumed that the more recent cones and lava were erupted through the pre-existing ignimbrite sheets. Plagioclase, clinopyroxene and olivine phenocrysts, as well as groundmass are the major constituents of these lava flows (Godoy et al., 2019). The origin of the Linzor lavas is linked to magma dominated by shallow assimilation of crustal melts that were derived from the Altiplano-Puna Magma Body (Godoy et al. 2014). Compositionally, the lava flows are classified as basaltic-andesite to rhyolite, with predominance of dacitic constituents. Plagioclase and orthopyroxene are the main phenocrysts found in these lava flows, with percentages of about 60-70% plagioclase and pyroxene microlites as well as glass. Partially resorbed quartz phenocrysts (see appendix) are also observed in Linzor lavas (Godoy et al., 2017).

Chao and the associated domes are located within the APVC, and younger than the flanking volcanoes of Paniri and Leon, on whose flanks it is constructed. The magmatic products of Chao erupted in several phases, as described by de Silva et al. (1994). The first phase (upper group) was explosive and produced ~1 km^3 of coarse, non-welded dacitic pumice deposits and later produced block and ash flows that form an apron in front of the main lava body. The second phase was dominantly effusive and erupted ~22.5 km^3 of magma in the form of a composite coulee. Phase 3 produced a 6 km-long, 3 km-wide flow that emanated from a collapsed dome. Chao's anomalous size is a function of both the relatively steep local slope (20°-3°) and the available volume of magma.

The duration for Chao's emplacement is thought to have been about 100 to 150 years, with maximum effusion rates of about 25 m^3s^{-1} for short periods. Petrological and physical similarities between Chao and neighbouring young domes suggest that they form part of the same magmatic episode. Conclusions made by de Silva et al. (1994), indicate a resemblance between the dacite domes and lavas with the older regional ignimbrites. This resemblance suggests that they all from a long lived silicic magmatic system below the APVC. Chao and the other young domes may have been derived from a waning magmatic system containing "old" volatile-poor silicic magma that was left after the eruption of the voluminous ignimbrites. Alternatively, they may represent a new crustal melting episode influenced by the intrusion of fresh and hot mafic magma (de Silva et al., 1994).

During the fieldwork, Chao dome (Figure 3.4) was the first location where sampling was done. Located between the composite cones of Leon and Paniri volcanoes, Chao is the largest known silicic lava flow on earth and the biggest dome sampled throughout the fieldwork. Considering the stagewise formation of the dome, samples were collected from down-up to cover most of the products of each development stage of the dome. Samples were collected from the seasonal stream flowing along the flanks of the dome, some high up the dome and then higher up. The samples ranged from intermediate, glassy and crystalline dacite to pumice, from the flanks to the top respectively. More dacite samples were collected from Turi lava, just a distance from Chao dome. The dacite from Turi lava also had flow-banding and were mineralogically like those from Chao, shown in Figure 3.5.

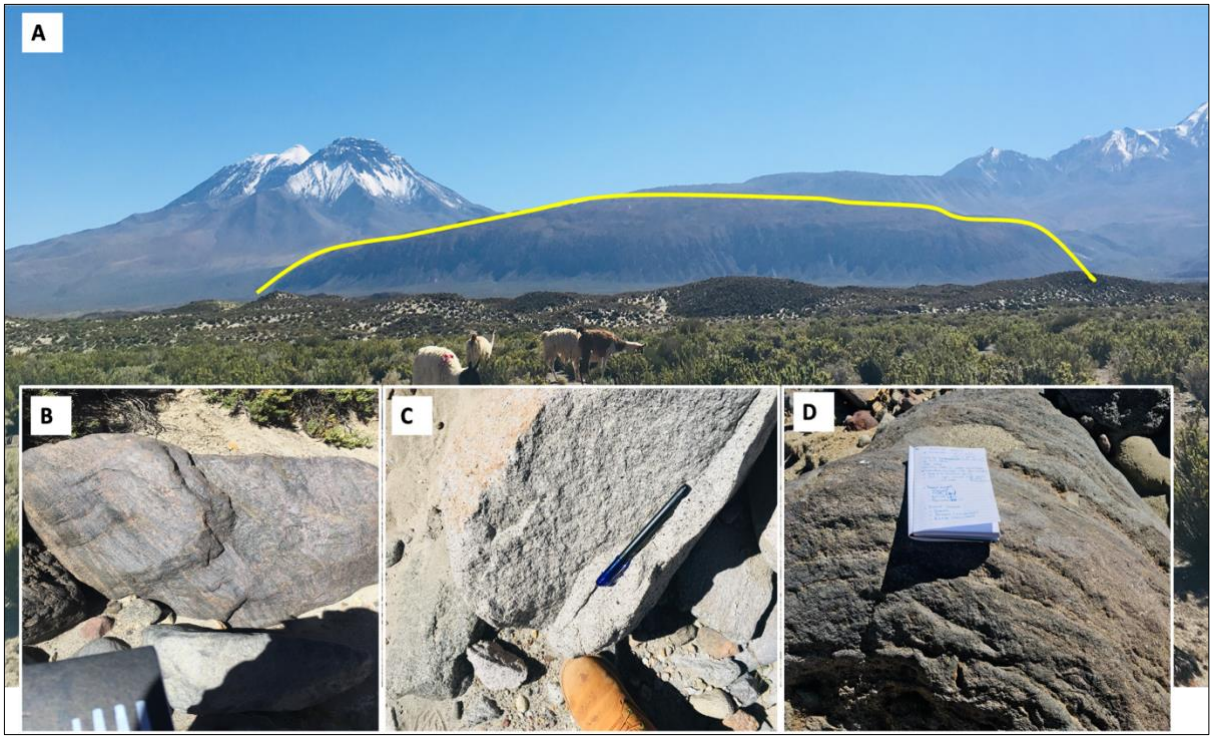

Figure 3.4: An image of Chao dome (main frame), with the yellow line showing the outline of the dome. Frame (B) shows the flow-banded dacite, frame (C) shows the crystalline dacite and the glassy dacite with flow banding is shown on frame (D), all sampled from the flanks of the dome.

Figure 3.5: Left; a flow-banded dacite lava boulder, probably from the Toconce flow, and an nonflow-banded dacite outcrop (right), both sampled in Turi.

Fresh and altered samples of dacite we taken in Cerro Overro, this is a maar generated from an eruption of basaltic andesite at the foot of Chiliques stratovolcano. This explosion crater cuts into the surrounding country rock and is surrounded by a ring of ejecta (White and Ross, 2011). The Cerro Overo maar explosion was likely phreatomagmatic (produced by a subsurface interaction between magma and water, at which the water flashed to steam, leading to rapid expansion and uplift), and accompanied by catastrophic degassing of the magma itself (e.g. White and Ross, 2011). However, a lack of fine-grained deposits or palagonite indicates that minimal amounts of water were involved. The crater is elliptical, approximately 480-600 m across and 60-80 m deep. A thin ejecta blanket surrounding the crater is partially-eroded, with an estimated original extent of 1-3 km from the eruption site and dominated by smaller (1-40 cm) lava clasts. Thicker, discontinuous and disparate deposits of lava are restricted to the crater rim and display surface flow textures (Figure 3.7) such as pahoehoe "ropes", cooling fractures, and oriented vesicles (White and Ross, 2011).

Flow-banding is also prevalent at the near surface of thicker deposits and microphenocryst plagioclase lathes and elongated vesicles display strong flow orientation in the banded regions of the samples. The dacite samples from the maar contain a lot of quartz phenocrysts. The basalt also contains enclaves of unaltered dacite and some of the dacite was in sharp contact with the basalt.

More sampling was done on the exposed, light, cliff-like structures around the maar rim (Figure 3.6, 3.7) and they were all dacitic in composition, with large and visible quartz crystals; these cliff-like structures appear to be weathered and friable. Towards the maar crater, outcrops of highly altered dacite, which some appeared glassy and pinkish in colour were found. Greenish and white samples of pumice were taken from the central part crater.

Figure 3.6: View of Cerro Overro maar, the yellow line marks the maar rim and the blue circled areas represent the dacitic country rock (Atana ignimbrite) outcrops where more samples were taken. The black scattered stuff are the ejecta from the explosion. The stratocones behind are Chiliques (left) and Lejia (right).

Figure 3.7: Flow textures on a glassy basalt (A), and a large dacite xenolith in the basalt (B) all found along the maar rim. Frame (C) shows a cliff-like outcrop of the country rock (ignimbrite) and (D) is a close-up image of the outcrop with clearly visible minerals and big quartz crystals.

Altered materials were relevant to this study, therefore sampled across the study area as well. Altered materials were sampled to investigate the nature of fluid-rock interactions and the availability of low-$\delta^{18}O$ source rocks. During alteration processes, an exchange of isotopes and/or elements take place at varying temperatures and the interaction involves dissolution-precipitation, chemical exchange reactions, redox reactions, diffusion, and their combinations. Shifts in $\delta^{18}O$ values can be to higher or lower values depending on the temperature and the $\delta^{18}O$ of the fluid (Vratislav et al., 2015).

Samples of altered dacite and ignimbrite were collected from Chillahuita dome, Cabanas sulfur mine, western Ollagüe and San Pedro de Atacama. Altered rocks from Chillahuita dome and Cabanas sulfur mine were crumbly and rich in sulfur crystals (Figure 3.8). A very beautiful and interesting mineralized zone was encountered during the ascent to Aucanquilcha dome. This zone has brecciated outcrops with opaline veins of varying shades (Figure 3.9).

Figure 3.8: Sulfur rich altered rock from Cabanas mine (left) and a sulfur rich altered dacite from Ollagüe (right).

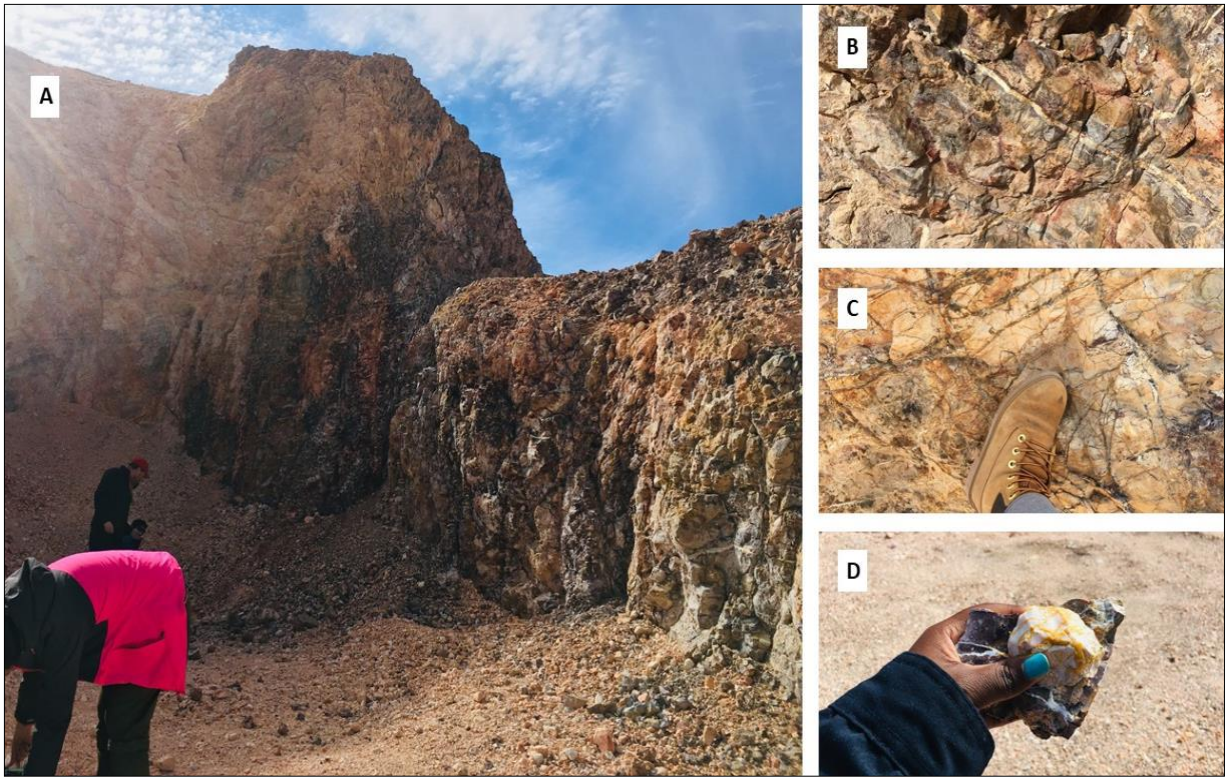

Figure 3.9: A view of the mined out mineralized zone (A). Frame (B) and (C) show the brecciated outcrops with a lot of veins. Frame (D) shows the opaline rock with shades of purple, white and yellow.

CHAPTER 4

Analytical Methods

This chapter describes all the analytical methods, materials that were employed. For this project, the analytical methods that were used include; Laser and conventional Fluorination, for the analysis of stable isotopes through the extraction of oxygen gas from the silicate mineral; Mass Spectrometry, for measuring the $\delta^{18}O$ values of the samples; X-Ray Fluorescence, for analysis of major and trace elements in our bulk rock samples.

4.1. Sample Preparation

The samples were separated according to their possibility of bearing separable quartz or to a lesser extent feldspar phenocrysts, which are the two minerals most favoured for isotopic analyses. Therefore, fifty-six rock samples were crushed through the primary crusher and jaw-crusher available at the UCT Geological Sciences crushing lab. A fraction of each crushed sample was bagged separately for milling to obtain powders for bulk rock analyses through XRF and ICP-MS. The remaining fraction was separated using a stack of sieves (1400µm and 650µm meshes) into coarse (1400µm) and medium (600µm) for the purpose of picking individual quartz or feldspar grains for oxygen isotope analysis. Medium particles were selected for picking since it is the most convenient size, this fraction was washed in water and oven dried for 24 hours. For conventional fluorination, whole rock samples were powdered in a mortar with acetone and dried in an oven at 50°C overnight.

4.2. Oxygen Isotope Analysis

The use of unaltered phenocrysts in igneous rocks (in this case, quartz and plagioclase) yields a better view of true magmatic $\delta^{18}O$ values than bulk rock and gives reliable proxies for their parental melts (e.g. Bindeman, 2008).

In this project, most of our rock samples were fresh with fine-grained or glassy groundmass, making it easy to pick out quartz phenocrysts. Quartz phenocrysts (refer to appendix) were individually picked while looking down a binocular microscope. Oxygen isotope analysis was then performed using the laser fluorination system (Figure 4.1) available at the University of Cape Town stable isotopes laboratory (Figure 4.2), adhering to the methods described by Harris and Vogeli (2011). This system uses a 25W (full capacity) New Wave CO_2 Laser, mounted on a moveable stage, sample chamber, Kel-F BrF_5 distillation tube and a vacuum extraction line. The sample chamber consists of a polished vertical stainless steel tube with a disconnect flange

for insertion and removal of samples; a BaF_2 window that acts as a transparent medium in the visible and infrared regions, with resistance to fluorine and its derivatives, the window is compressed between two soft Teflon O-rings that serve as a tight seal for the vacuum; and a nickel sample holder, with 12 holes that contain each sample/standard.

The sample holder was loaded with ten quartz (or plagioclase) grains of about 2-3 mg per sample, as well as two MON GT garnet samples that served as standards. Prior to insertion of the holder into the reaction chamber, it was placed in an oven at 110°C for at least an hour to remove any absorbed moisture from the samples and the Ni disc. Once loaded into the reaction chamber and pumped out overnight, the samples were pre-fluorinated for 30 seconds and pumped out, then pre-fluorinated overnight. The next day, each grain was heated by the laser in the presence of about 10 kPa BrF_5. Different gaseous species (O_2, Br_2, F_2) along with oxygen gas are produced upon sample reaction, therefore purification of the O_2 is required.

The excess BrF_5 and produced Br were cryogenically removed. The remaining gases were passed through a KCL filter that retains F_2 and releases CL_2, the CL_2 was passed through a U-trap dipped into LN_2 to obtain pure O_2. Glass bottles containing 5Å molecular sieve were used to trap the pure O_2 inside and frozen into LN_2. These were used as carriers for transporting the liberated oxygen gas to the mass spectrometer. A gas source Finnegan Mat Delta XP mass spectrometer in the Department of Archaeology (UCT) was used to measure the isotope ratio in a dual inlet mode and reported the measurements in the standard δ-notation relative to SMOW; where, (Equation 1):

$$\delta^{18}O = \left(\frac{R_{Sample}}{R_{Standard}} - 1\right) \times 1000 \qquad \text{Eq (1)}$$

R_{Sample} and $R_{Standard}$ are absolute ratios of $^{18}O/^{16}O$ and the standard.

The oxygen isotope data for all the samples were normalized to a standard MONGT garnet value of 5.38‰. The in-house garnet standard MONGT was analysed in duplicate with each batch of 10 samples. MONGT has a $\delta^{18}O$ value of 5.38‰ calibrated against the UWG-2 garnet standard of Valley et al. (1995), assuming a $\delta^{18}O$ value of 5.80‰ for UWG-2. The average $\delta^{18}O$ value of the MONGT for each LF run was used to normalise the raw data to the SMOW scale (Harris and Vogeli, 2010). The long-term average difference between duplicates of MONGT obtained by laser fluorination is 0.12‰ (n=283), corresponding to a 2σ value of 0.16‰.

Conventional Fluorination was used to determine $\delta^{18}O$ in bulk rock samples, using the vacuum line available at the UCT Geological Sciences Department. For each analysis, about 10 mg of whole rock powder is required, and the procedures described by Harris and Ashwal (2002) were followed. The powdered samples were loaded into nickel tubes and degassed at 200°C, eight whole rock samples and two quartz standards were done per run.

The liberation of oxygen was done by reacting the samples with ClF_3 for about three hours at 550°C. Unwanted reaction products and excess ClF_3 were retained by immersion of the reaction tubes in N_2. Oxygen gas was converted to CO_2 by a hot carbon rod, the CO_2 was then frozen in tight sealed tubes and taken to the mass spectrometry lab for oxygen analysis. Duplicate splits of the in-house quartz standard MQ were run with each batch of 8 samples to monitor analytical precision and convert the raw data to the SMOW scale using the $\delta^{18}O$ value of 10.1‰ for MQ (calibrated against a $\delta^{18}O$ value of 9.64‰ NBS-28). The long-term variability of MQ suggests a 2σ error of 0.20‰.

Figure 4.1: Laser Fluorination system in the Stable Isotopes Lab with Laser, traps ,kBr trap, sample bottles, etc (Department of Geological sciences UCT).

4.3. X-Ray Fluorescence (XRF) Analysis

Fusion discs and pellets were prepared for performing an XRF analysis. This analysis was done at the XRF laboratory in the Geological Sciences Department at UCT. Upon preparation of fusion discs for major elements, about 2 g of a powdered sample was added into a crucible of known mass and dried in an oven for at least four hours at 110°C. The samples were allowed to cool, re-weighed, and put into a furnace overnight at about 850-1000°C. Another round of re-weighting of the samples was done prior to transferring them from the crucibles to glass tubes. At 450°C, a lithium tetraborate flux was dried in furnace overnight and let to cool thereafter, 6 g of this flux was used as a releasing agent. From each sample, 0.7 g was measured into glass tubes and sealed with mylar film and lid. The fusion discs were made by fusing the flux and the sample together into a Claisse gas burner.

The XRF pellets for trace elements were made by weighing out 6 g of a powdered sample and mixed it with a binding agent (about 3 drops), thorough mixing of the agent and the sample was done, and the mixture was tipped into a mould. Pressure of 10 tons was applied to the mixture to make a desirable pellet shape and boric acid was added to the mould, with a cylinder inserted onto the sample and the acid. A pressure of about 10 tons was applied on the mould in a hydraulic press, the pellet was then removed from the mould and labelled accordingly.

XRF analysis was carried out using a Panalytical Axios XRF spectrometer available in the Geological Sciences Department (UCT). The selected samples were analysed for bulk rock major oxides and trace elements separately and both calibrated using standards set by known organizations (e.g. United States Geological Survey, the Geological Society of Japan, MINTEK, etc). These standards were prepared following the same procedures that were followed in preparation of the analysed samples for this project. All necessary corrections and calibrations were applied on the elementary concentrations, absorption and enhancement effects and spectral line overlaps.

4.4. Hydrogen Isotope Analysis

Hydrogen isotopes were measured on between 27 and 130 mg of whole-rock powders on the hydrogen silicate line, using the method of Vennemann and O'Neil (1993), with reduction by "Low-blank Indiana Zinc" (Schimmelmann and DeNiro, 1993). The amount of powder was chosen on the basis of the LOI, and the aim was to obtain about 2 mg of water for analysis. For D/H determination, the in-house Serina Kaolinite standard (Serina bulk kaolinite, D= −57‰, H_2O= 12.4 wt%) (Harris et al., 1999 sample SB8) was analysed in triplicate with the silicates, and internal water standards CTMP2010 (Cape Town Millipore Water 2010, D= −7.4‰) and RMW (Rocky Mountain Water, D= −131.4‰) were used to convert raw data to the Standard Mean Ocean water (SMOW) scale and correct for scale compression. Water concentrations ($H2O^+$) were determined from the voltage measured on the mass 2 collector of the mass spectrometer, using identical sample inlet volume (Vennemann and O'Neil, 1993). The expected voltage per milligram of water was determined from accurately measured amounts of the 5 standard waters analysed with the samples. The precision for δD for the internal kaolinite standard were ±2‰ (1σ, n=3). The typical precision for water amounts based on many measurements of water and kaolinite standards is ±0.1wt%. The average standard kaolinite gave a δD value of −63‰, after all the corrections to the raw data were applied. All data were adjusted to the accepted kaolinite value of −57‰. The obtained water was trapped cryogenically and transferred to pyrex tubes containing Zn. The hydrogen isotope composition of the H_2O was determined using the closed tube Zn reduction method of Vennemann and O'Neil (1993). Note that sample CS-19-11 contained insufficient water for analysis and that for CS-19-41, the quartz glass tube burst during pyrolysis, presumably due to the high non-water volatile content.

CHAPTER 5

Petrography

Thin sections of 10 selected rock samples that are representative of the CVZ were made to identify the phenocrysts and alteration mineral textures (Table 3). Photomicrographs of some of the samples are shown in Figures 5.1 to 5.3.

Dacites from the CVZ have coarse to medium sized grains, with mostly light colors (white, grey, pinkish and light brown). They have inequigranular textures with clearly visible phenocrysts in hand specimen. There is a 30-50% of crystals in most of the dacites. These dacites are really fresh, and in most cases, it was hard to clearly distinguish between quartz and plagioclase phenocrysts. The mineral constituents present in these dacites include quartz, plagioclase, biotite and hornblende. Quartz/plagioclase phenocrysts are dominant, making approximately 35% of the 40% crystal percentage ratio; followed by biotite (~3%), and hornblende (~2%). The quartz/plagioclase phenocrysts are large and generally angular in shape, and biotite flakes are sub-angular. In some of the dacites, the groundmass is glassy and sugary, especially the dacites from Cerro Overo maar.

The CVZ ignimbrites have similar composition as the dacites. Some dacites (Chao dome) are pyroclastic with vesicular textures (of pumice). These ones have relatively less crystal content with; however, numerous inclusions of andesite and some sands. Some are welded with small, rounded hornblende crystals. The lavas are fine textured and are light colored to reddish, they have small crystals of equigranular texture. The modal percentage is approximately 10%. Their mineral composition (rhyo-dacitic) consists of quartz/plagioclase, biotite, minor hornblende and oxides. Most of the lavas have flow-banding textures with a glassy appearance. Lavas from Chao are monotonous, crystal-rich and dacitic in composition. They have prominent phenocrysts of quartz, plagioclase, biotite and large hornblendes (up to about 1.6 cm). These lavas have a holocrystalline texture, with crystal percentages going up to approximately 40%. The plagioclase shows simple twinning and zoning (Figure 5.1), and quartz have minor resorption. There is also some twinning in the large hornblendes. The matrix is colorless to white, with high silica, and some have rhyolitic glass.

Altered dacites, ignimbrites and lavas from the CVZ have varying textures, but mostly coarse-grained and visible. Their colors vary from pinkish to reddish, while some are whitish to cream. The altered rocks all have alteration textures and indicators, from oxidation to weathering patterns. The crystals in altered rocks are not really visible, but in some, ~3% of crystals are visible. Quartz phenocrysts in altered dacites and ignimbrites prevail, and plagioclase and biotite are almost completely altered in some of the rocks. Some altered rocks have sulfur crystals in them, e.g., the ones from high elevations close to the domes and the ones from Cabanas sulfur mine. The altered rocks from Ollagüe have hydrothermal alteration textures, such as veins. In this zone, the dacitic rocks contains opal veins that are white to yellow. Some have the entire rock altered to a pseudoglass of opaline appearance, with varying colors (yellow, white, red).

Table 3: Petrographic summary of CVZ thin sections.

Sample	Mineral composition	Modal %	Grain Size (mm)	Description	Texture	Rock type
CS-19-08	Quartz/Plagioclase	30	>3	Euhedral, simple twinning, zoning	Fine, with plagioclase and quartz enclaves, vesicular	Lava
	Biotite	1	>1	Subhedral, anhedral		
	Hornblende	4	>2	Euhedral, subhedral		
	Groundmass	65				
CS-19-11	Plagioclase	20	>2	Subhedral to euhedral, simple twins and zoning	Vesicular, welded, with phenocrysts of plagioclase	Ignimbrite
	Hornblende	>5	>1	Subhedral, euhedral		
	Groundmass	75				
CS-19-25	Plagioclase/Quartz	22	>3	Subhedral to euhedral, simple twins and zoning	Fine with quartz and plagioclase enclaves, alteration patterns	Altered lava
	Biotite	3	>4	Subhedral, anhedral		
	Hornblende	4	>5	Subhedral, euhedral		
	Olivine	1	>1			
	Groundmass	70				
CS-19-28	Plagioclase	20	>2	Subhedral,euhedral, with twinning and zoning	Vesicular, with andesite and sandy inclusions	Ignimbrite
	hornblende	4	>4	Euhedral		
	Biotite	1	>2	Anhedral, subhedral		
	Groundmass	75				
CS-19-37	Quartz/Plagioclase	10	>2	Subhedral to euhedral, zoning and simple twins	Fine with little crystals of quartz, plagioclase and hornblende	Ignimbrite
	Biotite	2	>1	Subhedral, anhedral		
	Hornblende	3	>2	Subhedral, euhedral		
	Groundmass	85				

CS-19-41	Plagioclase/Quartz	35	>3	Subhedral to euhedral, zoning and simple twins	Porphyritic with quartz, plagioclase, biotite phenocrysts.	Dacite
	Biotite	>1	>1	Subhedral, anhedral		
	Hornblende	3	>2	Subhedral, euhedral		
	Olivine	>1	>1			
	Groundmass	60		The matrix is glassy		
CS-19-48	Quartz/Plagioclase	35	>4	Euhedral to subhedral, lamellar twins and zoning	Medium to coarse with plagioclase and quartz enclaves	Dacite
	hornblende	>5	>1	Euhedral, subhedral		
	Groundmass	60				
CS-19-56	Plagioclase/quartz	30	>4	Subhedral to euhedral, simple twining and oscillatory zoning	Coarse with quartz and plagioclase enclaves and large biotite flakes	Ignimbrite
	Biotite	>4	>4	Subhedral, anhedral		
	Olivine	>1	>2			
	Groundmass	75				
CS-19-58	Quartz/Plagioclase	>5	>3	Subhedral to euhedral	Fine textured with pumice and andesite inclusions	Ignimbrite
	Biotite	>2	>1	Anhedral, subhedral		
	Hornblende	>3	>2	Euhedral to subhedral		
	Groundmass	90		Volcanic ash		
CS-19-65	Plagioclase/quartz	25	>3	Twinning, zoning	Medium, welded, with pumice grains	Ignimbrite
	Pyroxene	5	>2	Anhedral to subhedral		
	Groundmass	70				

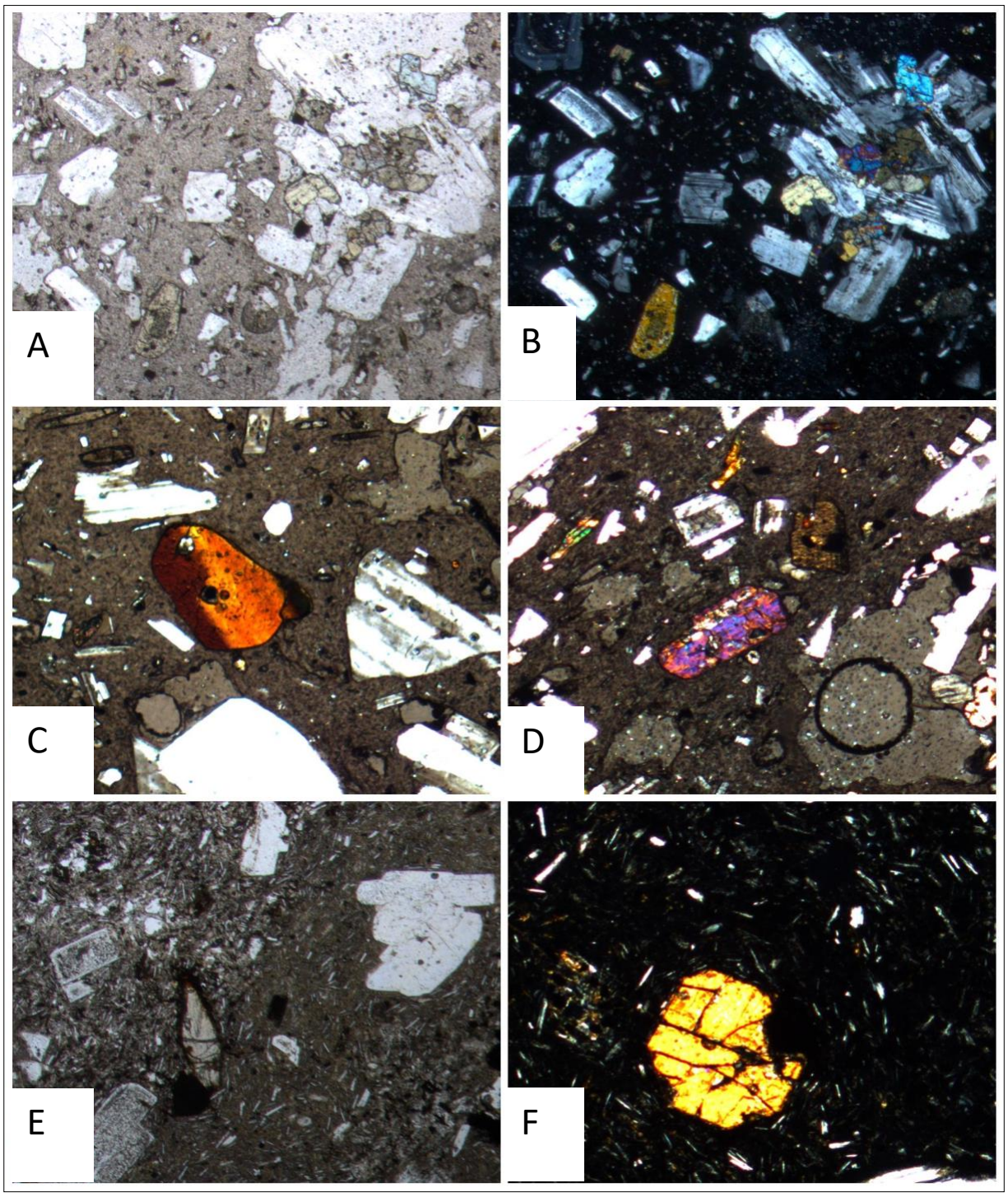

Figure 5.1: Photomicrograph of some samples from the CVZ; (A) and (B) Plagioclase and clinopyroxene in glass groundmass in PPL and XPL, (C) Biotite and plagioclase, (D) Plagioclase and clinopyroxene, (E) Plagioclase showing partly dissolved cores and orthopyroxene in PPL, (F) Clinopyroxene and plagioclase microcrysts in XPL.

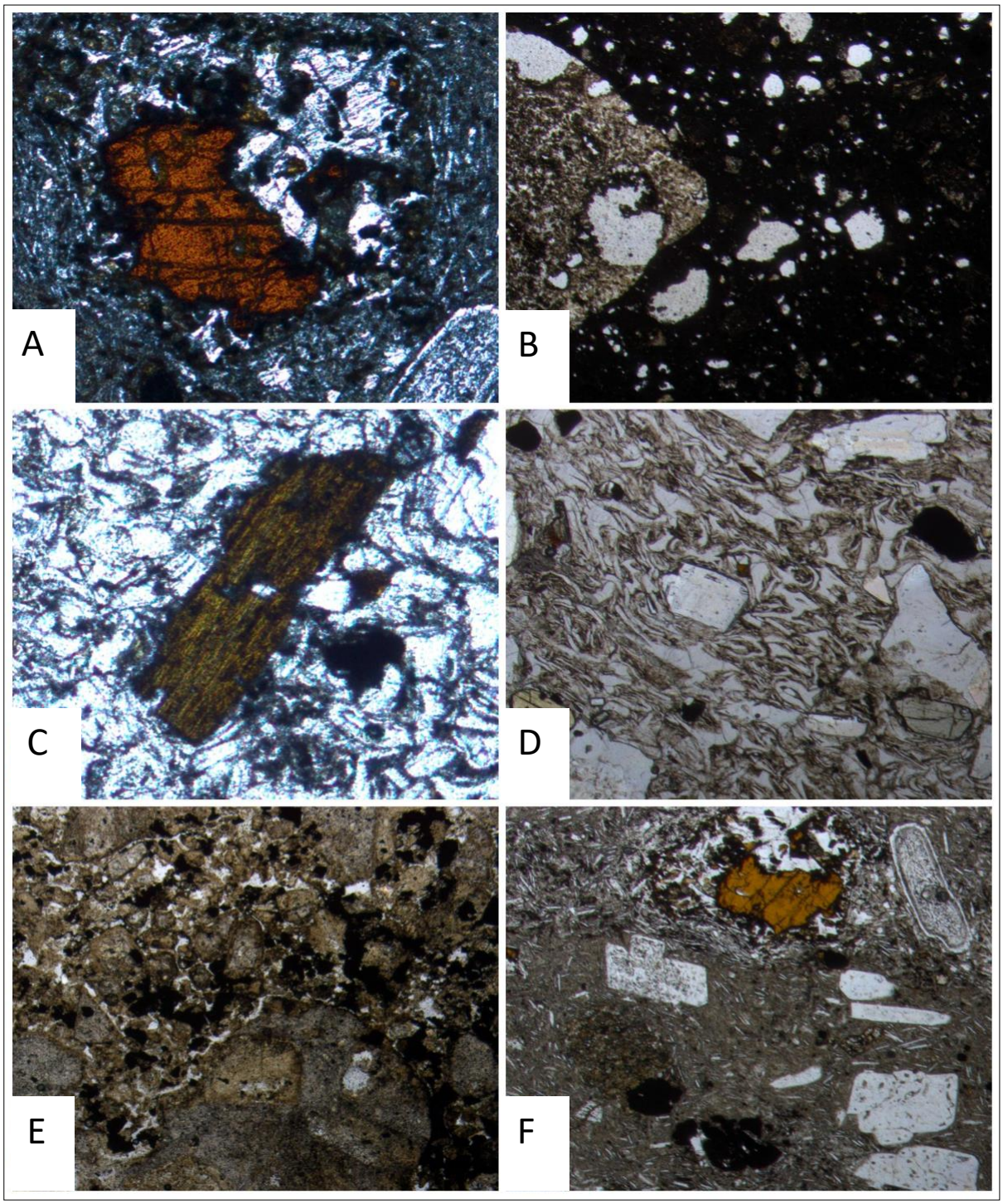

Figure 5. 2: (A) Brown hornblende in PPL, (B) Altered sample with fine grained dark groundmass and altered plagioclase, (C) Biotite in PPL, (D) Plagioclase and clinopyroxene crystals in groundmass with flattened pumice, (E) Highly altered sample with sulphur in PPL, (F) Hornblende and plagioclase in fine-grained groundmass with plagioclase microcrysts.

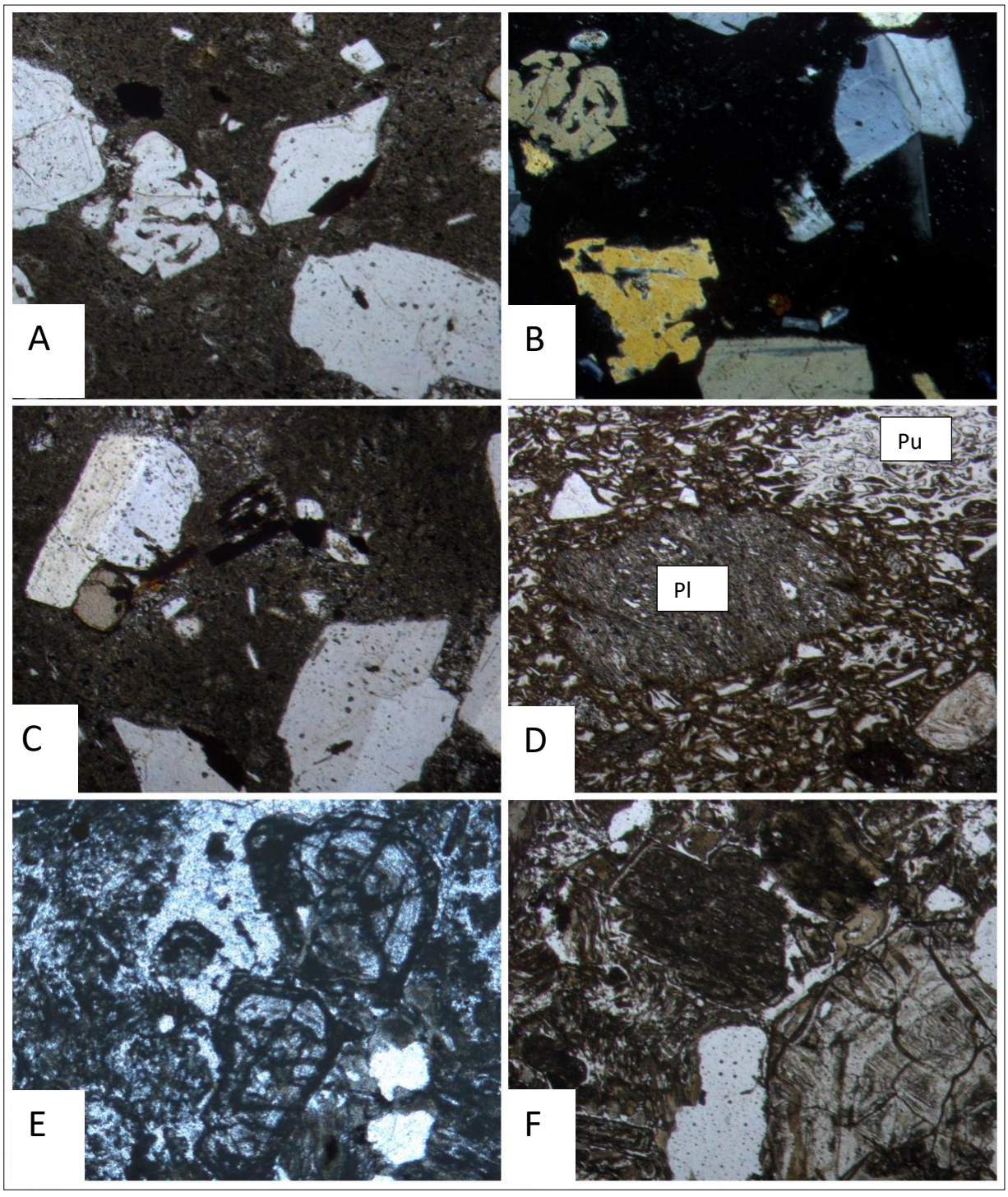

Figure 5. 3: (A) Quartz and plagioclase in fine-grained groundmass in PPL, (B) XPL version of (A) slightly rotated to show interference colours, (C) Plagioclase and clinopyroxene in PPL, (D) Pumice fragment (Pu) and altered plagioclase crystal (Pl), (E) and (F) Zoned unidentified mineral (could be Sulphur/Zeolite/Alunite)

CHAPTER 6

Results

In this chapter, results obtained are presented (Table 4). These include oxygen isotope data ($\delta^{18}O$ values) for quartz and plagioclase phenocrysts, and whole rock are presented as well as bulk rock major and trace element data from the analysis of the samples.

6.1. Oxygen Isotopes

A total of 52 samples were analysed for stable isotopes; of these, 41 quartz phenocrysts were analysed and 2 quartz seemed to be feldspar during lasing. All 52 samples were analysed for whole rock O-isotopes by conventional fluorination, and these whole rock samples include dacites, lava flows and ignimbrites, which are the dominant rocks found in the study area.

Oxygen isotope composition of quartz phenocrysts and whole rocks are presented in Table 4. The overall range of $\delta^{18}O$-quartz is wide and contains the lowest value of this dataset, as it ranges from 5.0 to 10.7‰. The average $\delta^{18}O$ value of quartz is 8.6‰ (n=41).

Most of our dacites and ignimbrites have $\delta^{18}O$-quartz values between 9.0-10.0‰, and quartz in lavas and altered rocks between 8.01-9.0‰. In the $\delta^{18}O$-whole rock dataset, most dacites and lavas have $\delta^{18}O$ composition between 9.01-11.0‰, whereas ignimbrites show high frequency at values between 7.01-9.0‰. Altered rocks show high frequencies at values between 11.01-13.0‰ (Figure 6.1).

The $\delta^{18}O$ values of whole rocks range from 5.0 to 22.3‰. Dacites (n=24) have the widest range of oxygen isotope composition (5.0- 22.3‰), and there is quite a variation in their values. The lowest whole-rock $\delta^{18}O$ value of dacites is 5.0‰, which is the only volcanic rock type with $\delta^{18}O$ value lower than those of mantle derived magmas (5.7‰) in this study. The dacites have an average $\delta^{18}O$ value of 10.4‰ with n= 24. Ignimbrites range from 8.3 to 14.9‰, with an average of 9.7‰, n=13. Ignimbrites have the lowest average $\delta^{18}O$ value as compared to the other rock types. Lava flows and altered rock range from 8.5 to 11.0‰ and 10.8 to 14.1‰ respectively. The average $\delta^{18}O$ value for altered rock is 12.0‰, and 10.2‰ for lava flows.

Table 4: Oxygen isotope composition of quartz (plagioclase) phenocrysts and whole rock species from the studied rocks of the Central Volcanic Zone of the Andes (reported in ‰).

		Coordinates				
Sample	**Location**	***Latitude***	***Longitude***	**Rock Type**	**$\delta^{18}O$ Quartz**	**$\delta^{18}O$ Whole Rock**
CS-19-01	Chao dome	22° 11' 41" S	68° 11' 33" W	Dacite	9.77	9.8
CS-19-02	Chao dome	22° 11' 41" S	68° 11' 33" W	Dacite		9.5
CS-19-03	Chao dome	22° 11' 41" S	68° 11' 33" W	Dacite		9.1
CS-19-04	Chao dome	22° 11' 41" S	68° 11' 36" W	Dacite	9.43	10.4
CS-19-05	Chao dome	19° 29' 04" S	68° 12' 27" W	Dacite	9.51	
CS-19-06	Chao dome	22° 11' 39" S	68° 11' 36" W	Dacite	9.48	10.4
CS-19-07	Turi lava	22° 14' 22" S	68° 10' 07" W	Dacite lava	9.53	11.0
CS-19-08	Turi lava	22° 14' 22" S	68° 10' 07" W	Lava		10.9
CS-19-10	To Toconce	22° 15' 28" S	68° 11' 47" W	Ignimbrite	9.33	10.9
CS-19-11	To Toconce	22° 15' 31" S	68° 11' 40" W	Ignimbrite	7.88	13.2
CS-19-12	Toconce village	22° 15' 57" S	68° 09' 45" W	Ignimbrite	9.37	11.9
CS-19-13	Upper San Pedro river	21° 56' 00" S	68° 31' 02" W	Ignimbrite	8.82	14.9
CS-19-14	Lower San Pedro river	21° 56' 30" S	68° 31' 48" W	Ignimbrite	7.64	8.3
CS-19-15	Toconce volcano	22° 05' 49" S	68° 03' 28" W	Dacite	9.70	11.1
CS-19-17	Chillahuita dome	22° 08' 54" S	68° 02' 44" W	Dacite	8.43	12.6
CS-19-18	Chillahuita dome	22° 08' 54" S	68° 02' 44" W	Dacite	10.66	9.7
CS-19-19	cabanas sulfur mine	22° 14' 24" S	67° 59' 02" W	Alt Rock	8.12	10.8
CS-19-22	Cabanas sulfur mine	22° 03' 52" S	68° 03' 31" W	Alt Rock	9.70	14.1
CS-19-23	Cabanas sulfur mine	22° 03' 52" S	68° 03' 31" W	Alt Rock		12.4
CS-19-24	Ollague	22° 00' 26" S	68° 19' 48" W	Dacite	7.93	11.8
CS-19-25B	West of Ollagüe	21° 12' 28" S	68° 22' 12" W	Alt Rock		16.1
CS-19-25C	West of Ollagüe	21° 12' 28" S	68° 22' 12" W	Alt Rock	7.02	8.8
CS-19-25D	West of Ollagüe	21° 12' 28" S	68° 22' 12" W	Alt Rock		9.5
CS-19-26	Ollagüe	21° 12' 07" S	68° 22' 42" W	Dacite	8.53	10.3
CS-19-27	Ollagüe	21° 11' 46" S	68° 22' 58" W	Alt Rock		12.6
CS-19-28	Ollagüe	21° 11' 46" S	68° 22' 58" W			19.9
CS-19-29	Ollagüe	21° 11' 34" S	68° 27' 15" W		8.28	9.1
CS-19-30	Ollagüe	21° 11' 34" S	68° 27' 15" W		7.94	8.7
CS-19-31	Ollagüe	21° 11' 34" S	68° 27' 15" W		8.26	8.2
CS-19-32	Ollagüe	21° 11' 19" S	68° 27' 01" W	Lava	8.18	8.5
CS-19-33	Ollagüe	21° 12' 34" S	68° 22' 06" W	Alt Rock	8.56	12.2
CS-19-35	Cerro Overo	23° 30' 56" S	67° 39' 38" W	Dacite	9.27	12.0
CS-19-36	Cerro Overo	23° 30' 55" S	67° 39' 38" W	Dacite	7.75	8.9
CS-19-37	Cerro Overo	23° 30' 55" S	67° 39' 38" W	Dacite	10.00	8.0
CS-19-38	Cerro Overo	23° 31’ 01" S	67° 39' 50" W	Dacite	8.96	8.6
CS-19-39	Cerro Overo	23° 31' 01" S	67° 39' 50" W	Dacite		8.8
CS-19-40	Cerro Overo	23° 31' 01" S	67° 39' 50" W	Dacite		8.5

CS-19-41	Cerro Overo	23° 31' 03" S	67° 39' 53" W	Dacite	7.02	6.8
CS-19-42	Cerro Overo	23° 31' 03" S	67° 39' 53" W	Dacite	10.02	12.5
CS-19-43	To salar de atacama	23° 25' 57" S	67° 46' 15" W	Dacite	7.71	10.3
CS-19-44	To salar de atacama	23° 19' 24" S	67° 47' 41" W	Ignimbrite	9.12	8.8
CS-19-45	To salar de atacama	23° 19' 04" S	67° 51' 46" W	Ignimbrite	7.15	8.7
CS-19-48	EL Laco	23° 50' 33" S	67° 29' 29" W	Lava	8.58	
CS-19-56	San Pedro De Atacama	23° 55' 05" S	67° 33' 06" W	Ignimbrite	7.20	8.4
CS-19-57	San Pedro De Atacama	23° 45' 10" S	67° 50' 09" W	Ignimbrite	7.62	8.9
CS-19-58	San Pedro De Atacama	23° 36' 58" S	67° 50' 52" W	Ignimbrite	7.10	12.7
CS-19-59	San Pedro De Atacama	22° 45' 07" S	68° 04' 22" W	Ignimbrite	9.68	9.7
CS-19-60	San Pedro De Atacama	22° 44' 31" S	68° 03' 58" W	Ignimbrite	9.89	10.3
CS-19-61	San Pedro De Atacama	22° 26' 21" S	67° 58' 48" W	Ignimbrite	9.44	9.6
CS-19-62	San Pedro De Atacama	22° 26' 07" S	67° 59' 14" W	Dacite	9.62	9.6
CS-19-64	San Pedro De Atacama	22° 25' 38" S	67° 59' 21'' W	Dacite		11.0
CS-19-65	San Pedro De Atacama	22° 25' 43" S	67° 59' 22" W	Dacite		22.3
CS-19-66	San Pedro De Atacama	22° 26' 14" S	67° 59' 21" W	Dacite	5.00	5.0

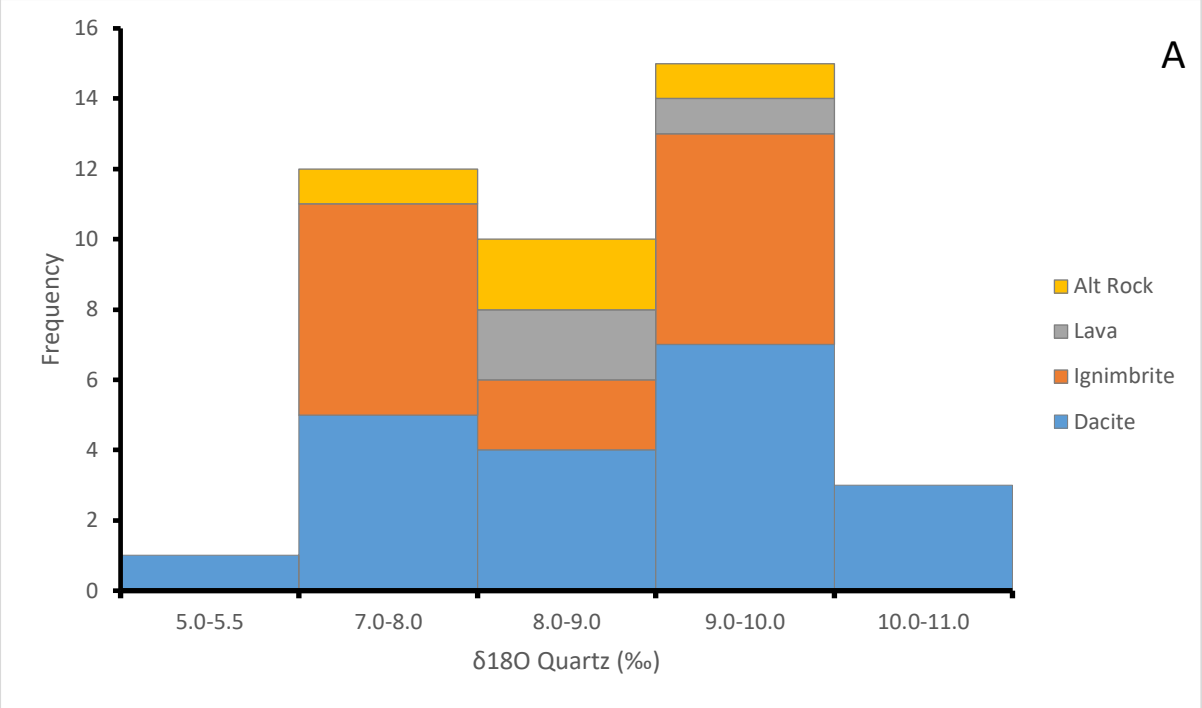

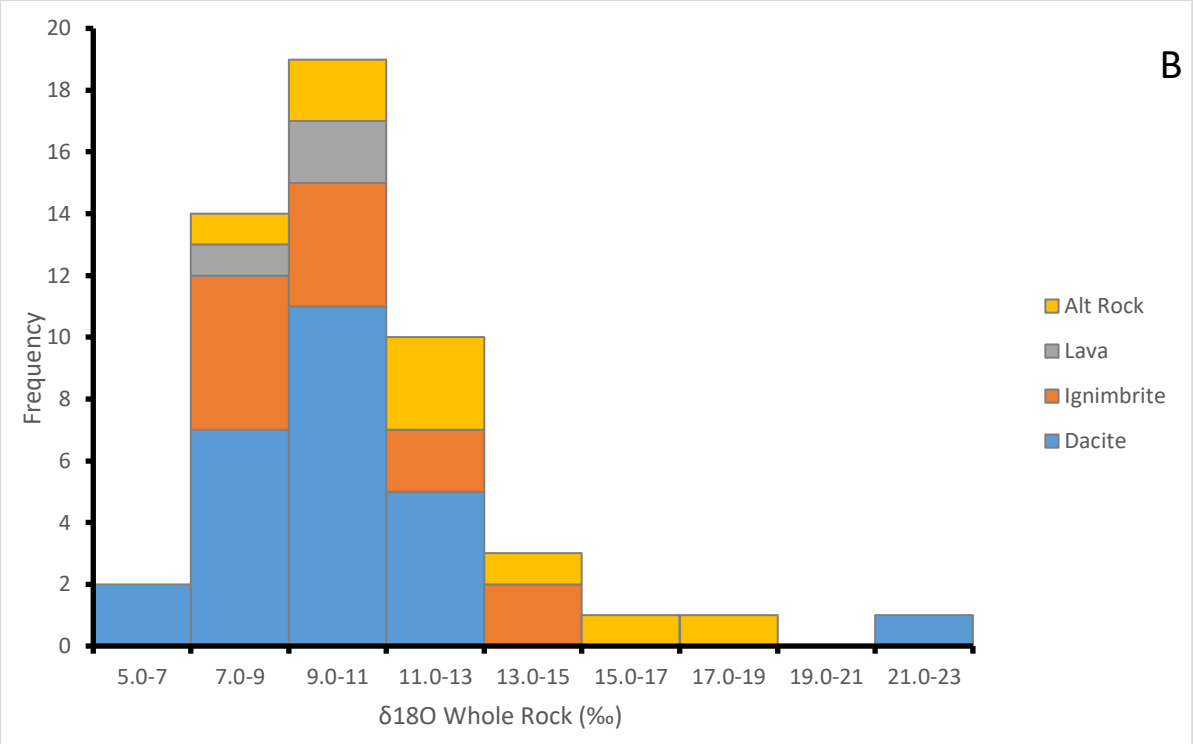

Figure 6.1: Histograms of quartz (A) and whole rock (B) $\delta^{18}O$ values showing the $\delta^{18}O$ compositions for the different rock types in the study; Alt Rock=Altered rock.

The relationship between quartz and whole-rock $\delta^{18}O$ composition with individual rock types is shown on Figure 6.2. Dacite domes show a moderate to strong positive correlation (r =1), where an increase in $\delta^{18}O$-quartz corresponds with a moderate increase in $\delta^{18}O$-whole rock composition. There is also a strong positive correlation (r =1) in altered rocks and lava, showing an increase in $\delta^{18}O$-whole rock with increasing $\delta^{18}O$-quartz composition. The correlation in ignimbrites is not strong (r =1).

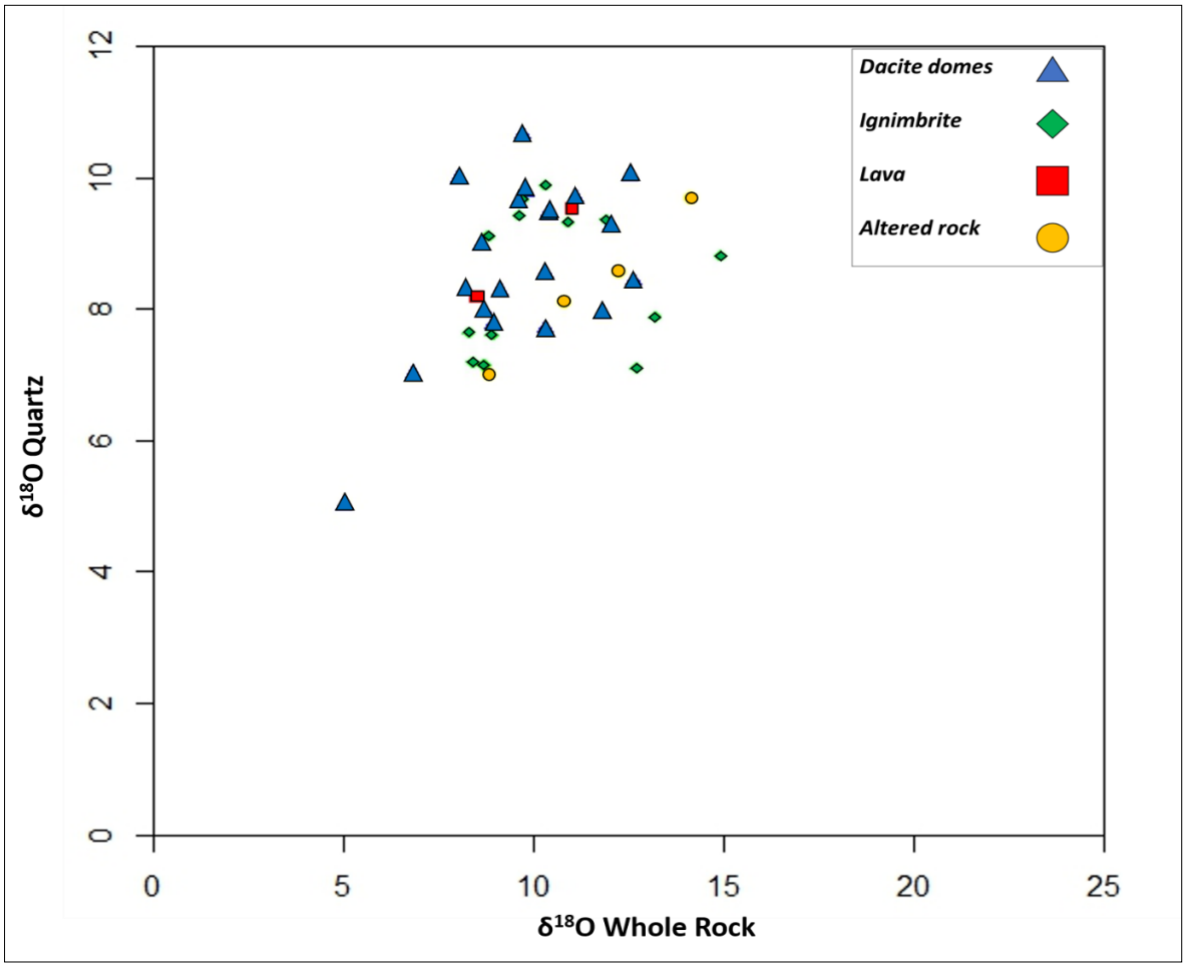

Figure 6.2: Plot of $\delta^{18}O$ quartz vs $\delta^{18}O$ whole rock in the same sample, and the correlation between these two variables in the individual rock types.

6.2. Hydrogen Isotopes

Nine samples were selected for hydrogen isotope analysis, two of these samples did not give out data, one of them did not have water (too fresh) and the other one's tube burst, possibly due to high sulphur content in the sample.) and the other burst out upon heating (may have too much volatiles). Table 5 presents the δD values and the water content in each rock sample. The whole-rock δD values for the CVZ dacites range from -32 to -102‰ and ignimbrites range from -74 to -119‰. The ignimbrites are independent of the water content (Figure 6.3). The dacite sample that has the highest δD value (-32), also has the highest water content (6.17 wt.%).

Table 5: δD values of selected rock samples from the CVZ and their water content (wt %).

Sample	**Rock type**	**δD Whole-rock**	**Wt % Water (H_2O^+)**
CS-19-08	Lava	-82	1.10
CS-19-14	Ignimbrite	-74	1.00
CS-19-25C	Altered rock	-118	0.29
CS-19-28	Dacite	-102	0.60
CS-19-37	Dacite	-85	1.53
CS-19-58	Ignimbrite	-119	1.56
CS-19-65	Dacite	-32	6.17

Notes: (wt %) water obtained by pyrolysis during H-isotope analysis

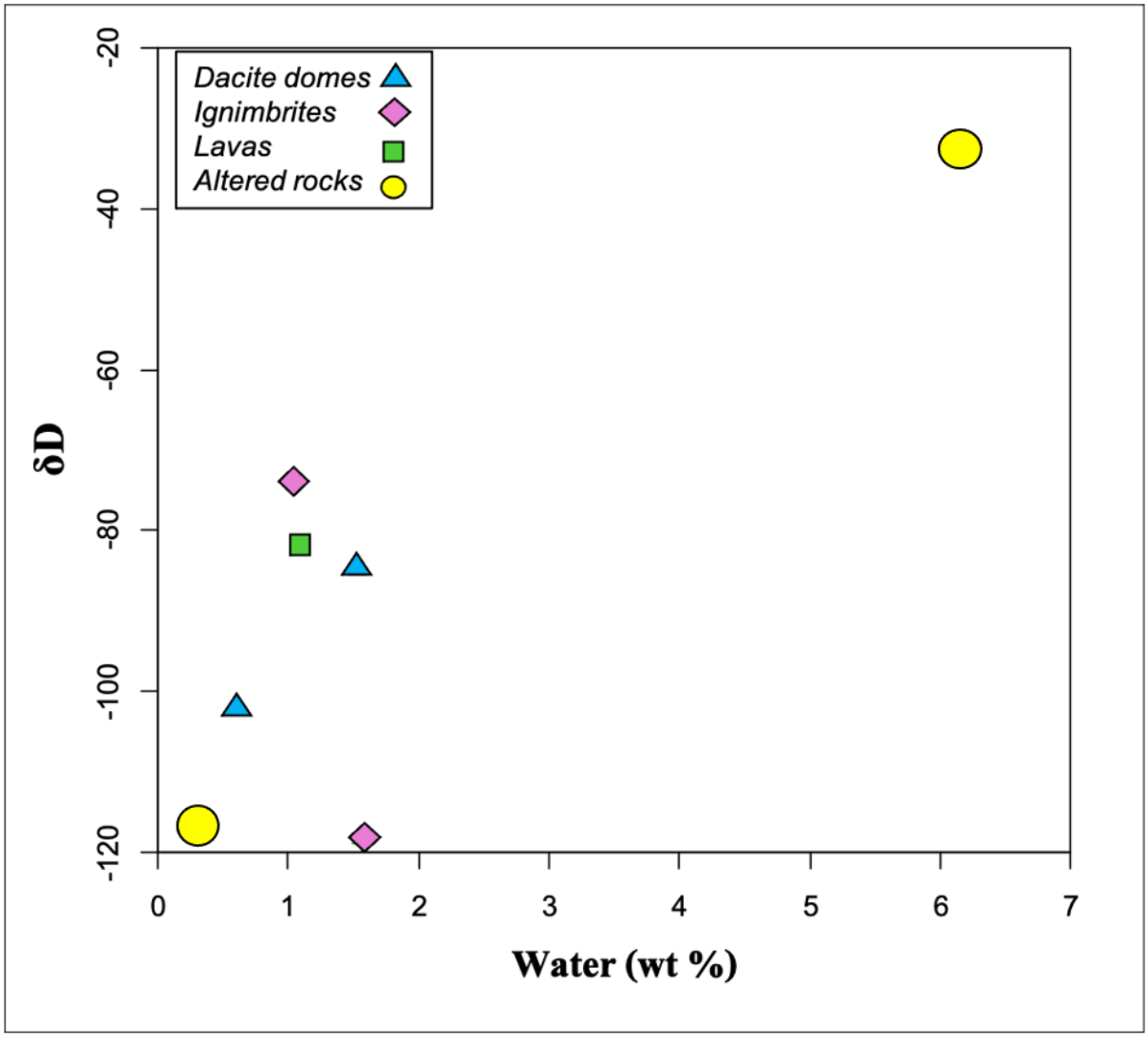

Figure 6.3: A plot of whole-rock δD (‰) values against water content (wt %) for selected rock samples from the CVZ.

6.3. Major and Trace Elements Geochemistry

Major and trace element analysis was done on nine selected bulk rock samples from the CVZ. Ignimbrites, dacites, lava and altered material are the rock types that were found across the study area and are all represented in this selection for the analysis of major and trace element geochemistry. Tables 6 and 7 present the major and trace element compositions of the selected whole rock samples, respectively.

6.3.1. Whole rock major element compositions

The SiO_2 values of the analysed rocks have a wide range, ranging from 55.5 to 90.5 wt%, corresponding to the felsic nature of all our samples in this study. In Figure 6.4, major oxides (TiO_2, Al_2O_3, Fe_2O_3, MgO, CaO, Na_2O, K_2O, P_2O_5) are plotted against SiO_2. With values ranging from 0.33-0.99 wt%, TiO_2 show a negative correlation with SiO_2 in dacites and ignimbrites, and the increase in TiO_2 corresponds with a decrease in SiO_2 composition. On the contrary, altered rocks show a strong positive correlation between SiO_2. An overall negative correlation is observed between Al_2O_3 and SiO_2, where Al_2O_3 decreases with increasing silica content in all the rock types. Na_2O (0.10-4.65 wt%) increases with SiO_2 in dacites and decreases drastically in altered rocks, ignimbrites also show a negative correlation between Na_2O and silica.

Table 6: Major oxide compositions of selected whole-rock samples of the CVZ.

Rock:	Ignimbrite			Dacite				Lava	Alt-Rock
Samples	CS-19-11	CS-19-14	CS-19-58	CS-19-28	CS-19-37	CS-19-41	CS-19-65	CS-19-08	CS-19-25C
Oxides (wt%)									
SiO_2	70.14	63.12	71.76	90.46	71.11	69.63	55.51	64.84	62.52
TiO_2	0.17	0.51	0.18	0.99	0.33	0.39	0.80	0.56	0.61
Al_2O_3	14.16	17.30	13.33	0.59	12.60	13.67	14.86	15.50	16.98
Fe_2O_3	1.36	3.65	1.59	0.14	2.23	3.14	3.18	3.84	5.73
MnO	0.10	0.07	0.13	0.03	0.11	0.12	0.04	0.10	0.09
MgO	0.02	1.44	0.17	0.02	0.05	0.36	0.03	1.36	0.60
CaO	1.34	4.15	1.24	0.09	1.89	1.61	0.29	3.63	4.22
Na_2O	3.64	4.65	3.61	0.10	3.08	3.83	1.23	3.21	4.27
K_2O	4.02	2.45	4.18	0.08	4.49	4.02	2.99	4.02	2.90
P_2O_5	0.06	0.24	0.06	0.05	0.09	0.09	0.12	0.15	0.20
SO_3	0.01	0.01	0.14	0.07	0.09	0.03	0.73	b.d	b.d
Cr_2O_3	0.02	b.d	b.d	b.d	b.d	0.01	b.d	0.01	b.d
NiO	0.02	b.d	b.d	b.d	b.d	0.02	b.d	0.04	b.d
H_2O-	0.29	0.14	0.37	5.14	0.18	0.21	0.96	0.22	0.30
LOI	4.02	1.31	2.48	1.31	3.00	2.18	18.16	1.64	0.87
Sum	99.38	99.08	99.24	99.10	99.25	99.29	99.34	99.13	99.30

Notes:

b.d. = "below detection" meaning that the concentration of the element was too low to quantify (generally <0.01 wt.% for major elements)

LOI = Loss On Ignition at 1000°C

H_2O^- = Loss of mass at 110°C

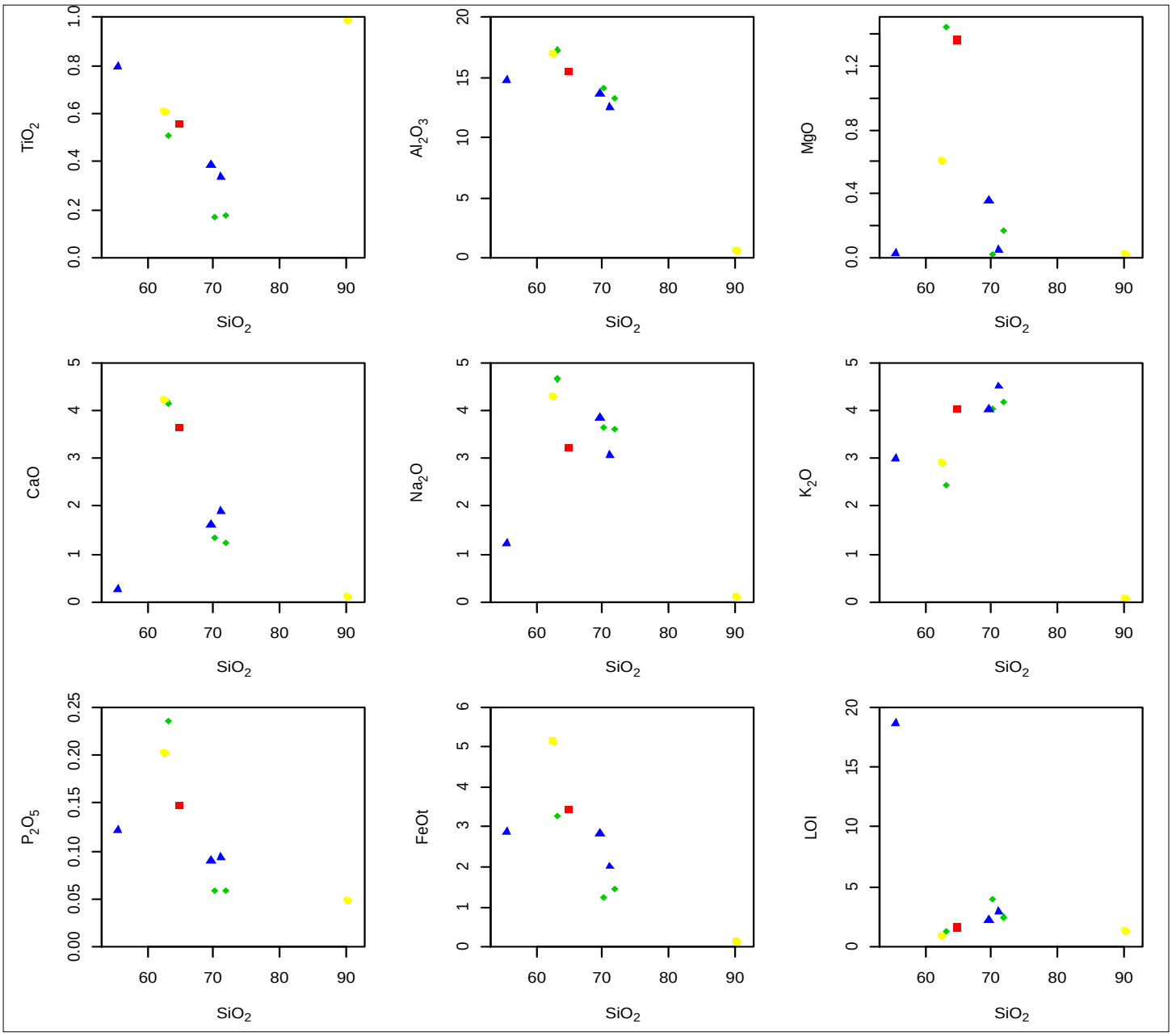

Figure 6.4: Major element variations of the studied rocks from the CVZ of the Andes plotted against SiO_2; ignimbrites, dacites, lava and altered rocks are presented in green, blue, red and yellow polygons, respectively.

6.3.2. Whole rock trace element compositions

The trace element concentrations are variable in the studied rocks. Table 7 shows all the trace elements that were analysed and the respective concentrations for each rock sample. The trace elements that have variable concentrations are plotted against SiO_2 in Figure 6.5 to observe the correlations that exist along the different rock types.

Table 7: Trace element compositions of selected whole rock samples of the CVZ (reported in ppm).

Rock Type:	Ignimbrite			Dacite				Lava	Alt-Rock
Samples	CS-19-11	CS-19-14	CS-19-58	CS-19-28	CS-19-37	CS-19-41	CS-19-65	CS-19-08	CS-19-25C
(ppm)									
Zn	46	36	32	<5	29	35	9	39	43
Cu	<5	45	<5	<5	<5	<5	<5	6	58
Ni	<5	<5	<5	<5	<5	<5	<5	<5	<5
Mo	<5	<5	<5	<5	<5	<5	<5	<5	<5
Nb	16	9	19	10	18	18	12	15	11
Zr	147	150	87	219	198	189	151	225	179
Y	24	13	25	12	27	28	8	19	15
Sr	214	883	140	119	103	171	353	374	649
Rb	138	60	163	2	195	179	96	197	130
U	<5	<5	<5	<5	<5	<5	<5	<5	5
Th	12	<5	11	<5	29	26	11	20	14
Pb	22	13	20	22	20	18	20	23	14
Co	6	<5	<5	<5	<5	<5	<5	<5	18
Mn	657	397	642	15	487	563	58	376	513
Cr	7	28	10	<5	36	20	92	71	36
V	47	76	84	89	<5	<5	81	75	97
F	161	759	210	972	440	121	114	270	115
S	273	287	486	438	290	270	11777	265	268
Cl	359	240	192	151	355	462	261	206	109
Sc	7	10	5	6	7	8	12	15	18
Ba	1235	1277	825	223	800	830	637	902	1109

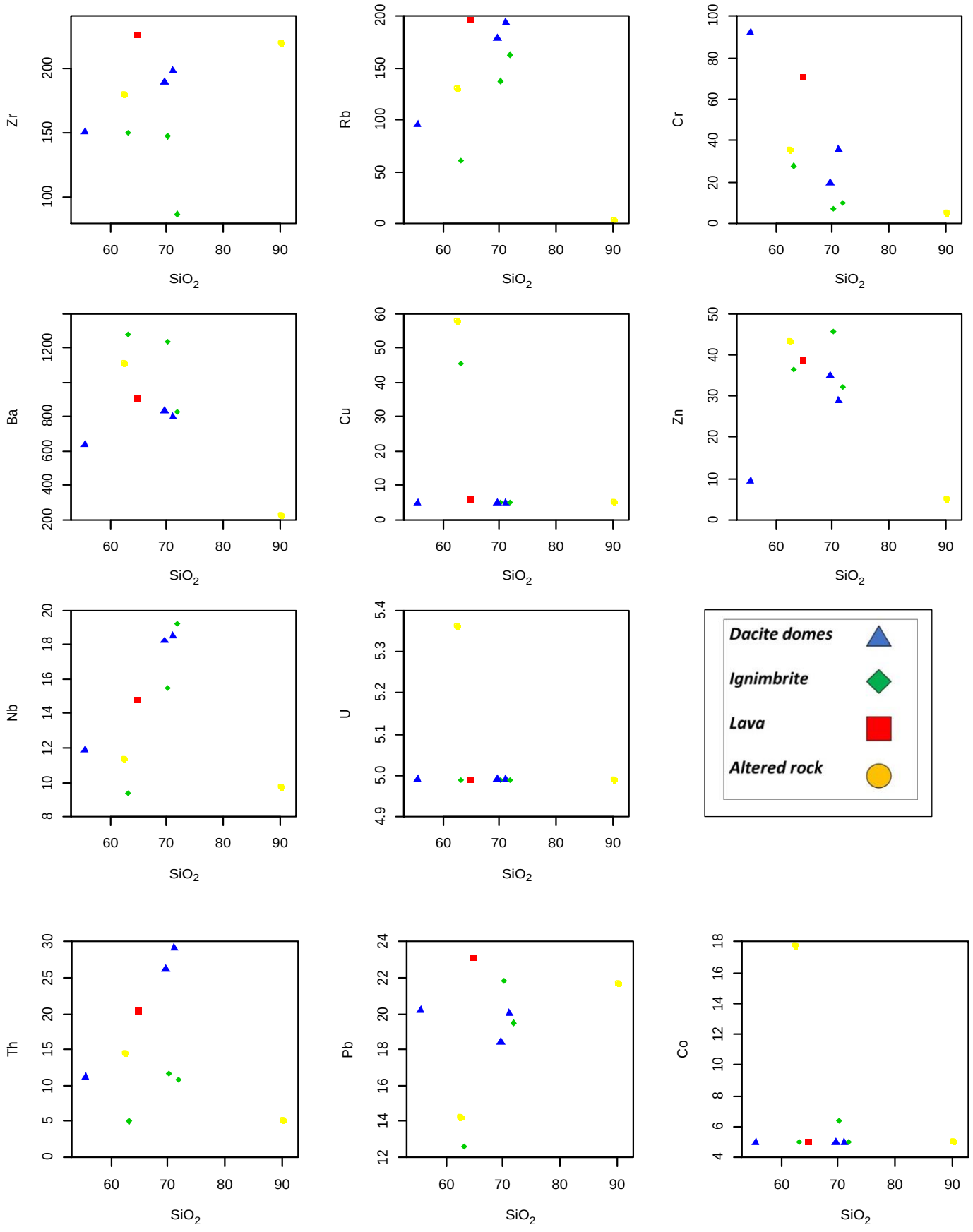
Zr
Rb
Cr
Ba
Cu
Zn
Nb
U
Th
Pb
Co
SiO2
Dacite domes
Ignimbrite
Lava
Altered rock

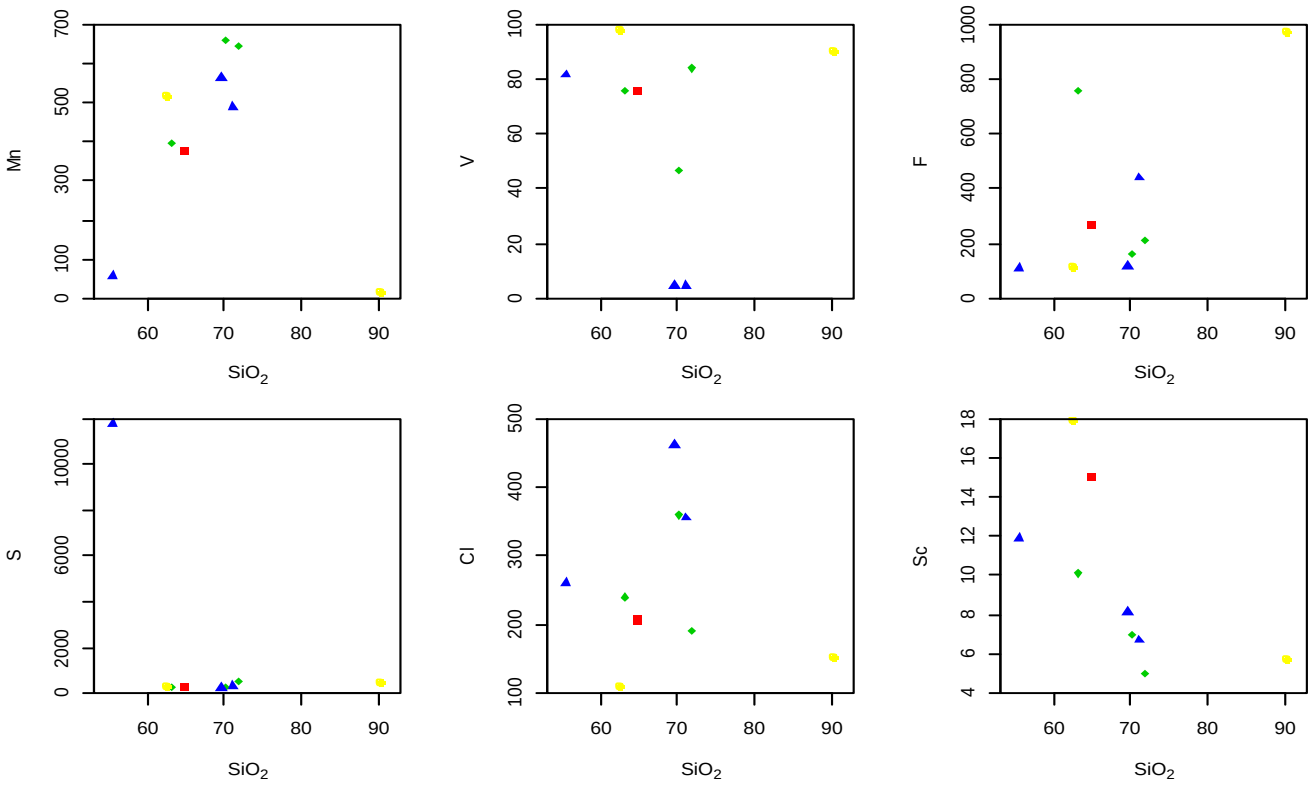

Figure 6.5: Trace element variation in the rocks from the CVZ of the Andes plotted against SiO_2.

Dacites and ignimbrites show a moderate positive correlation between Rb and SiO_2; however, in altered rocks, decreasing Rb corresponds with increasing SiO_2. A similar trend is observed Nb and Zn. Cr decreases as the silica concentrations of all the rock types increase, this correlation is also observed between Sc and SiO_2. Ignimbrites and altered rocks show a decreasing Ba trend with increasing SiO_2, whereas dacites demonstrate a positive correlation in this case. Th concentrations in dacites and ignimbrites increase with increasing SiO_2, showing a moderate positive correlation, Th then decreases in altered rocks with increasing SiO_2. In altered rocks and dacites, Zr increases as SiO_2 increases, the correlation begins to lack definition in ignimbrites. Pb and F increases with SiO_2 in altered rocks, F then continues to increase with SiO_2 in dacites whereas Pb decreases. There is a similar correlation between Co, Mn against SiO_2 in altered rocks, showing a negative trend. The other trace elements (V, S, Cl) do not demonstrate any significant correlation with SiO_2.

CHAPTER 7

Discussion

This chapter is aimed at discussing the key findings of this study, which include explaining the variation of $\delta^{18}O$ values and their spatial distribution across the Central Volcanic Zone. As discussed above, the main aim of this study was to determine (i) if low-$\delta^{18}O$ rocks and magmas exist and (ii) to answer the question why low-$\delta^{18}O$ magmas seem to be absent from subduction zone settings like the Andes.

7.1. Chemical Variation and Classification

The rocks show a variation on the TAS diagram (Figure 7.1), from dacite to rhyolite/trachyte. The lavas are all dacitic in composition and the ignimbrites vary from the dacite/trachydacite boundary, to rhyolite.

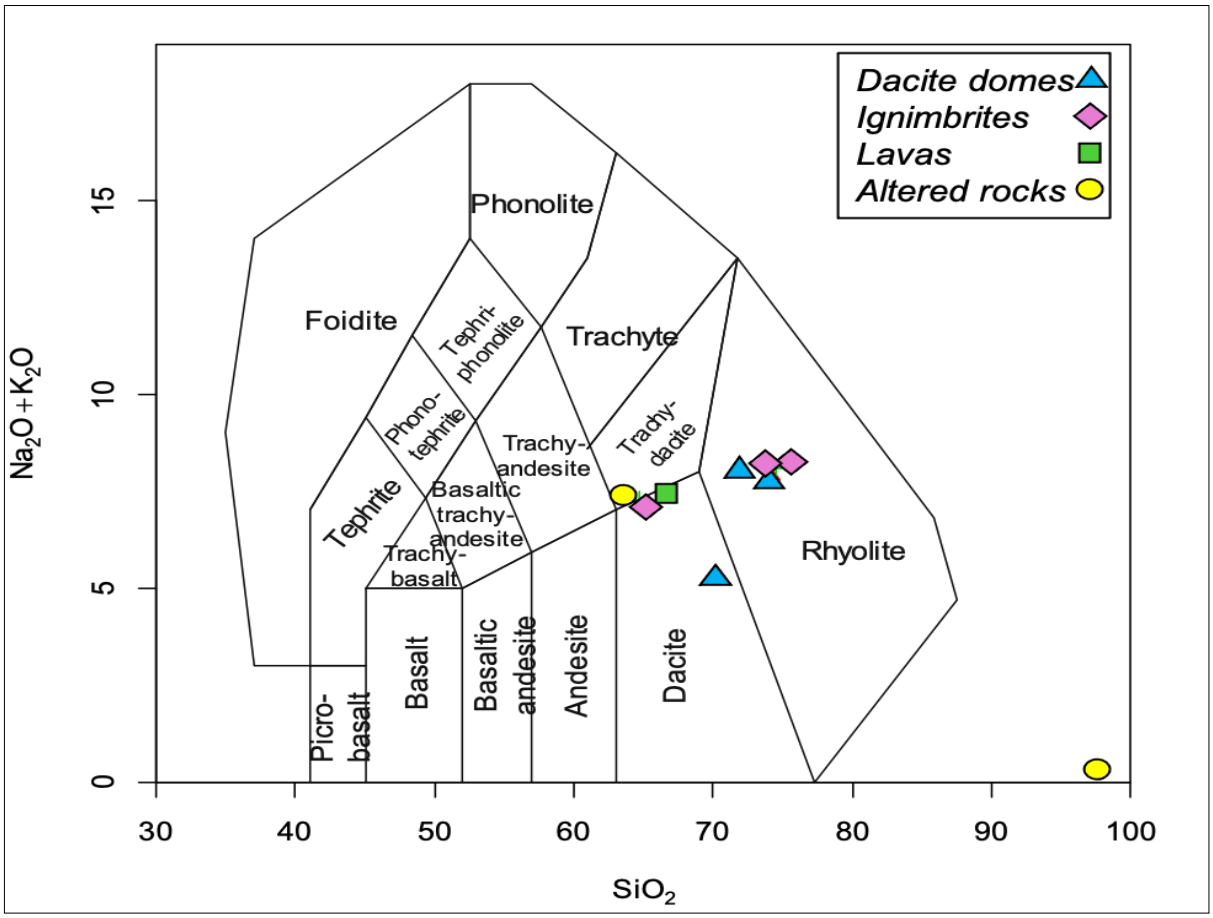

Figure 7.1: Total-Alkali vs. Silica (TAS) diagram for selected rock samples from the CVZ. The red, green, blue and yellow represent the lavas, ignimbrites, dacite domes and altered rocks respectively.

The altered rocks range from dacite to rhyolite. CVZ rocks have a medium-K calc-alkaline character, their TiO_2, Fe_2O_3, MnO, Al_2O_3 and CaO compositions decrease, and K_2O increase as the SiO_2 composition increases (Figure 5.3). These variations are consistent with the fractionation of plagioclase, pyroxenes and Fe-Ti oxides as is typical for magmas of this type and tectonic setting, e.g. Stern (2004).

Although it was not the purpose of this thesis to investigate the major and trace element variation and petrogenesis of the magmas in detail, it can be concluded that the petrological features observed in the CVZ rocks show that fractional crystallization played a major role in the origin of the dacites from andesitic/basaltic magmas. Magma mixing has occurred, coupled with fractionation processes, as signified by the disequilibrium textures (resorption and inverse zonations in plagioclase). This signifies mineralogical disequilibria and geothermometric effects (Matthews et al., 1994; Matthews et al., 1999; and Lindsay et al., 2001). CVZ magmas are considered hybrid, with crustal proportions of about 70% and 30% of mantle-derived basaltic andesites (e.g. Schmitt et al., 2001). There are more recent ideas around the end-member magma compositions and crustal contributions; where Blum-Oeste and Wörner (2016) and Freymuth et al. (2015) suggest that all magmas in the CVZ are derived from three end-end member compositions with varying amounts of crustal input. de Silva et al. (2016) described the rates of magma fluxes and the corresponding relationships of the crust to creating variable compositions of hybrid magmas.

7.2. Stable Isotope Variations in the CVZ

The quartz $\delta^{18}O$ values recorded in this study for the CVZ are higher than 7‰, which suggests that the magmas from which they crystallized have higher $\delta^{18}O$ values than expected in mantle-derived felsic magmas (up to ~6.5‰, e.g., Bindeman, 2001). The $\delta^{18}O$-quartz for this study range from 7.02 to 10.70‰, these O-isotope composition suggest involvement with assimilation and crustal melting processes. The variation in dacites is larger than the other rock types. Their whole rock $\delta^{18}O$ values range between 5.0 to 22.3 per mil. The lowest $\delta^{18}O$ value in this study is 5.0‰ and represents certain implications of mantle-derived magmatism. The ignimbrites range from 8.3 to 14.9‰, with an average of 9.7‰, they display the lowest average $\delta^{18}O$-value as compared to the other rock types. Lava flows and altered rocks range from 8.5 to 11.0‰ and 10.8 to 14.1‰ respectively. In essence, these values signify an increase in $\delta^{18}O$ and this is most likely to be the result of low-temperature alteration.

At 1000ºC, the fractionation factor between quartz and magma is 0.6‰ and is 0.2‰ between plagioclase and magma (e.g. Harris et al., 2018). The whole rock $\delta^{18}O$ values obtained for this study are significantly higher (average difference = 1.9‰) than those of the analysed phenocryst phases (quartz and plagioclase). This can be explained if oxygen isotope disequilibrium exists between phenocryst and matrix. Such behaviour is termed 'open system' and is most often influenced by low-temperature weathering (e.g. Muehlenbachs and Clayton, 1972). The variation of $\delta^{18}O$ values is wider in whole rocks and narrow in quartz/plagioclase phenocrysts of the same rocks in the CVZ. As explained by Taylor and Epstein (1962), the phenocrysts in a volcanic rock presumably coexisted simultaneously with enclosing groundmass, unlike in plutonic rocks where the minerals are often zoned and crystallized at different stages. In this regard, the $\delta^{18}O$ values of quartz/plagioclase phenocrysts and whole rock may differ significantly. In this study, we observe the same pattern; the dacites, ignimbrites and altered rocks all have very high $\delta^{18}O$-whole rock values when compared to their $\delta^{18}O$-quartz/plagioclase values. The lavas seem to show a close range of $\delta^{18}O$-whole rock and quartz values; ranging from 8.5 to 11.0‰ and 8.2 to 10.0‰ respectively. Considering this, the phenocrysts in the lavas are more suitable to provide reliable estimates of the original whole rock $\delta^{18}O$ values.

Figure 7.2 shows the variation of whole rock $\delta^{18}O$ values plotted against the $\delta^{18}O$ values of quartz phenocryst separates from the same rock samples. These results show that some of the quartz $\delta^{18}O$ values closely approach the expected values in equilibrium with the whole-rock, considering that these crystals are visibly pristine and the isotopic fractionations are smaller. When looking at the whole rock $\delta^{18}O$ values, larger differences between quartz and whole-rock $\delta^{18}O$ are observed, with the whole-rock $\delta^{18}O$ values about 0.5-5.0‰ higher than the quartz phenocryst values of the same rock sample. The variation in whole-rock $\delta^{18}O$ values is larger than that of quartz. In altered rocks, for every 2‰ increase in whole-rock $\delta^{18}O$, there is a 1‰ increase in $\delta^{18}O$ of quartz, the alteration seem to affect quartz to some extent as observed on Figure 7.2. Quartz is generally considered to be unaffected by low-T alteration, so it is most likely that shifts in whole-rock $\delta^{18}O$ values have occurred.

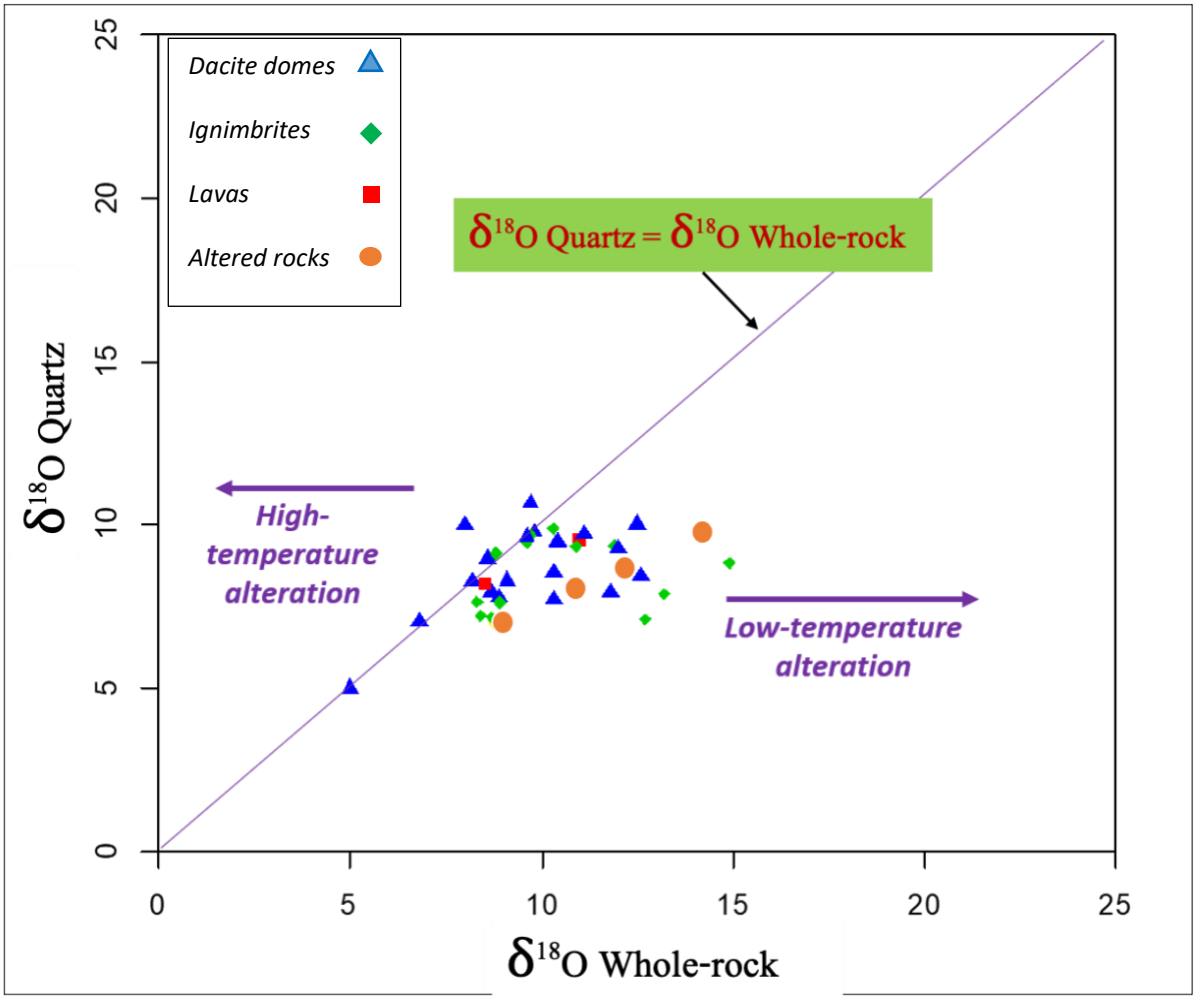

Figure 7.2: Oxygen isotope values of quartz mineral separates in the CVZ vs whole-rock $\delta^{18}O$ values. The diagonal line indicates fractionation $\delta^{18}O$ quartz = $\delta^{18}O$ whole-rock, and the arrows schematically illustrate the effect of low and high-temperature alteration on whole rock $\delta^{18}O$ values, increasing form either sides of the magmatic equilibrium line.

In the whole rocks of this study, the groundmass in 49 samples out of 51 were enriched in $\delta^{18}O$, which then contributes to the higher $\delta^{18}O$ values relative to their phenocrysts. The $\delta^{18}O$ values of the quartz phenocrysts in this study are not consistent with contamination by a low-$\delta^{18}O$ material, but instead require the presence of a crustal component with high $\delta^{18}O$ values. In the Southern Volcanic Zone (SVZ) of the Andes, Grunder (1987) documented $\delta^{18}O$ values that are lower, relative to those common in the CVZ (Figure 7.3).

These values range from 5.0 to 6.3‰, and belong to the Calabozos Caldera Complex. The slightly low-$\delta^{18}O$ values of the lavas in the Calabozos Caldera were found to have been caused by a low-$\delta^{18}O$ contaminant; a long-lived intermediate-to-silicic magma reservoir, which acted as a driving force for extensive meteoric hydrothermal circulation. The SVZ contains a thinner continental crust (~30 km), whereas the CVZ has thicker continental crust, reaching a thickness of about 70 km; this could explain the differences in the amount of crustal input in $\delta^{18}O$ values for the different Andean regions.

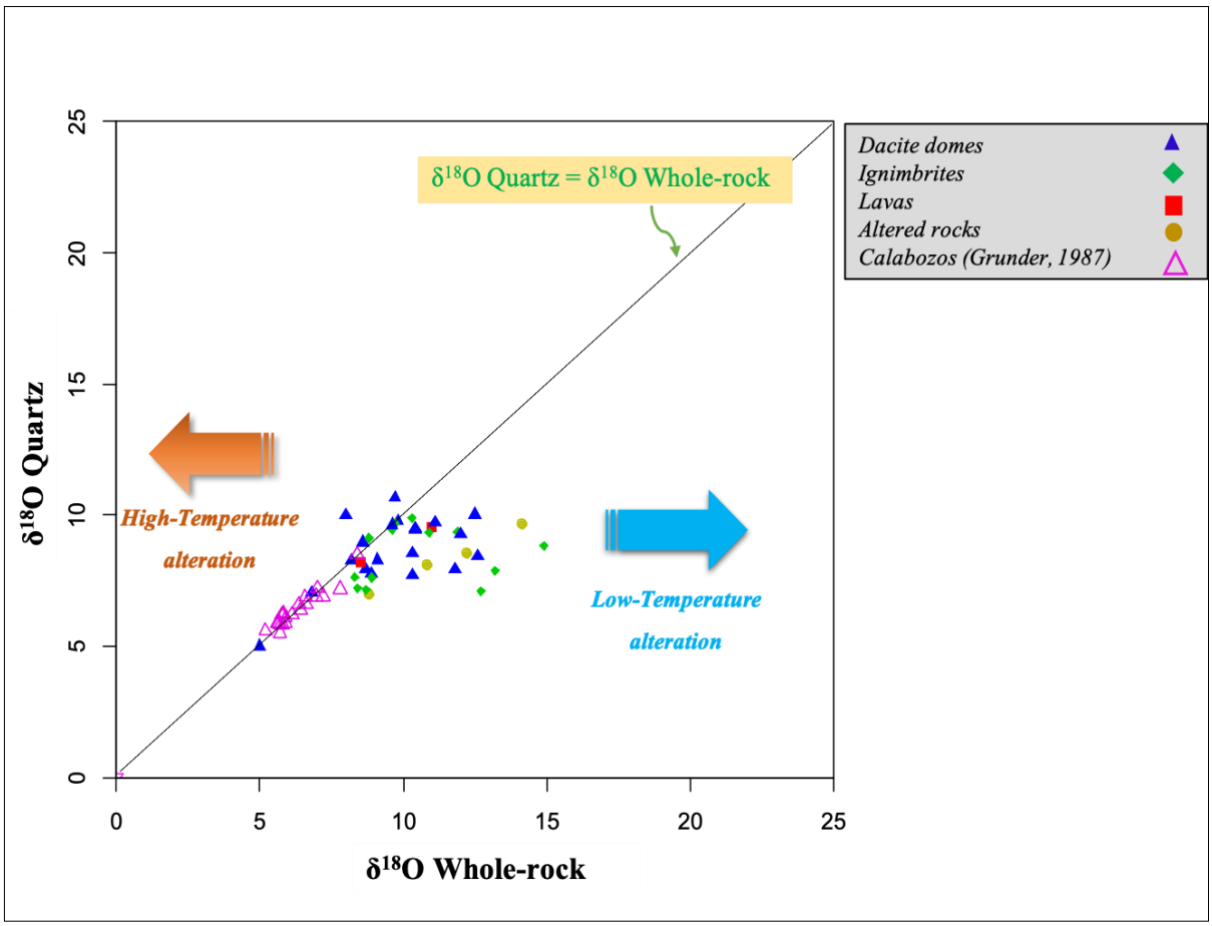

Figure 7.3: A plot of $\delta^{18}O$ quartz versus whole-rock, showing the comparison between the CVZ samples of this study and SVZ (Calabozos) samples from a study by Grunder (1987).

It is also worthy to note the relationship between $\delta^{18}O$ of quartz and whole rock against SiO_2 (Figure 7.4). Increasing silica content generally brings about a progressive but small increase in $\delta^{18}O$ of the melt, when an equilibrium is maintained during the process (Whittington et al., 2009). The SiO_2 composition in whole-rocks is variable, with a wide range (60 to 75 wt.%), with one sample of very altered rock with the highest value (91 wt.%). These correspond with the variability of the $\delta^{18}O$ of whole rocks, signifying a certain degree of O-isotope enrichment. The $\delta^{18}O$ values of quartz phenocrysts do not show any significant dependence on the wt.% of SiO_2.

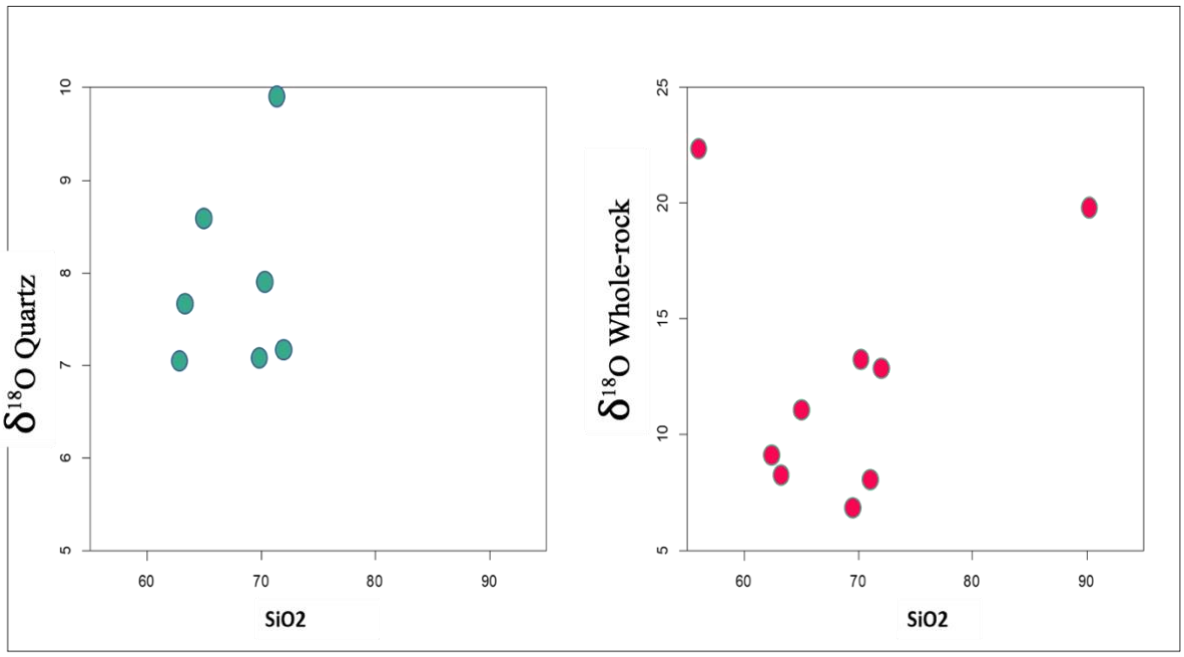

Figure 7.4: Relationship between $\delta^{18}O$ and silica content for selected rock samples from the CVZ.

7.3. Hydrogen Isotopes

The whole-rock δD values for the CVZ dacites range from -32 to -102‰ and ignimbrites range from -74 to -119‰ (see Table 5). The ignimbrites are independent of the water content (see Figure 6.3). The altered rock sample that has the highest δD value (-32), also has by far the highest water content (6.17 wt.%). In this sample, there may have been a direct addition of water or hydrothermal reaction during the alteration process that raised the δD value, as there is little fractionation during these processes. The overall δD data in this study do not show very negative values. This indicates that there is a lack of interaction between rock and low-δD water in the CVZ. Water with low- $\delta^{18}O$ values (and implication of low-δD) is a requirement for low-$\delta^{18}O$ rocks to occur. This confirms the O-isotope data in this study that there is no evidence for interaction with meteoric water with low-δD. This data corresponds with low-temperature alteration and hydration by water that is not δD-depleted, which generally lowers the δD signatures of the material (Kyser and O'Neil, 1984; Kyser, 1986; Chacko et al., 2001).

7.4. Spatial Variation of $\delta^{18}O$ Across the CVZ

There is no clear relationship between $\delta^{18}O$ values of either quartz and whole-rock with latitude/longitude across the study area in this study (Figure 7.5). The distribution of the $\delta^{18}O$ is mostly a function of the rock types and the volcanic units to which the rocks belong to (Table 8), the $\delta^{18}O$ values are therefore directly related to how the different rock types are distributed across the area. All the rocks in this study belong to the Altiplano-Puna Volcanic Complex (illustrated in Figure 7.5), which is major volcano-tectonic province that developed in response to the late Miocene ignimbrite flare-up that took place in the CVZ. The volcanic centres that were sampled in this study include the Chao dome, Turi lava, Toconce volcano, Chillahuita dome, Ollagüe, Cerro Overo and San Pedro de Atacama volcanoes; these individual but connected volcanoes form a chain that traverses across the Chilean Central Andes. There is varying distribution of $\delta^{18}O$ values in the rocks across this chain.

Table 8: The $\delta^{18}O$ values of different rock types at different latitudes across the studied volcanoes of the CVZ.

Location		**$\delta^{18}O$ Values (‰)**		
Latitude	**Volcanic unit**	***$\delta^{18}O$-Quartz***	***$\delta^{18}O$-Whole Rock***	***$\delta^{18}O$-QzWR Average***
21ºS	Ollague	7.02-8.56‰	8.2-19.9‰	10.0‰
22ºS	Chao dome	9.43-9.77‰	9.1-10.4‰	9.7‰
	Turi lava	9.33-9.53‰	10.9-13.2‰	10.4‰
	Toconce volcano	7.64-9.70‰	8.3-14.9‰	10.2‰
	Chillahuita dome	8.12-10.66‰	9.7-14.1‰	10.7‰
	San Pedro de Atacama volcanoes	5.00-9.89‰	5.0-22.3‰	9.0‰
23ºS	Cerro Overo maar	7.02-10-02‰	6.8-12.5‰	9.1‰

There is no relationship between $\delta^{18}O$ values and latitude (Figure 7.6 and Table 8). The variation in O-isotopic signatures across the CVZ can be related to the nature of each volcanic centre; these could be the magma composition, the age and the nature of the crust that has been traversed by the different volcanic regions across the CVZ. Crustal thickening, crustal shortening, magmatic underplating and lithospheric hydration all may have played a role in influencing the $\delta^{18}O$ values of the rocks in the study area. The area that was studied, the Altiplano-Puna Volcanic Complex (illustrated in Figure 7.5), belongs to an Andean region (Central) with the thickest crust (up to <70 km). Prior studies (e.g. Isacks, 1988; Tosdal et al., 1984; Victor et al., 2004) have suggested that this thick crust is a result of crustal shortening and magmatic underplating or both, with more crustal shortening on the Eastern Cordillera and more magmatic underplating and lithospheric hydration below the Western Cordillera.

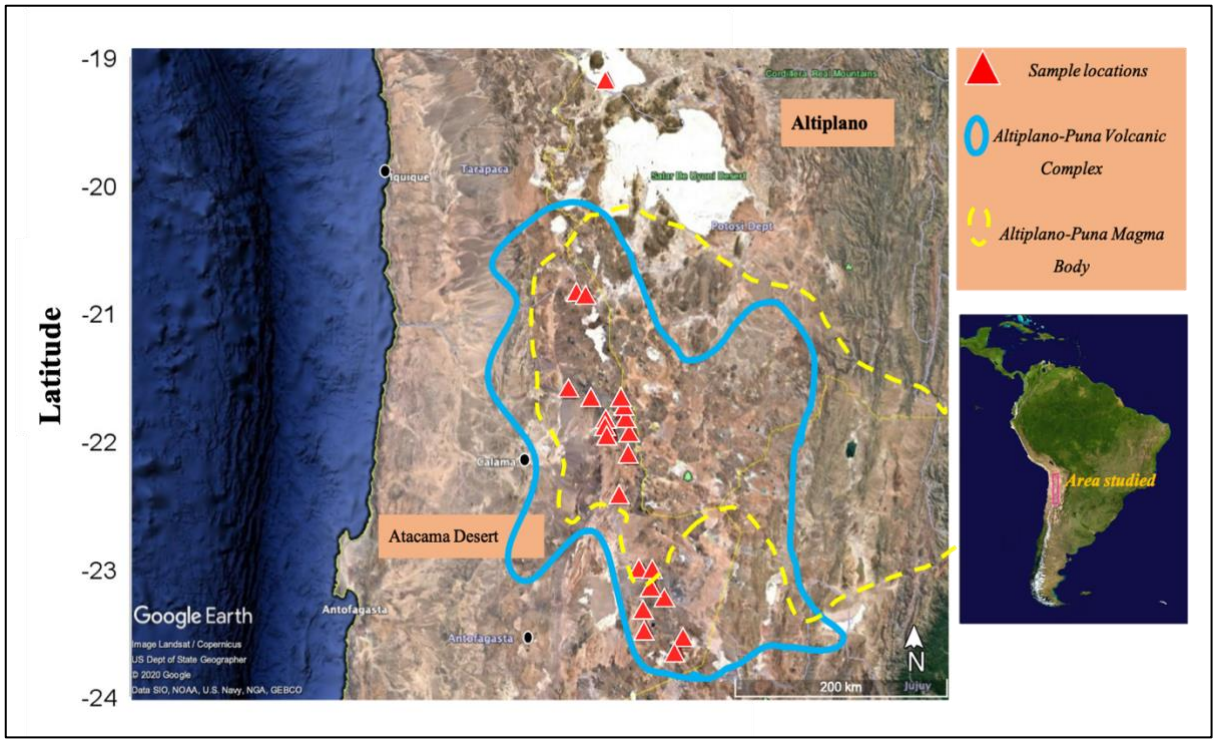

Figure 7.5: Location map of the APVC (solid blue line), with the sampled volcanic centres (red triangles) and the geographic outline of the APMB in dotted yellow lines (Adapted from Godoy et al., 2019).

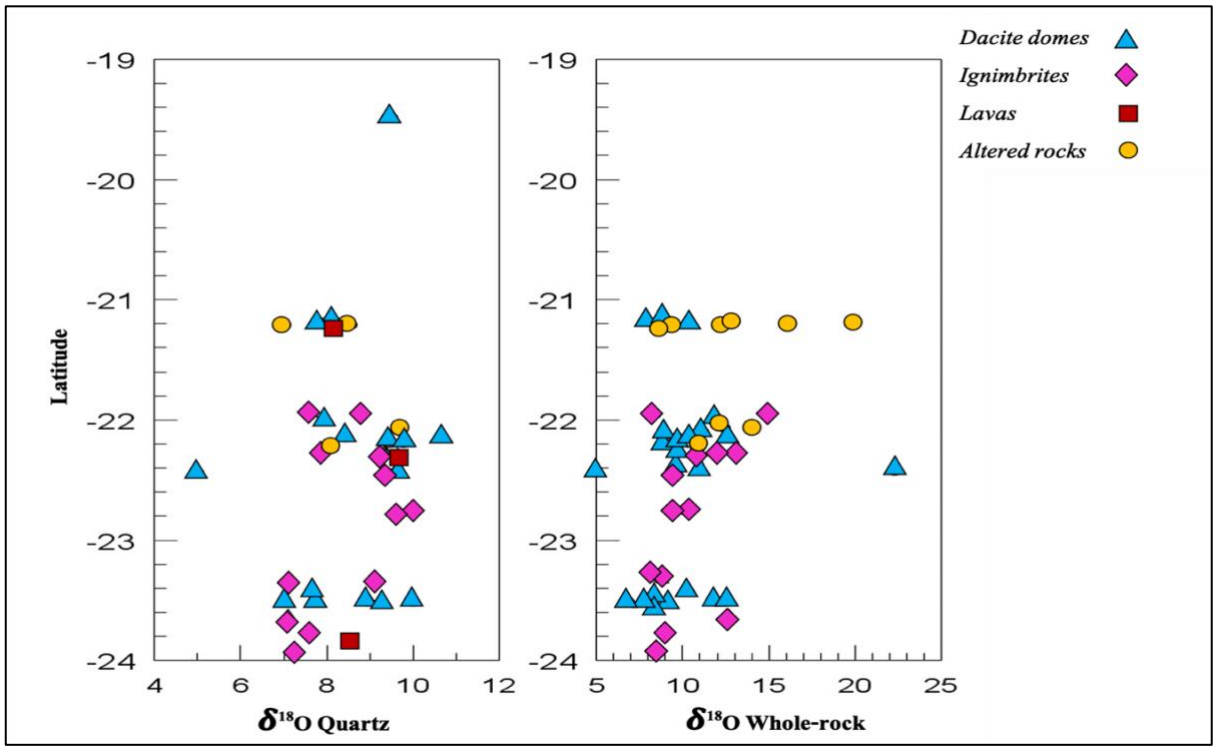

Figure 7.6: Variation of $\delta^{18}O$ values of whole-rock and quartz/plagioclase phenocrysts with latitude across the study area, per rock type.

CVZ magmas have elevated $^{87}Sr/^{86}Sr$ as well as high $\delta^{18}O$ values (as data from this study also shows), they also have lower $^{143}Nd/^{144}Nd$ than magmas in the Southern Andes (Schmitt et.al., 2002). These data are consistent with greater amounts of the continental crust that have been incorporated in the CVZ than in the SVZ. The CVZ has an extremely thick crust and high rates of subduction erosion, these aspects play a role in determining what is being incorporated into the magma, thus defining the composition of the magma (James, 1982; Wörner et al., 1988; Barrero, 1984; Davidson et al., 1991; Francis and Hawksworth, 1994; Schmitt et al., 2002). Stern (1990) also concluded that there is a good correlation between increased subduction erosion, source region contamination and increased importance of crustal components, which in turn influence the isotopic composition of magmas; in the CVZ, temporal variations indicate that the extent of crustal contamination of volcanic rocks has increased through time, from prior Miocene to Recent, with the crust thickening up to ~>70 km. This could mean a shift in magmatic compositions through time to more upper crustal. Ignimbrites are the oldest rock units in this study (12 Ma), these ignimbrites were followed by the formation of most of the Recent rock units in the area (andesitic and rhyodacitic stratovolcanoes). In the CVZ (this thesis) and in the findings of Feeley and Sharp (1995) on Volcàn Ollagüe, they have $\delta^{18}O$ values that are higher than the older rocks.

7.5. Controls on the Variation in $\delta^{18}O$ Across the CVZ

The $\delta^{18}O$ values of the magma depend on the source of the magma and fractional crystallization as well as assimilation. In this study, the magma could be melted crust or mantle-derived with accompanying assimilation processes. The average quartz $\delta^{18}O$ value is about 9‰ in this study, which is consistent with a melted crust. Feeley and Davidson (1994) established that; mantle-derived magmas at Ollagüe volcano in the CVZ have evolved by contamination and fractional crystallization to basaltic-andesitic composition. These processes reduce the density of the magmas and allow them to migrate to shallow crustal levels, where they accumulate magma chambers that are stratified and periodically refilled with basaltic-andesitic magmas. Feeley and Sharp (1995); Figueroa (2009); Matthews et al. (1994) identified an open system magmatic differentiation, that played a role in the change in isotopic compositions with indices of magmatic differentiation, which was interpreted as a result of assimilation plus fractional crystallization. The isotopic compositions in this study relate to the findings by Wörner et al. (1992) and Aitcheson et al. (1995); as they indicate an important part of crustal contamination of CVZ magmas that occurred by intracrustal assimilation, coupled with crystallization of these magmas, and these compositions are difficult to model because there is no apparent

exposure of the crust. Quartz-magma fractionation also define the O-isotopic values in this study. In most cases, the $\delta^{18}O$ of quartz equals that of the magma. In this study, the quartz-magma fractionation factor is about 0.6‰.

The wide variation in O-isotopes is generally a result of a complex petrogenetic evolution that involves primary mantle-derived magmas, as established in the works of Hawksworth et al. (1982); Schneider (1987); and Davidson and de Silva (1995), similar variations are observed in this study. These magmas are then modified by deep crustal interactions to produce magmas with baseline isotopic compositions that are parental to those that erupted at the surface. Parental magmas have subsequently evolved at shallower levels through assimilation-crystallization processes that involve the upper crust and magma mixing with restrictions to a low-isotopic contrast end-member (Stern, 1988).

Rogers and Hawksworth (1989) suggested that the enrichment of isotopic values in the CVZ are due to an increasing involvement of ancient enriched subcontinental lithospheric mantle as magmatism migrated eastward during the Miocene. The increased enrichment of the arc magmas is a result of the gradual enrichment of the mantle-wedge due to the increased influence of the subducting components and asthenospheric mantle influx (Jones et al., 2015; Parada, 1990). The influence of subducting components on the melt source region and increased contamination of arc magmas with existing continental crust en-route to the surface are the two prominent processes that have been identified to have played a significant role in the enrichment of the CVZ magmas. Both processes are attributed to the shallowing angle of the subducting Nacza plate and increased compression along the margin as well as continued crustal thickness (Jones et al., 2016).

7.6. Alteration

A spring from the El Tatio geothermal field in Calama (-22º13'46"S/-68º16'52"W) was sampled in this study to get an overview of the $\delta^{18}O$ values of the meteoric waters in the area, noting that the upper crust is an important source of these meteoric waters and a host for most geochemical processes. This geothermal field has chloride-rich and sulfate-rich waters; the isotopic signatures of the chloride-rich waters are controlled by magma degassing and water-rock interactions, whereas the sulfate-rich waters are fed by shallow meteoric water that is heated by descending gases (Cortecci et al., 2005).

At 200°C, the fractionation factor between 'rock and water' is 6‰, and 1.3‰ at 400°C (Figure 7.7). Here, the 'rock' fractionation is assumed to be that of plagioclase (An_{30}). Interaction between rock and water at 200°C would result in a rock having a $\delta^{18}O$ of -2.5‰, if they reached equilibrium (i.e. the water/rock ratio was extremely large). At high temperature, the $\delta^{18}O$ of the rock after interaction would be <-2.5 per mil. The rock values are all much higher in this study.

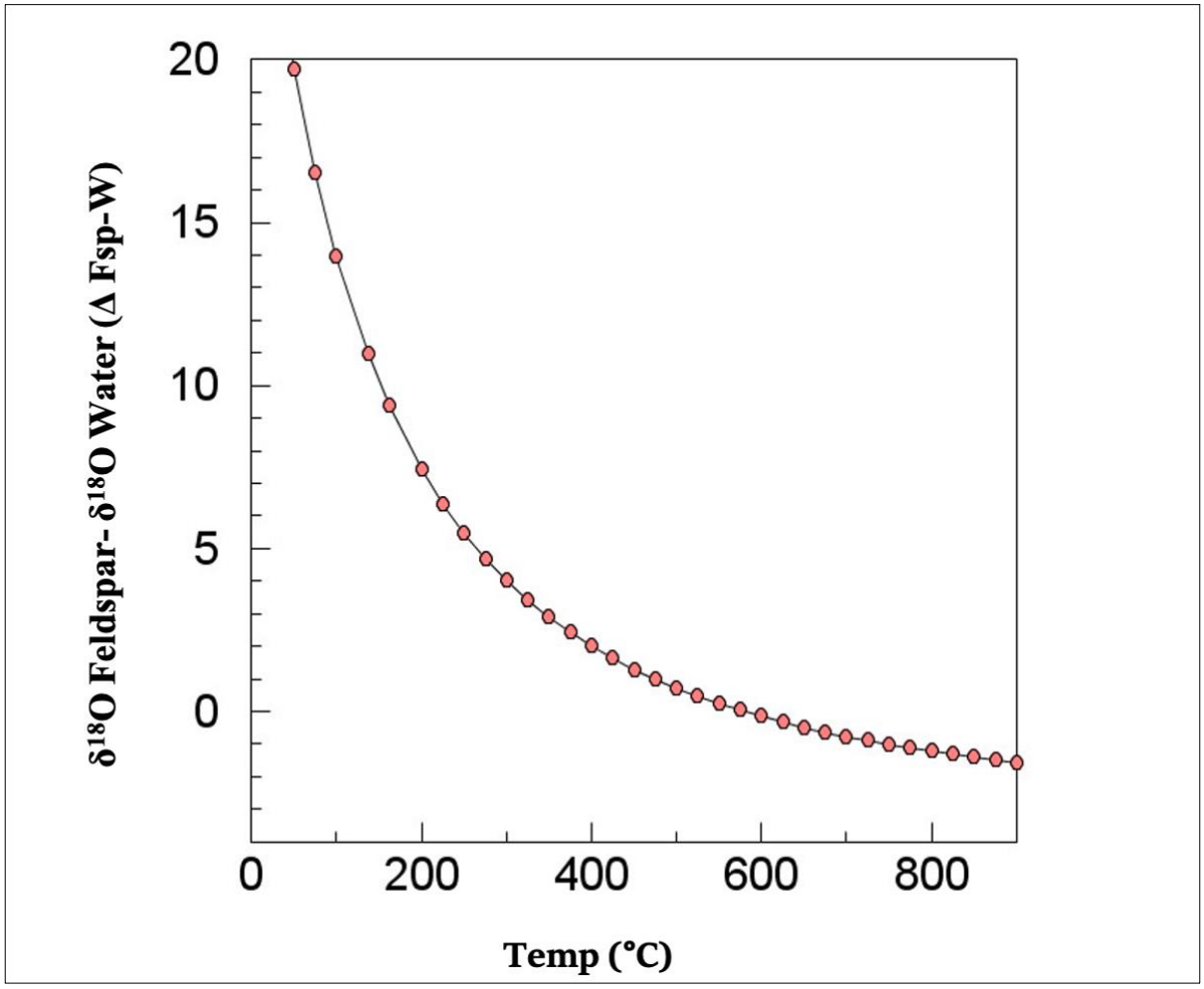

Figure 7.7: Plot of $\delta^{18}O$-Fsp- $\delta^{18}O$ water vs temperature, where feldspar is plagioclase An_{30} (using equations of Clayton et al., 1972).

Whole rock O-isotope data in this study represent influence of secondary alteration, these effects are generally dependant on the $\delta^{18}O$ of water (which also depends on temperature, altitude and water-rock ratios). The study area is dominated by arid climate and this reduces the potential for hydrothermal alteration processes.

Cortecci et al. (2005) found the meteoric waters in the El Tatio geothermal field to have H and O isotopic values that range from δD= -58 to -47‰ and $\delta^{18}O$ of -8.8 to -6.8‰. In this study, a single sample of El Tatio water in Calama had $\delta^{18}O$ and δD values of -8.5‰ and -50‰ respectively; these values are within the range of Cortecci et al. (2005). These isotopic values indicate the composition of the meteoric waters that interact with the magmas in the region and the hydrothermal alteration thereof.

In shallow intrusions that are emplaced into rocks charged with groundwater, there will be an exchange or influx of hydrothermal material into the magma. This can result in a large reduction in the $\delta^{18}O$ value of the magma, this is because meteoric waters are much lower in $\delta^{18}O$ than the common igneous rocks, especially in magmas emplaced at high altitudes (Taylor, 1968). The lowest $\delta^{18}O$ value recorded in this study is 5.0‰ for both quartz and whole-rock, this dacite could have been partially melted by a hydrothermal material that has depleted $\delta^{18}O$ signatures. It is important to note that the interaction at both 200°C and 400°C would give a low-$\delta^{18}O$ rock.

7.7. Why Are There No Low-$\delta^{18}O$ Magmas in the CVZ?

Rocks from this study belong to the Neogene Central Andean Ignimbrite province. This, in the words of de Silva et al. (2006) is a surface manifestation of a subduction-related magmatic flare-up. It was concluded by de Silva et al. (2006) that the Central Andean ignimbrite flare-up produced temporally and spatially homogeneous magmas with high $\delta^{18}O$ values. In this study, the average $\delta^{18}O$ value for quartz is 8.6‰ and 10.5‰ for whole rock, this agrees with the conclusions of Folkes et al. (2013), that there is a 'close member resemblance' over ~10 Ma. It has been established in this study that meteoric water interaction with volcanic rocks had little or no effect on bulk rock $\delta^{18}O$ values; if anything, raising rather than lowering them. The isotope composition of meteoric water, and the extent of hydrothermal alteration (the water/rock ratio), are the two main factors that were expected to have lowered the $\delta^{18}O$ values of bulk rock in the region under study. Folkes et al. (2013) discussed the enriched $\delta^{18}O$ character of the Central Andean rocks using quartz phenocryst $\delta^{18}O$ values as a proxy for magma $\delta^{18}O$ values, particularly for the rhyodacitic ignimbrites. In attempt to account for this $\delta^{18}O$ enrichment, factors such as the tectonic history and climatic conditions were placed at the centre of this $\delta^{18}O$ enrichment in the region. In this study, both quartz phenocrysts and whole-rock $\delta^{18}O$ values have been presented. The latter are essential to assess the nature of near surface hydrothermal alteration, and to see if source material for low-$\delta^{18}O$ magmas exist in the CVZ.

Convergence and climate on meteoric-hydrothermal alteration

The CVZ magma $\delta^{18}O$ values in the CVZ appear to increase with the increasing rates of crustal thickness and elevation. Folkes et al. (2013) compared these CVZ conditions with Kamchatka in the USSR, where Chesko (1994) and Bindeman et al. (2004) documented low-$\delta^{18}O$ values that correlated with a decrease in average crustal thickness and elevation, as well as increase in the amount of precipitation and presumably interaction with extremely low-$\delta^{18}O$ glacial melt waters. In the CVZ we observe the opposite of this; there is known evidence for low precipitation (100-350 mm/year), high aridity and high elevation (>3500 m) in the last 10 Ma, and few glaciers if any (Strecker et al., 2007). This period coincides with the eruption of large scale silicic volcanism from which the studied rocks were formed. In this regard, there is possibility that the prevailing climatic and tectonic conditions in the CVZ may have resulted in the lack of $\delta^{18}O$ rock and magmas in the region. Folkes et al. (2013), concluded that there has been a limited supply of meteoric water in the Central Andes, and that these conditions may have been in place since at least the last 10 Ma (period of the major silicic volcanism). Folkes et al. (2013) concluded that this is the main cause of the lack of low-$\delta^{18}O$ values.

The El Tatio and Sol de Mañana are the only prominent geothermal fields in the CVZ (de Silva and Francis, 1991). In this study, waters from El Tatio were sampled and the δD and $\delta^{18}O$ values were determined. The $\delta^{18}O$ of the meteoric water were certainly low enough (-8.5‰) to cause low-$\delta^{18}O$ values in the rocks that interacted with it at >200°C. Balsley and Gregory (1998) also suggested that lack of water content in whole rocks indicates that they did not exchange with meteoric waters. The rocks of this study have relatively low water content (1.8 wt.%) (Table 4). In view of this, we conclude that water-rock ratios were low during any alteration. When the water/rock ratio is low, the O-isotope composition of the fluid is shifted towards that of the rock. Thus, the findings of this thesis do not preclude interaction of the altered rocks with water of surface (meteoric) origin, just that the effects of alteration did not extend to lowering the $\delta^{18}O$ values of the rocks.

Studies by Barnes and Ehlers (2009), Bywater-Reyes et al. (2010) and Strecker et al. (2007) have established that the CVZ region is generally a highly elevated, arid plateau with very low precipitation and high evaporation rates, steep and relatively narrow drainage basis as well as deep-level water tables.

These conditions combined are thought to limit amounts of low-$\delta^{18}O$ meteoric and groundwater from permeating down the shallow to intermediate crustal depths, and also limit hydrothermal alteration of shallow crustal material required to produce low-$\delta^{18}O$ magmas. This study has shown that even though there is alteration and hydrothermal systems within the vicinity of the study area, no low-$\delta^{18}O$ rocks were identified. It is known that in order to make low-$\delta^{18}O$ magmas, low-$\delta^{18}O$ rocks are required, either to partially melt or to contaminate mantle-derived magmas, thereby lowering the $\delta^{18}O$ values in the magma. In this regard, assimilation of low-$\delta^{18}O$ material produced through hydrothermal alteration did not occur during the production of the silicic magmas in the CVZ because the low-$\delta^{18}O$ altered material did not exist in sufficient quantity. As suggested by Folkes et al. (2013), extremely low precipitation and evaporation rates due to high elevations limit large scale hydrothermal systems from developing. Supporting this are the findings from the isotopic studies of the Great Basin in Nevada (subduction-related), which has been found to have the highest $\delta^{18}O$ signatures (9.5-10.1‰) in North America. This region is associated with a dry climate, thickened crust and high elevations, as does the Central Andes (Best et al., 2009 and DeCelles, 2004).

CHAPTER 8

Concluding Remarks

This study has attempted to address the possible reasons why low-$\delta^{18}O$ magmas have not been found in the CVZ of the Andes. Initially, a search for these magmas in the CVZ was conducted during the field work stage of this study. Whole rocks and quartz were analysed on altered rocks that were deliberately sampled; seeing that there is neither low-$\delta^{18}O$ magmas nor low-$\delta^{18}O$ altered rocks found, the following conclusions have been drawn in attempt to address why the region does not have tangible evidence for low-$\delta^{18}O$ magmas:

1. Whole rock analyses of the studied rocks reveal the composition of the major rock types in the CVZ (dacites, ignimbrites, lavas and altered rocks) to be dacitic and rhyolitic.
    i. CVZ rocks have a medium calc-alkaline character, which is consistent with the fractionation of plagioclase, pyroxenes and Fe-Ti oxides.
    ii. CVZ magmas are considered hybrid, having crustal proportions of ~70% and 30% of mantle-derived basaltic andesites.
    iii. Petrological features observed in the CVZ rocks show disequilibrium textures, which indicate that fractional crystallization, magma mixing and fractionation processes have played a major role in the origin of the dacites from andesitic/basaltic magmas.

2. The overall range for δD in this study is -32 to -119‰
    i. These are typical δD values for igneous rocks.
    ii. The δD values of altered rocks (-32‰) suggest alteration in fluids and not meteoric, given that El Tatio has a δD value of -50‰.

3. The $\delta^{18}O$ values of quartz phenocrysts range from 5.0 to 10.7‰ (average $\delta^{18}O$=8.6‰ ; n=41), and whole-rock $\delta^{18}O$ values range from 5.0 to 22.3‰ (average $\delta^{18}O$=10.5‰ ; n=51).
    i. The quartz $\delta^{18}O$ values suggest that the magmas from which these rocks crystallized have higher $\delta^{18}O$ values than expected in mantle-derived felsic magmas.
    ii. The $\delta^{18}O$ enrichment in the CVZ magmas is most likely to be a result of low-temperature alteration.

iii. There is an oxygen-isotope disequilibrium that exists between phenocryst and matrix in the studied rocks, which explains why the whole-rock $\delta^{18}O$ are significantly higher than those of the analysed phenocryst phases in this study.

iv. The whole-rock $\delta^{18}O$ values were controlled by large oxygen-isotope fractionations at low temperatures.

v. The rocks in this study do not have correlated variations of $\delta^{18}O$ with increasing SiO_2 content, Davidson et al. (1990, 1991) explained these isotopic features to be typical of a complex petrogenetic evolution that involves primary mantle-derived magmas that are modified by deep crustal interactions to produce magmas with baseline isotopic compositions that are parental to those that erupted at the surface.

4. Several factors control the variation of $\delta^{18}O$ in CVZ magmas in general. The $\delta^{18}O$ signatures of the magma depend on the source of the magma, fractional crystallization and assimilation processes.

   i. In this study, the magma could be melted crust or mantle-derived; however, influenced by assimilation processes. The ~9‰ average $\delta^{18}O$ in this study signifies a melted crust. Mantle-derived magmas in the CVZ have evolved by contamination and crystal fractionation to basaltic-andesitic composition, this crustal contamination has occurred by intracrustal assimilation, coupled with crystallization of these magmas.

   ii. The lowest $\delta^{18}O$ value recorded in this study is 5.0‰ for both quartz and whole-rock, this dacite could have been partially melted by a hydrothermal material that has depleted $\delta^{18}O$ signatures.

   iii. The highest $\delta^{18}O$ values for quartz and whole rock are 10.7‰ and 22.3‰, respectively.

5. The variation in $\delta^{18}O$ values across the CVZ is related to magma composition, age and the geodynamics of each volcanic centre in the different regions of the area (Altiplano-Puna Volcanic Complex). There is no clear relationship between $\delta^{18}O$ values with latitude, longitude and altitude across the CVZ.

   i. Crustal thickening, crustal shortening, magmatic underplating and lithospheric hydration may have played a big role influencing the $\delta^{18}O$ of the rocks in the area.

ii. CVZ magmas, have elevated $^{87}Sr/^{86}Sr$ and lower $^{143}Nd/^{144}Nd$ (Schmitt et al., 2002) as well as elevated $\delta^{18}O$ values, this suggests that greater amounts of crust have been incorporated. Gonzalez-Maurel et al. (2020) suggest that most primitive rocks in the CVZ (La Poruña) have $\delta^{18}O$ values of 7.0‰, based on olivine data. The Andes is at its highest average altitude and width in the CVZ, this is where the largest amount of upper crustal shortening has occurred (Leier et al., 2013), this extremely thick crust and high rates of subduction erosion play a role in determining what is being incorporated into the magma, which also define the isotopic composition of the magma.

iii. Younger rocks in the CVZ have $\delta^{18}O$ compositions that are more crustal than the older rocks. A shift in magmatic compositions to more upper crustal through time has been revealed by temporal variation data, which indicate that the extent of crustal contamination of volcanic rocks in the CVZ has increased from prior Miocene to Recent, as the crust has thickened up to ~70 km (Stern, 1990). Supporting this conclusion is a PhD study by Walker (2011), who presented an extensive suit of $\delta^{18}O$ data for Aucanquilcha volcano (11 Ma). The $\delta^{18}O$ values were consistent over the history of the volcano, with a slight increase in $\delta^{18}O$ values over time, suggesting evidence of temporal variation.

6. In attempt to account for the lack of low-$\delta^{18}O$ magmas in the CVZ, the conclusions of Folkes et al. (2013) have been integrated with the results of this study to explain why there were no low-$\delta^{18}O$ magmas found. The following conclusions are based on factors such as the tectonic history and climatic conditions, which are considered to have had an impact on the $\delta^{18}O$ values across the study area:

   i. There has been low precipitation (100-350mm/year), high aridity and high elevation (>3500m) in the last 10 Ma in the CVZ (Strecker et al., 2007). It is concluded that there is possibility that the prevailing climatic and tectonic conditions in the CVZ may have been the driving forces in the enrichment of $\delta^{18}O$ signatures in the region.

   ii. Based on the conclusions of Folkes et al. (2013), it seems that there may be a limited supply of meteoric water in the Central Andes, and that these conditions may have been in place since at least the last 10 Ma (period of the major silicic volcanism). The $\delta^{18}O$ values of the rocks show that the effects of meteoric water

interaction with lavas had little or no effect on bulk rock $\delta^{18}O$ values. This work shows almost no low-$\delta^{18}O$ rock exist in the CVZ.

iii. The $\delta^{18}O$ values of the sampled spring water from El Tatio indicate that the $\delta^{18}O$ of the meteoric water were low enough (-8.5‰) to cause low-$\delta^{18}O$ values in the rocks that interacted with it at >250°C, it is concluded that there ought to be low-$\delta^{18}O$ rocks.

iv. Highly altered rocks have high rather than low-$\delta^{18}O$ values. This must reflect low water/rock ratio in hydrothermal systems close to the surface.

v. The meteoric water values in this study for a spring water from the El Tatio geothermal field are -8.5‰ and -50‰ for $\delta^{18}O$ and δD respectively, these isotopic signatures are symbolic of the type of meteoric waters that interact with the magmas in the region and the hydrothermal alteration thereof.

vi. The CVZ region is a highly elevated, arid plateau with very low precipitation and high evaporation rates, steep and relatively narrow drainage basins as well as deep-level water tables. As suggested by Folkes et al. (2013), extremely low precipitation and high evaporation rates due to high elevations limit large scale hydrothermal systems from developing. This study has shown that even though there is alteration and hydrothermal systems within the vicinity of the study area, no low-$\delta^{18}O$ rocks were identified, therefore assimilation of low-$\delta^{18}O$ material produced through hydrothermal alteration did not occur during the production of the silicic magmas in the CVZ because the low-$\delta^{18}O$ altered material did not exist in sufficient quantity.

9. REFERENCES

Aitcheson, S.J., Harmon, R.S., Moorbath, S., Schneider, A., Soler, P., Soria-Escalante, E., Steele, G., Swainbank, I., and Wörner, G. (1995). 'Pb isotopes define basement domains of the Altiplano, central Andes', *Geology*, 23 (6), pp. 555–558.

Allmendinger, R.W., Jordan, T.E., Kay, S.M., and Isacks, B.L. (1997). 'The evolution of the Altiplano-Puna plateau of the Central Andes', *Annual Reviews Earth Planetary Sciences,* 25, pp. 139-174

Bacon, C.R., Adami, L.H., and Lanphere, M.A. (1989). 'Direct evidence for the origin of low-$\delta^{18}O$ silicic magmas - quenched samples of a magma chambers partially fused granitoid walls, Crater Lake, Oregon', *Earth and Planetary Science Letters,* 96, pp. 199–208.

Bacon, C.R., and Lowenstern, J.B. (2005). 'Late Pleistocene granodiorite source for recycled zircon and phenocrysts in rhyodacite lava at Crater Lake, Oregon', *Earth and Planetary Science Letters,* 233, pp. 277–293.

Barreiro, B.A. (1984). Lead isotopes and Andean magma genesis. In *Andean magmatism, chemical and isotopic constraints*. Harmon, R.S., Barreiro, B.A. Eds. Shiva, Bristol, pp. 21-30

Barnes, J., and Ehlers, T. (2009). 'End member models for Andean Plateau uplift', *Earth-Science Reviews,* 97, pp. 105–132.

Balsley, S.D., and Gregory, R.T. (1998). 'Low-$\delta^{18}O$ silicic magmas: why are they so rare?', *Earth and Planetary Science Letters,* 162, pp. 123–136.

Baker, M.C.W., and Francis, P.W. (1978). 'Upper Cenozoic volcanism in the Central Andes: Ages and volumes', *Earth and Planetary Science Letters,* 41, pp. 175–187.

Beard, J.S., Ragland, P.C., and Crawford, M.L. (2005). 'Reactive bulk assimilation: a model for crust-mantle mixing in silicic magmas', *Geology,* 33, pp. 681–684.

Beck, S., Zandt, G., Myers, S., Wallace, T., Silver, R., and Drake, L. (1996). 'Crustal-thickness variations in the Central Andes', *Geology,* 24, pp. 407–410.

Beck, S.L., and Zandt, G. (2002). 'The nature of orogenic crust in the central Andes', *Journal of Geophysical Research*, 107. DOI: http://dx.doi.org/10.1029/2000JB000124

Best, M., Barr, D., Christiansen, E., Gromme, S., Deino, A., and Tingey, D. (2009). 'The Great Basin Altiplano during the middle Cenozoic ignimbrite flareup: insights from volcanic rocks', *International Geology Review*, 51 (7), pp. 589–633.

Best, M.G., Christiansen, E.H., de Silva, S., and Lipman, P.W. (2016). 'Slab-rollback ignimbrite flareups in the southern Great Basin and other Cenozoic American arcs: a distinct style of arc volcanism', *Geosphere*, 12, pp. 1097-1135.

Bindeman, I.N. (2008). 'Oxygen isotopes in mantle and crustal magmas as revealed by single crystal analysis', *Reviews in Mineralogy and Geochemistry*, 69, pp. 445–478.

Bindeman, I.N., and Valley, J.W. (2001). 'Low-$\delta^{18}O$ rhyolites from Yellowstone: Magmatic evolution based on analyses of zircons and individual phenocrysts', *Journal of Petrology*, 42, pp. 1491–1517.

Bindeman, I.N., and Valley, J.W. (2002). 'Oxygen isotope study of the Long Valley magma system, California: isotope thermometry and convection in large silicic magma bodies', *Contributions on Mineralogy and Petrology*. 144, pp. 185–205.

Bindeman, I.N., Fournelle, J.H., and Valley, J.W. (2001). 'Low-$\delta^{18}O$ tephra from a compositionally zoned magma body: Fisher Caldera, Unimak Island, Aleutians', *Journal of volcanology and geothermal research*, 111, pp. 35-53.

Bindeman, I.N., Ponomareva, V.V., Bailey, J.C., and Valley, J.W. (2004). 'Volcanic arc of Kamchatka: a province with high-$\delta^{18}O$ magma sources and large scale $^{18}O/^{16}O$ depletion of the upper crust', *Journal of Geochemistry and Cosmochemistry*, 68, pp. 841– 865.

Bindeman, I.N., Eiler, J.M., Yogodzinski, G.M., Tatsumi, Y., Stern, C.R., Grove, T.L., Portnyagin, M., Hoernle, K., and Danyushevsky, L.V. (2005). 'Oxygen isotope evidence for slab melting in modern and ancient subduction zones', *Earth and Planetary Science Letters*, 235 (3–4), pp. 480–496.

Bindeman, I. N., Leonov, V. L., Izbekov, P. E., Ponomareva, V. V., Watts, K. E., Shipley, N. K., et al. (2010). 'Large-volume silicic volcanism in Kamchatka Ar-Ar and U-Pb ages,

isotopic, and geochemical characteristics of major pre-Holocene caldera-forming eruptions', *Journal of Volcanology and Geothermometry*, 189, pp. 57–80. DOI: 10.1016/j.jvolgeores.2009.10.009

Bindeman, I. N., Anikin, A. P., and Schmitt, A. K. (2016). 'Archean xenocrysts in modern volcanic rocks from Kamchatka: Insight into the basement and paleo-drainage', *Journal of Geology*, 124, pp. 684833. DOI: 10.1086/684833

Blum-Oeste, M., and Wörner, G. (2016). 'Central Andean magmatism can be constrained by three ubiquitous endmembers', *Terra Nova*, 28, pp.434-440.

Boroughs, S., Wolff, J., Bonnichsen, B., Godchaux, M.M., and Larson, P.B. (2005) 'Large-volume, low-$\delta^{18}O$ rhyolites of the central Snake River Plain, Idaho, USA', *Geology*, 33, pp. 821–824.

Bowen, N.L. (1947). 'Magmas', *Bulletin of the Geological Society of America*, 58, pp. 263-280.

Burns, D.H., de Silva, S.L., Tepley, F III., Schmitt, A.K., and Loewen, M.W. (2015). 'Recording the transition from flare-up to steady-state arc magmatism at the Purico–Chascon volcanic complex, northern Chile', *Earth and Planetary Science Letters*, 422, pp. 75-86.

Bywater-Reyes, S., Carrapa, B., Clementz, M., and Schoenbohn, L. (2010). 'Effect of late Cenozoic aridification on sedimentation in the Eastern Cordillera or northwest Argentina (Angastaco basin)', *Geology*, 38, pp. 235–238.

Chacko, T., Cole, D.R. and Horita, J. (2001). Equilibrium oxygen, hydrogen, and carbon isotope fractionation factors applicable to geological systems. In *Stable Isotope Geochemistry, Mineralogical Society of America/Geochemical Society, Reviews in Mineralogy and Geochemistry.* Valley, J.W. and Cole, D.R. Eds. 43, pp. 1-81.

Chesko, A. (1994). '$^{18}O/^{16}O$, and $^{3}He/^{4}He$ data on the formation of the main types of thermal waters in the Kurile–Kamchatka region', *Geochemistry International*, 32, pp. 988–1001.

Clayton, R.N., Hurd, J.M., and Mayeda, T.K. (1972). Oxygen isotope abundances in Apollo 14 and 15 rocks and minerals', *Lunar Science III, Lunar Science Institute Contribution,* 88, pp. 144-143.

Coira, B., Davidson, J., Mpodozis C, and Ramos, V. 1982. Tectonic and magmatic evolution of the Andes of northern Argentina and Chile. In *Magmatic evolution of the Andes*. Linares, E., Cordani, U.G., and Munizaga, F. Eds. Amsterdam: Elsevier. 18, pp. 303-332.

Clinton, C.P and Lithgow-Bertelloni, C (2004). 'The temporal evolution of plate driving forces: Importance of "slab suction" versus "slab pull" during the Cenozoic', *Journal of Geophysical Research: Solid Earth*, 109 (B10), pp. 407. DOI:10.1029/2004JB002991

Cortecci, G., Mussi, M., Boschetti, T., Lameli, C.H., Mucchino, C., and Barbieri, M. (2005). 'New chemical and isotopic data on waters from El Tatio geothermal field, Northern Chile', *Geochemical Journal*, 39, pp. 547-571.

Davidson, J.P and de Silva, S.L., (1995). 'Late Cenozoic magmatism of the Bolivian Altiplano', *Contributions in Mineralogy and Petrology*, 119, pp. 387-408.

Davidson, J.P., Harmon R.S., and Wörner, G. 1991. The source of Central Andean magmas: some considerations. In *Andean Magmatism and its Tectonic Setting*. Harmon R.S, Rapela C.W. Eds. Geological Society of America Special Paper, 265, pp. 233-244.

Davidson, J.P., McMillian, N., Moorbath, S., Wörner, G., Harmon, R. S., and Lopez-Escobar, L. (1990). 'The Nevados de Payachata volcanic region (18°S/69°W, N. Chile): II. Evidence for widespread crustal involvement in Andean magmatism', *Contributions of Mineralogy and Petrology*, 105, pp. 412–432.

DeCelles, P. (2004). 'Late Jurassic to Eocene evolution of the Cordilleran thrust belt and foreland basin system, western U.S.A', *American Journal of Science,* 304, pp. 105–168.

DePaolo, D.J. (1981). 'Trace element and isotopic effects of combined wall-rock assimilation and fractional crystallization', *Earth and Planetary Science Letters*, 53, pp. 189–202.

de Silva SL. (1989). 'Altiplano-Puna volcanic complex of the Central Andes', *Geology*, 17, pp. 1102-1106.

de Silva, S.L. and Francis, P.W. 1991. *Volcanoes of the Central Andes*. Springer-Verlag, Berlin, pp. 216

de Silva, S.L., Self, S., Francis, P.W., Drake, R.E., and Ramirez, R.C. (1994). 'Effusive silicic volcanism in the Central Andes: the Chao dacite and other young lavas of the Altiplano–Puna Volcanic Complex', *Journal of Geophysics*. Res. 99 (B9), pp. 17805–17825.

de Silva, S. L., Zandt, G., Trumbull, G., Viramonte, J. G., Salas, G., and Jimenez, N. (2006). 'Large ignimbrite eruptions and volcano-tectonic depressions in the Central Andes: a thermomechanical perspective in Mechanisms of Activity and Unrest at Large Calderas'. C. Troise, et al. Eds. *London: Geological Society of London Special Publication*, pp. 47–63.

de Silva, S.L. and Gosnold, W.D. (2007). 'Episodic construction of batholiths: insights from the spatiotemporal development of an ignimbrite flare-up', *Journal of Volcanology and Geothermal Research,* 167, pp. 320-325.

de Silva, S. L., Riggs, N. R., and Barth, A. P. (2015). 'Quickening the pulse: fractal tempos in continental arc magmatism', *Elements*, 11, pp. 113–118.

de Silva, S.L. and Kay, S.M. (2018). 'Turning up the heat: high-flux magmatism in the Central Andes', *Elements,* 14, pp. 245-250.

Ducea, M.N. and Barton, M.D. (2007). 'Igniting flare-up events in Cordilleran arcs', *Geology*, 3, pp. 1047–1050. DOI: 10.1130/G23898A.1

Dungan, M.A. and Davidson, J.P. (2004). 'Partial assimilative recycling of the mafic plutonic roots of arc volcanoes: an example from the Chilean Andes', *Geology,* 32, pp. 773–776.

Eiler, J.M., Mc Innes, B., Valley, J.W., Graham, C.M., and Stolper, E. (1998). 'Oxygen isotope evidence for slab-derived fluids in the sub-arc mantle', *Nature,* 393, pp. 777–781.

Ellis, B.S., Szymanowski, D., Wotzlaw, J.F., Schmitt, A.K., Bindeman, I.N., Troch, J., Harris, C., Bachmann, O., and Guillong, M. (2017). 'Post-caldera volcanism at the Heise volcanic field: implications for petrogenetic models', *Journal of Petrology*, 58, pp. 115–136.

Feeley, T.C., Davidson, J.P., and Armendia, A. (1993). 'The volcanic and magmatic evolution of volcan Ollagüe, a high-K, late Quaternary stratovolcano in the Andean Central Volcanic Zone', *Journal Volcanology and Geothermal Research*, 54, pp. 221-245.

Feeley, T.C. and Davidson, J.P. (1994). 'Petrology of calc-alkaline lavas at Volcan Ollagüe and the origin of compositional diversity at Central Andean stratovolcanoes', *Journal of Petrology*, 35(5), pp. 1295–1340.

Feeley, T.C. and Sharp, Z.D. (1995). '$^{18}O/^{16}O$ isotope geochemistry of silicic lava flows erupted from Volćan Ollagüe, Andean Central Volcanic Zone', *Earth and Planetary science letters*, 33, pp. 239-254.

Feeley, T.C. and Hacker, M.D. (1995). 'Intracrustal derivation of Na-rich andesitic and dacitic magmas: an example from Volcan Ollagüe, Andean Central Volcanic Zone', *Journal Geology*, 103, pp. 213-225.

Francis, P.W., McDonough, W.F., Hammill, M., O'Callaghan, L.J., and Thorpe, R.S. 1984. The Cerro Purico shield complex, north Chile. In *Andean magmatism; chemical and Isotopic constraints*. Harmon, R., and Barreiro, B. Eds. Nantwich: Shiva Publishing Limited. pp. 106–123.

Francis, P.W. and Hawkesworth, C.J. (1994). 'Late Cenozoic rates of magmatic activity in the Central Andes and their relationships to continental crust formation and thickening', *Journal of the Geological Society of London,* 151, pp. 845-854.

Figueroa, O., Déruelle, B., and Demaiffe, D. (2009). 'Genesis of adakite-like lavas of Licancabur volcano (Chile-Bolivia, central Andes)', *Contributions to Geoscience*, 341(4), pp. 310–318. DOI: https://doi.org/10.1016/j.crte.2008.11.008

Freymuth, H., Brandmeier, M., and Wörner, G. (2015). 'The origin and crust/mantle mass balance of Central Andean ignimbrite magmatism constrained by oxygen and strontium isotopes and erupted volumes', *Contributions to Mineralogy and Petrology,* 169.

Folkes, C.B., Raymond, A.F., de Silva, S.L., and Bindeman, I.N. (2013). 'Tectonic and climate history influence on the geochemistry of large silicic magma: New $\delta^{18}O$ data from the Central Andes with comparison to N America and Kamchatka', *Journal of Volcanology and Geothermal research*, 252, pp. 90-103.

Garcia, M. O., Ito, E., Eiler, J. M., and Pietruszka, A. J. (1998). 'Crustal contamination of Kilauea volcano magmas revealed by oxygen isotope analyses of glass and olivine from Puu Oo eruption lavas', *Journal of Petrology*, 39(5), pp. 803-817.

Geise, P., Scheuber, E., Schilling, F., Schmitz, M., and Wigger, P. (1999). 'Crustal thickening process in the Central Andes and the different natures of the Moho-discontinuity', *Journal of South American Earth Sciences*, 12 (2), pp. 201-220.

Godoy, E., Wörner, G., Kojima, S., Aguilera, F., Simon, K. and Hartmann, G., (2014). 'Low-pressure evolution of arc magmas in thickened crust: The San Pedro-Linzor Volcanic Chain, Central Andes, Northern Chile', *Journal of South American Earth Sciences*, 52, pp. 24–42.

Godoy, B., Wörner, G., Le Roux, P., de Silva, S. L., Parada, M. A., Kojima, S., Gonzalez-Maurel, O., Morata, D., Polanco, E., and Martnez, P. (2017). 'Sr- and Nd- isotope variations along the Pleistocene San Pedro-Linzor volcanic chain, N. Chile: Tracking the influence of the upper crustal Altiplano-Puna Magma Body', *Journal of Volcanology and Geothermal Research*, 341, pp. 172-186.

Godoy, B., Taussi, M, González-Maurel, O., Renzulli, A., Hernández-Prat, L., le Roux, P., Morata, D., and Menzies, A. (2019). 'Linking the mafic volcanism with the magmatic stages during the last 1 Ma in the main volcanic arc of the Altiplano-Puna Volcanic Complex (Central Andes)', *Journal of South American Earth Sciences*, 95.

González-Maurel, O., Godoy, B., le Roux, P., Rodríguez, I., Marín, C., Menzies, A., Bertin, D., Morata, D et al. (2019). 'Magmatic differentiation at La Poruña scoria cone, Cental Andes, northern Chile: Evidence for assimilation during turbulent ascent processes, and genetic links with mafic eruptions at adjacent San Pedro volcano', *Lithos*, 338-339, pp. 128-140.

Götze, H. J. and Krause, S. (2002). 'The Central Andean gravity high, a relic of an old subduction complex?', *Journal of South American Earth Sciences*, 14, pp. 799–811.

Grunder, A.L. (1987). 'Low $\delta^{18}O$ silicic volcanic rocks at the Calabozos Volcanic Complex. Southern Andes: evidence for upper crustal contamination', *Contributions to Mineralogy and Petrology*, 88, pp. 133-149.

Grunder, A.L., Thompson, J.M., and Hildreth, W. (1987). 'The hydrothermal system of the Calabozos caldera, central Chilean Andes', *Journal of Volcanology and Hydrothermal Research*, 32, pp. 287-298.

Grunder, A.L., Klemetti, E.W., Feeley, T.C., and McKee, C.M. (2006). 'Eleven million years of arc volcanism at the Aucanquilcha Volcanic Cluster, Northern Chilean Andes: Implications for the life span and emplacement of plutons', *Transactions of the Royal Society of Edinburgh-Earth Sciences*, 97, pp.415-436.

Hamilton, T.D. 1994. Late Cenozoic glaciation of Alaska Peninsula. In *The Geology of North America; Geology of Alaska, G-1*. Plafker, G., Berg, H.C. Eds. Boulder: Geological Society of America. pp. 759-779.

Harris, C., Compton, J.S., Bevington, S.A. (1999). 'Oxygen and hydrogen isotope composition of kaolinite deposits, Cape Peninsula, South Africa: low-temperature, meteoric origin'. *Economic Geology,* 94, pp. 1353-1366.

Harris, C. and Ashwal, L.D. (2002). The origin of low-$\delta^{18}O$ granites and related rocks from the Seychelles', *Contributions to Mineralogy and Petrology*, 143, pp. 366–376.

Harris, C. and Vogeli, J. (2010). 'Oxygen isotope composition of garnet in the Peninsula Granite, Cape Granite Suite, South Africa: Constraints on melting and emplacement mechanisms', *South African Journal of Geology*, 113, pp. 385–397.

Harris, C., Mulder, K., Sarkar, S., Whitehead, B., and Roopnarain, S. (2018). 'Petrogenesis of low-$\delta^{18}O$ quartz porphyry dykes, Koegel Fontein complex, South Africa', *Contributions to Mineralogy and Petrol*ogy, 173, pp. 30.

Hawkesworth, C.J., Hammill, M., Gledhill, A.R., van Calsteren, P., and Rogers, G. (1982). 'Isotope and trace element evidence for late-stage intra-crustal melting in the High Andes', *Earth and Planetary Science Letters*, 58, pp. 240–254.

Hildreth, W., Grunder, A., and Drake, R. (1984). 'The Loma Seca Tuff and the Calabozos Caldera: a major ash-flow and caldera complex in southern Andes of central Chile', *The Geological Society of America Bulletin,* 95 (1), pp. 45-54.

Hildreth, W. and Moorbath, S. (1988) 'Crustal contributions to arc magmatism in the Andes of central Chile', *Contributions to Mineralogy and Petrology*, 98, pp. 455-489

Isacks, B. (1988). 'Uplift of the Central Andean plateau and bending of the Bolivian orocline', *Journal Geophysical Research*, 93, pp. 3211-3231.

James, D.E. (1971). 'Andean crustal and upper mantle structure', *Journal of Geophysics*, Res. 76.

James, D.E. (1982). 'A combined O, Sr, Nd and Pb isotopic and trace element study of crustal contamination in the central Andean lavas, Local geochemical variations', *Earth and Planetary Science Letters*, 57, pp. 47-52.

James, D.E. and Sacks, S. 1999. Cenozoic formation of the Central Andes: a geophysical perspective. In *Geology and Mineral Deposits of Central Andes*. Skinner, B. Ed. Society of Economic Geology. pp. 1-25.

Jones, R.E., Kirstein, L.A., Kasemann, S.A., Dhuime, B., Elliott, T., Litvak, V.D., Alonso, R., and Hinton, R. (2015). 'Geodynamic controls on the contamination of Cenozoic arc magmas in the southern Central Andes: insights from the O and Hf isotopic composition of zircon', *Geochimica et Cosmochimica*, 164, pp. 386–402.

Jones, R.E., Kirstein, L.A., Kasemann, S.A., Litvak, V.D., Poma, S., Alonso, R.N., Hinton, R., and EIMF. (2016). 'The role of changing geodynamics in the progressive contamination of Late Cretaceous to Miocene arc magmas in the southern Central Andes', *Lithos*, 262, pp. 169-191.

Kay, S.M., Mpodozis, C., Ramos, V.A., and Munizaga, F. 1991. Magma source variations for mid to late Tertiary volcanic rocks erupted over a shallowing subduction zone and through a thickening crust in the Main Andean Cordillera (28°-33°S). In *Andean Magmatism and its Tectonic Setting*. Harmon, R.S. and Rapela, C.W. Eds. Geological Society of America. pp. 113-137.

Kay, S.M., Coira, B., and Viramonte, J. (1994). 'Young mafic back-arc volcanic rocks as indicators of continental lithospheric delamination beneath the Argentine Puna Plateau, Central Andes', *Journal of Geophysical Research*, 99, pp. 24323-24339.

Kay, S.M., Mpodozis, C., Coira, B. 1999. Magmatism, tectonism and mineral deposits of the Central Andes (22°-33°S latitude). In *Geology and Ore Deposits of the Central Andes*. Skinner, B.J. Ed. Society of Economic Geology. pp. 27-59.

Kay, S., Coira, B., Caffe, P., and Chen, C. (2010). 'Regional chemical diversity, crustal and mantle sources and evolution of central Andean Puna plateau ignimbrites', *Journal of Volcanology and Geothermal Research*, 198, pp. 81–111.

Kent, C.C. (2016). 'Crustal and Mantle Evolution', *Earth as an Evolving Planetary System*, Academic Press, pp. 147–199.

Klemetti, E.W., and Grunder, A.L. (2006). 'Volcanic evolution of Volcàn Aucanquilcha: A long-lived dacite volcano in the Central Andes of northern Chile', *Bulletin of Volcanology*, 70, pp.633-650.

Kyser, T.K. 1986. Stable isotope variations in the mantle. In *Stable Isotopes in High-Temperature Geological Processes, Reviews in Mineralogy*. J.W. Valley, H.P. Taylor, J.R. O'Neil Jr. Eds. 16, pp. 141– 164.

Kyser, T.K. and O'Neil, J.R. (1984). 'Hydrogen isotope systematics of submarine basalts', *Geochimica et Cosmochimica*, 48, pp. 2l23-2133.

Lamb, S. and Hoke, L. (1997). 'Origin of the high plateau in the Central Andes, Bolivia, South America', *Tectonics*,16, pp. 623-649.

Larson, P.B. and Taylor Jr., H.P. (1986). '$^{18}O/^{16}O$ ratios in ash-flow tuffs and lavas erupted from the central Nevada caldera complex and the central San Juan caldera complex, Colorado', *Contributions to Mineralogy and Petrology*, 92, pp. 146–156.

Larson, P.B. and Geist, D.J. (1995). 'On the origin of low-^{18}O magmas: evidence from the Casto Pluton, Idaho', *Geology*, 23, pp. 909-912

Lazcano, J., Godoy, B., Aguilera, F., and Wilke, H.G. 2012. Volcanological evolution of Paniri volcano, central Andes, northern Chile. In *AGU Fall Meeting Abstracts*. San Francisco, USA. 21A-2759

Leir, A., McQuarrie, N., Garzione, C., and Eiler, J. (2013). 'Stable isotope evidence for multiple pulses of rapid surface uplift in the Central Andes, Bolivia', *Earth and Planetary Science Letters*, 371-372, pp. 49-58.

Lindsay, J. M., Schmitt, A. K., Trumbull, R. B., De Silva, S. L., Siebel, W., and Emmermann, R. (2001). 'Magmatic evolution of the La Pacana caldera system, central Andes, Chile:

compositional variation of two cogenetic, large-volume ignimbrites', *Journal of Petrology*, 42, pp. 459–486.

Lipman, P.W. and Friedman, I. (1975). 'Interaction of meteoric water with magma: An oxygen-isotope study of ash-flow sheets from Southern Nevada', *Geological Society of America Bulletin*, 86, pp. 695–702

Loewen, M., and Bindeman, I. N. (2016). 'Oxygen isotope thermometry reveals high magmatic temperatures and petrogenetic differences between hot-dry Yellowstone/ Snake River Plain and Icelandic rhyolites compared to cold-wet systems', *American Mineral*ogist, 101, pp. 1222–1227. DOI: 10.2138/am-2016-5591

Longstaffe, F. J., Claek, A. H., McNutt, R. H. and Zentilli, M. (1983). 'Oxygen isotopic composition of Central Andean plutonic and volcanic rocks, latitudes 26°-29° south', *Earth and Planetary Science Lett*ers, 64, pp. 9–18.

López, C., 2014. *Evolución geológica del Volcán Toconce, Región de Antofagasta, Chile*. Dissertation, Bachelor's Degree Thesis. Universidad de Atacama, Copiapó, Chile

Mamani, M., Wörner, G. and Sempere, T. (2010). Geochemical variations in igneous rocks of the Central Andean orocline (13°S to 18°S): tracking crustal thickening and magma generation through time and space', *Geological Society of America Bulletin,*122, pp. 162–182

Mancini, R., Díaz, D., Brasse, H., Godoy, B., and Hernández, M.J. (2019). 'Conductivity distribution beneath the San Pedro-Linzor volcanic chain, North Chile, using 3D magnetotelluric modelling', *Journal of Geophysics*, 124 (5), pp. 4386–4398.

Martínez, P., 2014. *Petrología y geoquímica de lavas recientes, al noroeste del Campo Geotermal del Tatio*. Dissertation, Bachelor's Degree Thesis. Universidad de Chile, Santiago, Chile.

Matthews, S. J., Jones, A. P. and Gardeweg, M. C. (1994). 'Lascar Volcano, northern Chile; evidence for steady-state disequilibrium', *Journal of Petrology*, 35, pp. 401–432.

Matthews, S., Sparks, S. and Gardeweg, M. (1999). 'The Piedras Grandes-Soncor Eruptions, Lascar Volcano, Chile: Evolution of a zoned magma chamber in the Central Andean Upper Crust', *Journal of Petrology*, 40, pp. 1891-1919

Mattioli, M., Renzulli, A., Menna, M., Flude, S. (2004). Petrology of a nearly aphyric basaltic andesite in the Andean Central Volcanic Zone: insight into the fast uprising of high-K calcalkaline magmas through the thick continental crust. *32nd IGC, Abstract Volume, part 1*. 20-28 August 2004. Florence, France.

Mattioli, M., Renzulli, A., Menna, M., & Holm, P. M. (2006). 'Rapid ascent and contamination of magmas through the thick crust of the CVZ (Andes, Ollagüe region): Evidence from a nearly aphyric high-K andesite with skeletal olivines', *Journal of Volcanology and Geothermal Research*, 158(1), pp. 87-105.

McGlashan, N., Brown, L.D., and Kay, S.M. (2008). 'Crustal thicknesses in the Central Andes from teleseismically recorded depth phase precursors', *International Journal of Geophysics*, 175, pp. 1013–1022.

Michelfelder, G. S., Feeley, T. C., Wilder, A. D., and Klemetti, E. W. (2013). 'Modification of the continental crust by subduction zone magmatism and vice-versa: Across-strike geochemical variations of silicic lavas from individual eruptive centres in the Andean Central Volcanic Zone', *Geosciences*, 3(4), pp. 633-667.

Mpodozis, C. and Ramos, V.A. (1990). The Andes of Chile and Argentina. In *Geology of the Andes and its relation to Hydrocarbon and Mineral Resources*. Ericksen, G.E., Cañas Pinochet, M.T., Reinemud, J.A. Eds. Houston: Circumpacific Council for Energy and Mineral Resources, Earth Sciences Series. 11, pp. 59-90.

Muehlenbachs, K. and Clayton, R.N. (1972). 'Oxygen isotope studies of fresh and weathered submarine basalts', *Canadian Journal of Earth Science*, 9, pp. 172.

Muehlenbachs, K., Anderson, A.T., and Sigvaldason, G.E. (1974). 'Low-^{18}O Basalts from Iceland', *Geochimica et Cosmochimica*, 38, pp. 577–588.

Naranjo, J. (1992). 'Chemistry and petrological evolution of the Lastarria volcanic complex in north Chilean Andes', *Geological Magazine*, 129, pp. 723-740.

O'Challagan, L.J., Francis, and P.W. (1986). 'Volcanological and petrological evolution of San Pedro volcano, Provincia El Loa, North Chile', *Journal of the Geological Society of London*, 143, pp. 275–286.

Olivier, C.G. (1967). Pediplain in Northern Chile and Andean Uplift', *Science*, 158, pp. 653-655.

Ort, M.H. (1993). 'Eruptive processes and caldera formation in a nested downsag-collapse caldera: Cerro Panizos, Central Andes', *Journal of Volcanology Geothermal Research*, 56(3), pp. 221–252.

Ortega, V. 2008. *Estudio petrográfico y petrológico de las rocas de los volcanes Láscar, Tilocalar Norte y Tilocalar Sur*. Dissertation, Bachelor's Degree Thesis. Universidad Católica del Norte, Antofagasta, Chile.

Parada, M.A. 1990. Granitoid plutonism in central Chile & its geodynamic implications, A review. In *Plutonism from Antarctica to Alaska*. Kay, S.M. and Rapela, C.W. Eds. Geological Society of America, Special Papers, 241, pp. 51–66

Raminez, C.F. and Huete, C. 1981. Geología de la Hoja Ollagüe, Región de Antofagasta. *Servicio Nacional de Geología y Minería, Carta Geológica de Chile*, 40, escala 1:250.000

Riishuus, M.S., Harris, C., Peate, D.W., Tegner, C., Wilson, J.R., and Brooks, C.K. (2015). 'Formation of low-$\delta^{18}O$ magmas of the Kangerlussuaq Intrusion by addition of water derived from dehydration of foundered basaltic roof rocks', *Contributions to Mineralogy and Petrology*, 169, pp. 1-16.

Rogers, G. and Hawkesworth, C.J. (1989). 'A geochemical traverse across the North Chilean Andes: evidence for crust generation from the mantle wedge', *Earth and Planetary Science Letterrs*, 9, 271-285.

Salisbury, M., Jicha, B., de Silva, S., Singer, B., Jimenez, N., and Ort, M. (2011). '$^{40}Ar/^{39}Ar$ chronostratigraphy of Altiplano–Puna volcanic complex ignimbrites reveals the development of a major magmatic province', *Geological Society of America Bulletin*, 123, pp. 821–840.

Scheuber, E. and Giese, P. (1999). 'Architecture of the Central Andes- a compilation of geoscientific data along a transect at 21˚S', *Journal of South American Earth Sciences*, 12, pp. 103-107.

Schimmelmann, A. and DeNiro, M.J. (1993). 'Preparation of organic and water hydrogen for stable isotope analysis: effects due to reaction vessels and zinc', *Analytical Chemistry*, 65, pp. 789-792.

Schmitt, A. (2001). 'Gas-saturated crystallization and degassing in large-volume, crystal-rich dacitic magmas from the Altiplano-Puna, northern Chile', *Journal of Geophysical Research*, 106 (B12), pp. 30561–30578.

Schmitt, A. K., De Silva, S. L., Trumbull, R. B. and Emmermann, R. (2002). 'Magma evolution in the Purico ignimbrite complex, northern Chile: evidence for zoning of a dacitic magma by injection of rhyolitic melts following mafic recharge', *Contributions to Mineralogy and Petrology*, 140, pp. 680–700.

Schmitz, M., Heinsohn, W.D., Schilling, F.R. (1997). 'Seismic, gravity and petrologic evidence for partial melt beneath the thickened Central Andean crust (21-23°S)', *Tectonophysics*, 270, pp. 313-326.

Schmitz, M., Lessel, K., Giese, F., Wigger, F., Araneda, M., Bribach, J., Graeber, F., Grunewald, S., Haberland, C., Lüth, S., Röber, F., Ryberg, T., and Schulze, A. (1999). 'The crustal structure beneath the Central Andean forearc and magmatic arc as derived from seismic studies: the PISCO 94 experiment in northern Chile (21°-23°S)', *Journal of South American Earth Sciences*. 12, pp. 237–260.

Schneider, A. (1987). Eruptive processes, mineralization and isotopic evolution of the Los Frailes, Kari Kari Region, Bolivia. *Revisita geologica de Chile.* 30, pp. 27–33.

Seligman, A., Bindeman, I. N., Jicha, B., Ellis, B., Leonov, V. L., and Ponomareva, V. V. (2014). 'Recognizing subtle evidence for silicic magma derivation from petrochemically-similar arc crust: isotopic and chemical evidence for the bimodal volcanic series of Gorely Volcanic Center, Kamchatka', *Russia Journal of Petrology*, 55, pp. 1561–1594.

Sharp, Z.D. (1990). 'A laser-based microanalytical method for the in-situ determination of oxygen isotope ratios of silicates and oxides', *Geochimica et Cosmochimica*, 54, pp. 1353– 1357.

Sigurdsson, H., Houghton, B., McNutt, S.T., Rymer, H., and Stix, J. Eds. (2015). *The Encyclopedia of Volcanoes.* 2nd Ed. Elsevier Inc, San Diego, USA.

Stelten, M.E., Cooper, K.M., Wimpenny, J.B., Vazquez, J.A., and Yin, Q. (2017). 'The role of mantle-derived magmas in the isotopic evolution of Yellowstone's magmatic system', *Geochemistry, Geophysics, Geosystems*, 18 (4), pp. 1350-1365.

Stern, C.R. (1990). 'Comment on "A geochemical traverse across the North Chilean Andes: evidence for crust generation from the mantle wedge" by G. Rogers and C.J. Hawkesworth', *Earth and Planetary Science Letters*, 101, pp. 129–133.

Stern, C.R. (1991). 'Role of subduction erosion in the generation of Andean magmas', *Geology* 19, pp. 78-81.

Stern, C.R. (1988). Source region versus intra-crustal contamination in the petrogenesis of the Quaternary volcanic centers at the northern end (33°-34°S) of the Southern Volcanic Zone. In *Congresso Geológico Chileno*. Santiago. 3, pp. 129-145.

Stern, C.R. (2004). Active Andean volcanism: its geologic and tectonic setting. Revista *Geológica de Chile*, 31(2), pp. 161-206.

Strecker, M., Alonso, R., Bookhagen, B., Carrapa, B., Hilley, G., Sobel, E., and Trauth, M. (2007). 'Tectonics and climate of the Southern Central Andes', *Annual Review of Earth and Planetary Sciences*, 35, pp. 747–787.

Tackley, P.J. (2000). 'Mantle Convection and Plate Tectonics: Toward an Integrated Physical and Chemical Theory', *Science*, 288 (5473), pp. 2002–2007.

Tassara, A., Götze, H.J., Schmidt, S., and Hackney, R. (2006). 'Three-dimensional density model of the Nazca plate and the Andean continent margin', *Journal of Geophysical Research*, 111.

Tatsumi, Y. (1989). 'Migration of fluid phases and genesis of basalt magmas in subduction zones', *Journal of Geophysical Research*, 94 (B4), pp. 4697-4707.

Taussi, M., Godoy, B., Piscaglia, F., Morata, D., Agostini, S., le Roux, P., González-Maurel, O., Gallmeyer, G., Menzies, A., and Renzulli, A. (2019). 'The upper crustal magma plumbing system of the Pleistocene Apacheta-Aguilucho Volcanic Complex area (Altiplano-Puna, northern Chile) as inferred from the erupted lavas and their enclaves', *Journal of Volcanology and Geothermal Research*, 373, 179–198.

Tosdal, R.M., Farrar, E., and Clark, A.H. (1984). 'K–Ar geochronology of the late Cenozoic volcanic rocks of the Cordillera Occidental, southernmost Peru', *Journal of Volcanology and Geothermal Research*, 10(1-3), pp. 157-173.

Troch, J., Ellis, B.S., Harris, C., Ulmer, P., and Bachmann, O. (2018). 'The effect of prior hydrothermal alteration on the melting behavior during rhyolite formation in Yellowstone, and its importance in the generation of low-$\delta^{18}O$ magmas', *Earth and Planetary Science Letters*, 481, pp. 338–349

Troch, J., Ellis, B., Harris, C., Ulmer, P., Bouvier, A.S., and Bachmann, O. (2020). 'Experimental melting of hydrothermally altered rocks: Constraints for the generation of low-δ18O rhyolites in the central Snake River Plain, USA', *Journal of Petrology*, 60(10), pp. 1881-1902.

Taylor, H.P. (1968). 'The oxygen isotope geochemistry of igneous rocks', *Contributions to Mineralogy and Petrology*, 19, pp. 1–71.

Taylor Jr., H.P. (1977). 'Water/rock interactions and the origin of H_2O in granitic batholiths', *Journal of Geological Society of London*, 133, pp. 509–558.

Taylor Jr, H.P. and Epstein, S. (1962). Relationship between $^{18}O/^{16}O$ ratios in coexisting minerals in igneous and metamorphic rocks. In *Applications to petrologic problems, Part 2. Geological Society of America Bulletin*. 73, pp. 480–498.

Taylor Jr, H.P. and Sheppard, S.M.F. (1986). 'Processes of isotopic fractionation and isotope systematics' *Reviews in Mineralogy,* 16, pp. 227–271.

Taylor, S.R. and McLennan, S.M. (1985). *The continental crust: its composition and evolution*. Blackwell, Oxford.

Taylor, S. R., and McLennan, S. M. (1995). 'The geochemical evolution of the continental crust', *Review in Geophysics*, 33, pp. 241–265. DOI: 10.1029/95RG 00262

Taylor, B and Martinez, F. (2002). 'Mantle wedge control on back-arc crustal accretion', *Nature*, 416 (6879), pp. 417–420.

van Alderwerelt, B.M.E.D. (2017). *Diverse Monogenetic Volcanism across the Main Arc of the Central Andes, Northern Chile*. PhD Thesis. The University of Iowa (Iowa), U.S.A.

Vennemann, T.W. and O'Neil, J.R. (1993). ‘A simple and inexpensive method of hydrogen isotope and water analyses of minerals and rocks based on zinc reagent’, *Chemical Geology (Isotope Geosciences Section)*, 103, pp. 227–234.

Victor, P., Oncken, O., and Glodny, J. (2004). ‘Uplift of the western Altiplano plateau: Evidence from the Precordillera between 20° and 21°S (northern Chile)’, *Tectonics*, 23(4). DOI:10.1029/2003TC001519.

Vratislav, H., Huraiovà, M., Slobodník, M., and Thomas, R. (2015). *Geofluids: Developments in Microthermometry, Spectroscopy, Thermodynamics and Stable Isotopes*. Elsevier Inc, Amsterdam, Netherlands.

Vroon, P.Z., Lowry, D., van Bergen, M.J., Boyce, A.J., and Mattey, D.P. (2001). ‘Oxygen isotope systematics of the Banda Arc; low- $\delta^{18}O$ despite involvement of subducted continental material in magma genesis’, *Geochimica et Cosmochimica*, 65, pp. 589-609.

Walker, B.A.K.E.W., Grunder, A.L., Dilles, J.H., Tepley, F.J., and Gile, D. (2013). ‘Crystal reaming during the assembly, maturation and waning of the eleven-million-year crustal magma cycle: Thermobarometry of the Aucanquilcha Volcanic Cluster’, *Contributions to Mineralogy and Petrology*, 165, pp.663-682.

Ward, K., Zandt, G., Beck, S.L., Christensen, D.H., and McFarlin, H. (2014). ‘Seismic imaging of the magmatic underpinnings beneath the Altiplano-Puna volcanic complex from the joint inversion of surface wave dispersion and receiver functions’, *Earth and Planetary Science Letters*, 404, pp. 43-53.

White, J.D. and Ross, P.S. (2011). ‘Maar-diatreme volcanoes: a review’, *Journal of Volcanology and Geothermal Research*, 201(1), pp. 1-29.

Whittington, A.G., Hofmeister, A.M., Nabelek, P.I. (2009). ‘Temperature dependent thermal diffusivity of the Earth’s crust and implications for magmatism’, *Nature*, 458, pp. 319–321.

Wood, C.A., McLaughlin, G., and Francis, P. (1987). ‘Segmentation of volcano rich arcs’, *Transactions of the American Geophysical Union (EOS)*,68, pp. 15-19

Wolff, J.A., Balsley, S.D., and Gregory, R.T. (2002). 'Oxygen isotope disequilibrium between quartz and sanidine from the Bandelier Tuff, New Mexico, consistent with a short residence time of phenocrysts in rhyolitic magma', *Journal of Volcanology and Geothermal Research*, 116, pp. 119-135

Wörner, G., Harmon, R.S., Davidson, J., Moorbath, S., Turner, D.L., McMillian, N., and Nye, C. (1988). 'The Nevados de Payachata volcanic region (18°S/69°W, N. Chile): Geological, geochemical and isotopic observations', *Bulletin of Volcanology*, 50, pp. 287–303.

Wörner, G., Moorbath, S., and Harmon, R.S. (1992). 'Andean Cenozoic volcanic centers reflect basement isotopic domains', *Geology*, 20, pp. 1103–1106.

Wörner, G., Moorbath, S., Entenmann, J., Davidson, J.D., and Lopez-Escobar, L. (1994). Large geochemical variations along the Andean Arc of northern Chile (17.5°-22°S). In *Tectonics of the Southern Central Andes: Structure and evolution of an active continental margin*. Reutter, K.J., Scheuber, E., Wigger, P.J. Eds. Berlin: Springer. pp. 77-91.

Wörner, G., Mamani, M., and Blum-Oeste. (2018). 'Magmatism in the Central Andes', *Elements*, 14: pp. 237-244.

Yuan, X., Sobolev. S., Kind, R. (2002). 'Moho topography in the central Andes and its geodynamic implications', *Earth and Planetary Science Letters*, 199, pp. 389-402.

Yurtsever, Y., and Gat, J.R. (1981). Atmospheric waters: Stable isotope hydrology. In *Deuterium and Oxygen-^{18} in the water cycle, Technical reports series*. Gat, J.R., and Gonfiantini, R. Eds. 210, pp. 103-142.

Zandt, G., Leidig, M., Chmielowski, J., Baumont, D., and Yuan X. (2003). 'Seismic detection and characterization of the Altiplano-Puna magma body, Central Andes', *Pure and Applied Geophysics*, 160, pp. 789-807.

Appendix

Images of the quartz/plagioclase phenocryst separates of the CVZ rocks from which analysed quartz/plagioclase were picked.

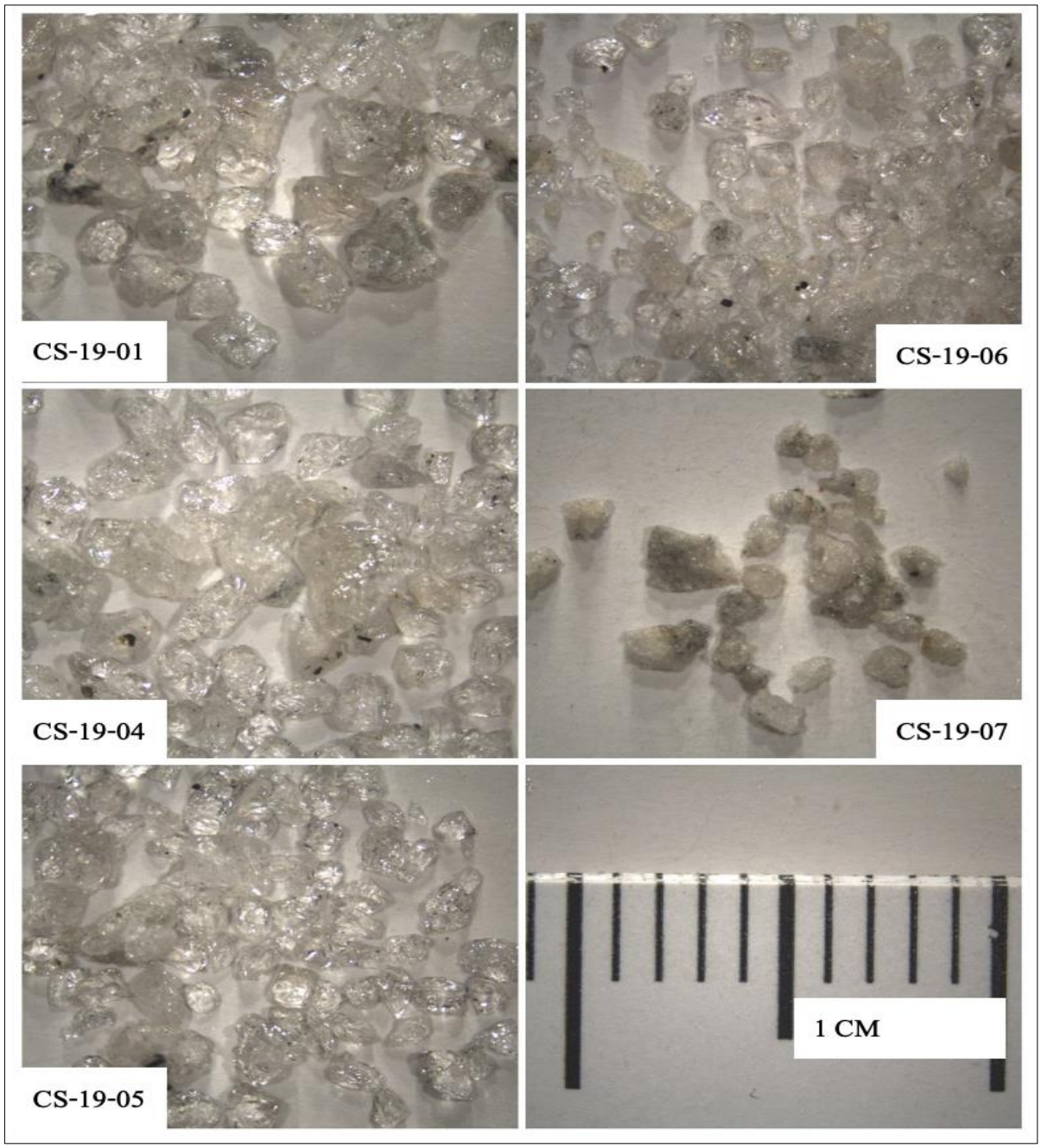

Notes

CS-19-07= Plagioclase

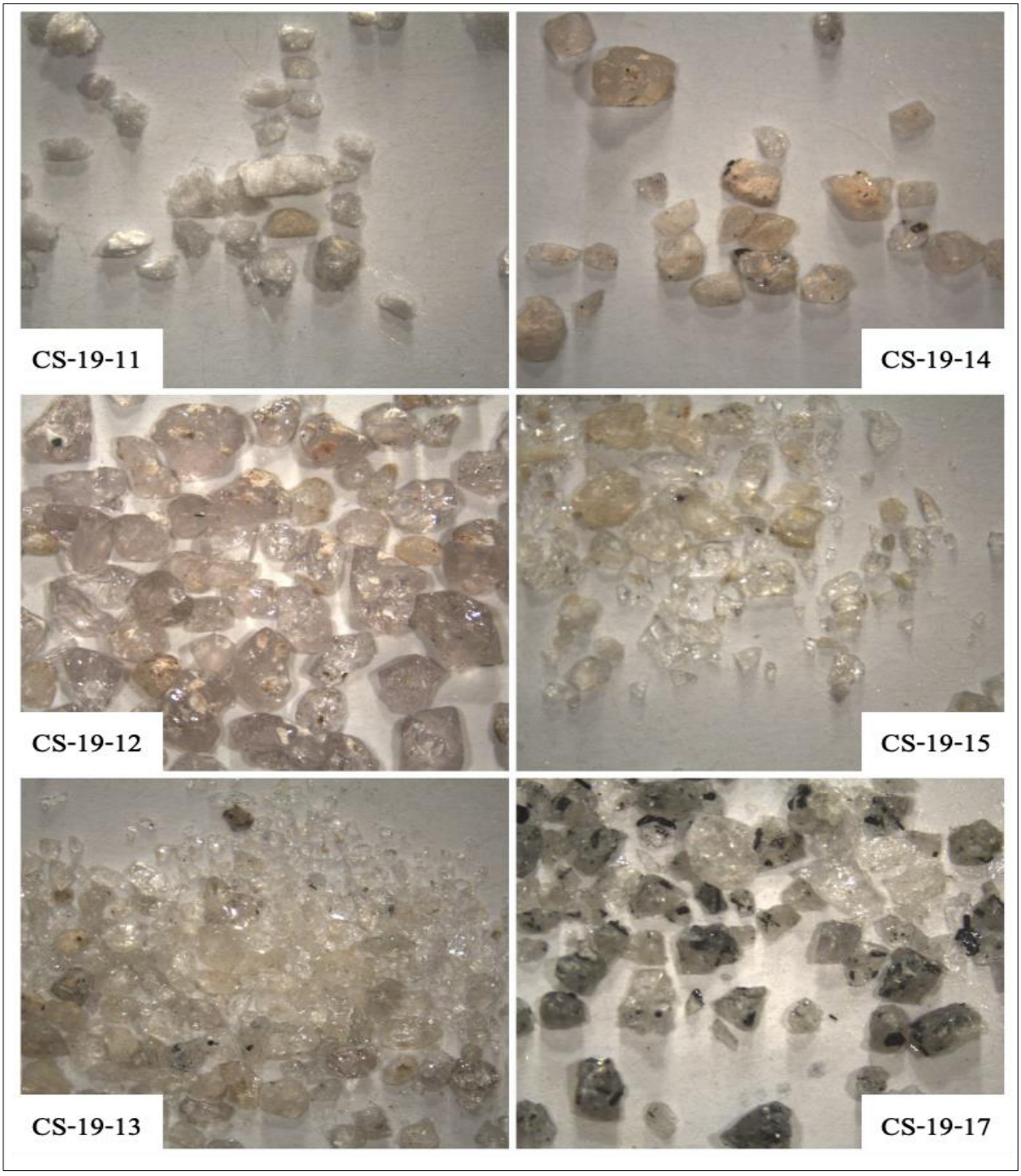
CS-19-11
CS-19-14
CS-19-12
CS-19-15
CS-19-13
CS-19-17

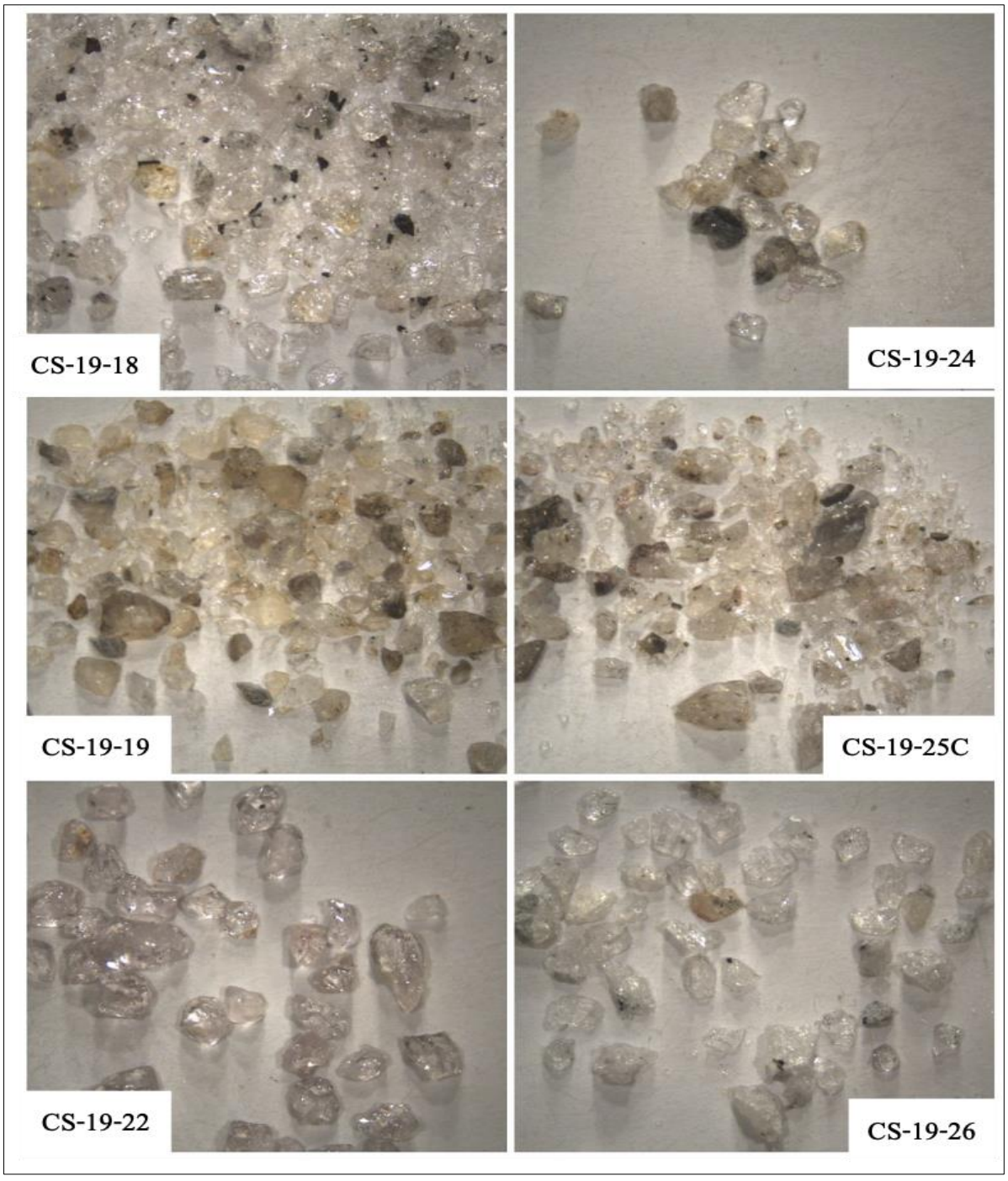
CS-19-18
CS-19-24
CS-19-19
CS-19-25C
CS-19-22
CS-19-26

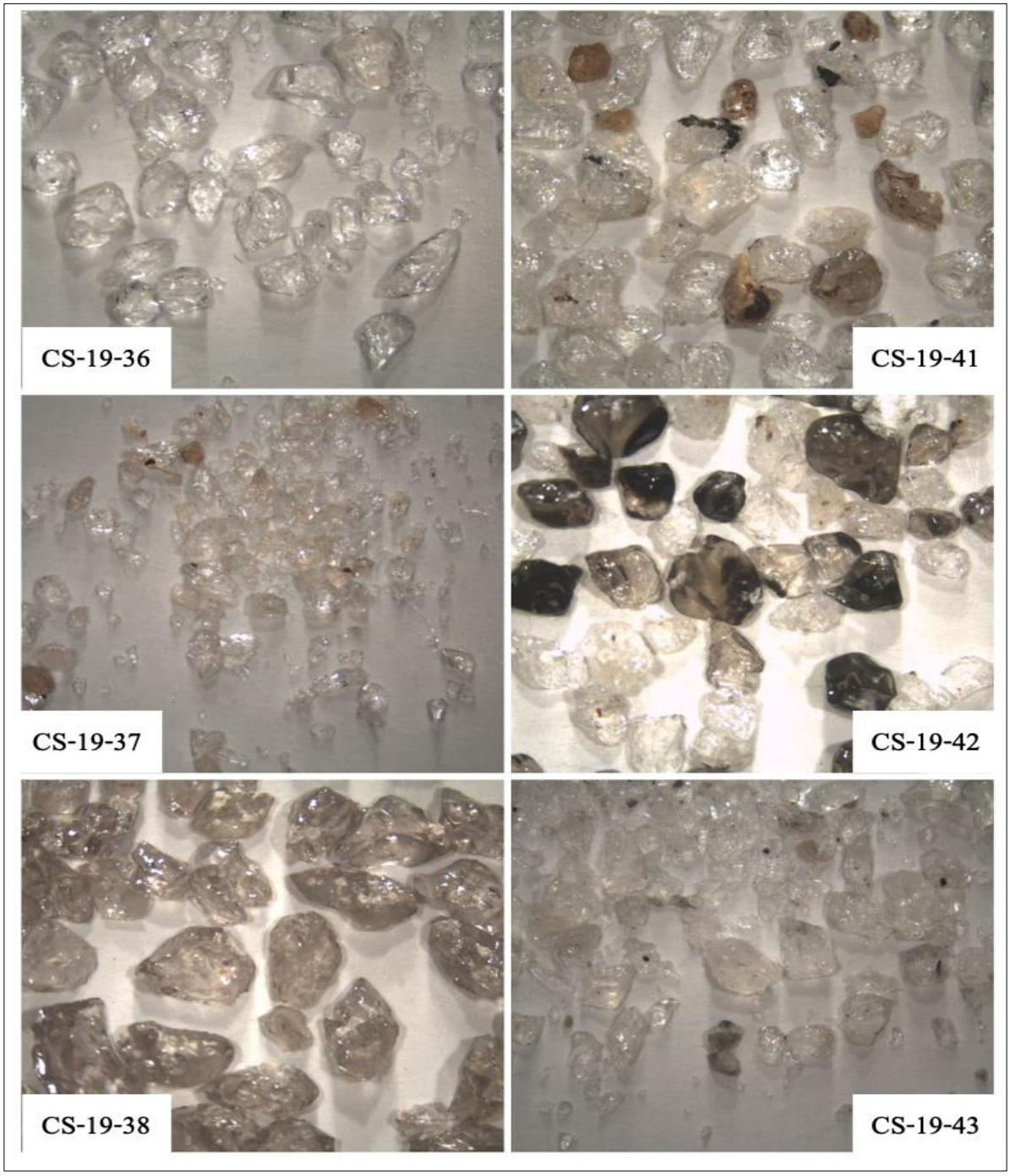

Notes

CS-19-42= The dark grains are possibly glass

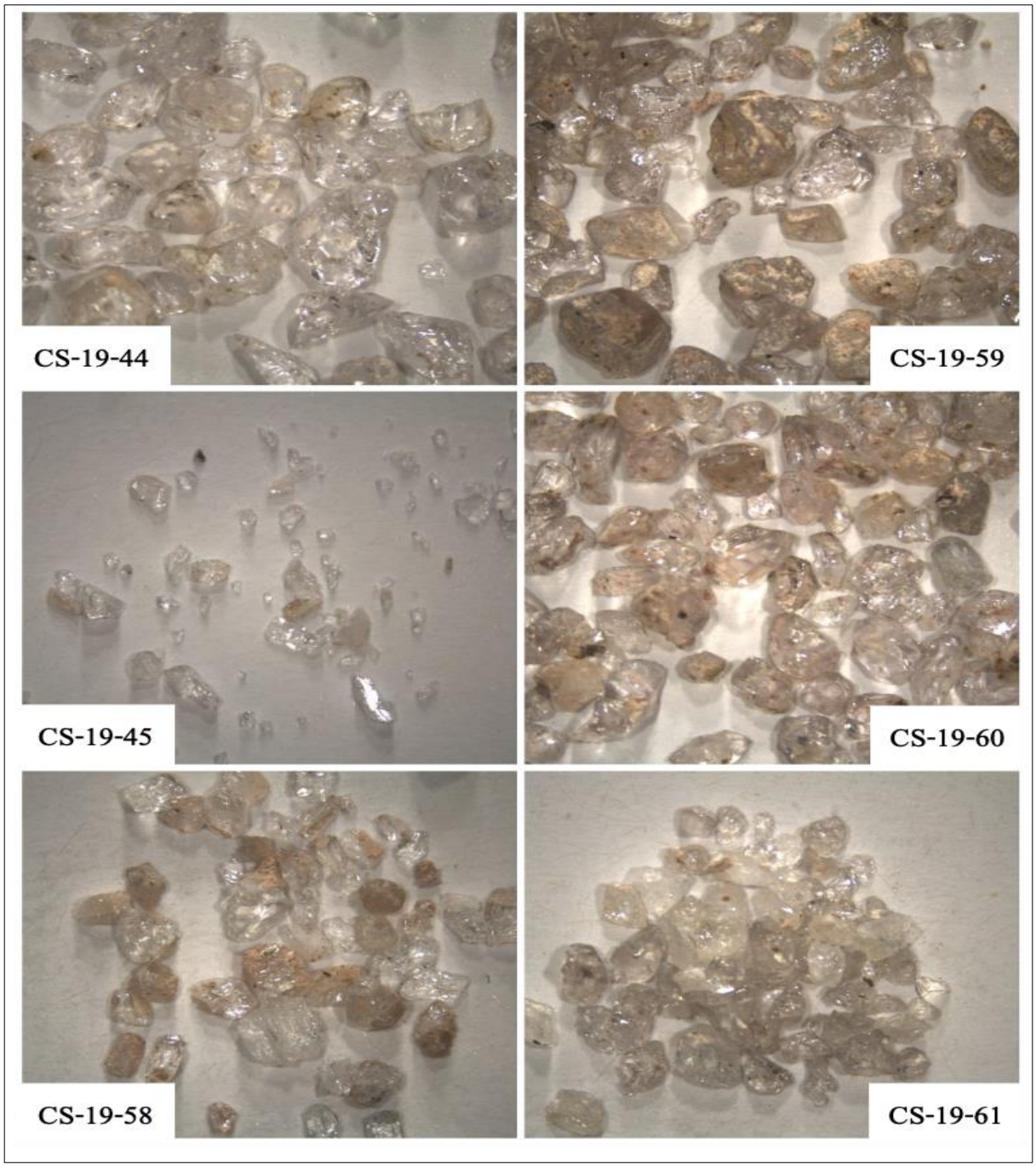
CS-19-44
CS-19-59
CS-19-45
CS-19-60
CS-19-58
CS-19-61